IUCAA - 8/94
February 94

BIRTH OF A NEUTRON STAR

Ramen Kumar Parui
Inter University Centre for Astronomy and Astrophysics,
Post Bag No 4, Ganeshkhind, Pune - 411007, India

Abstract : We have discussed various sources from which birth of a neutron star is possible, their discripancies with observed values, how new born neutron stars are different from usual cold ones, to what extend they are spun up by the contraction in the subsequent cooling stage evolving to cold stars.

Contents:

a

1. INTRODUCTION

Study of birth of a neutron star is of particular interest not only from the astrophysical view point but also from the view point of a new form of dense matter under extreme conditions. The matter from which neutron stars at the birth era are made, namely, supernova matter, is characterized by

i) almost constant entropy per baryon ($s \simeq 1\text{-}1.5$)[1]

ii) a high and almost constant lepton fraction ($Y_l \simeq 0.3 - 0.4$)[1,2] throughout the density

iii) the maximum density would amount to several times nuclear density ρ_0 ($\sim 2.8 \times 10^{14}$ g/cc)

iv) the temperature T could be as high as $T \simeq 10 - 50$ MeV

It is believed that type II supernova explosion[3-11], the end point of the evolution of massive stars, lead to the formation of neutron stars or blackholes. Whether a neutron star or a blackhole is formed depends on the size of the collapsing Fe core and the maximum neutron star mass, which is somewhat uncertain[12]. A major uncertainty is the lack of a complete understanding of type II supernova explosions with prompt mechnism, in which collapse core at bounce, can cause the ejection of the outer envelope.

It is also believed that a prototype of a neutron star with a radius ~ 100 Km is formed in the central part of the collapsing supernova core as a result of the bounce and successful supernova explosion (which is not yet well understood). The protoneutron star thus formed contracts rapidly (from radius ~ 100 Km to ~ 10 Km) and very soon goes into quasi hydrostatic equilibrium. According to Burrows and Lattimer[12] this rapid contraction almost

terminates within the first 0.1 - 1 s after the bounce. After wards, due to diffusion of neutrinos, this hot neutron star cools down and gradually contracts in a time scale of 10-20 s toward a typical cold neutron star.

The remaining promising mechanism is a Delayed Explosion caused by neutrino heating on a time scale of seconds (i.e. diffusion time scale of neutrinos from the core). The total energy release by the Fe core collapse in neutrinos of 2-3 x 10^{53} erg equals the gravitational binding energy of neutron star, because neutrinos and the particles with the longest mean free path being able to carry away that energy in the fastest fashion. This prompt mechanism still have some difficulties to explain such energies [13,14].

The other route for the formation of neutron stars is through white dwarfs. Various observations and calculations have forced to entertain this additional scenarios for the formation of neutron stars. There are three possibilities :

a) A white dwarf more massive than the Chandrasekhar limit could in principle be stabilized by thermal energy or rotation.
b) An extremely tight coalescing binary consisting of twoi white dwarfs
c) Accretion induced collapse of a white dwarf in a binary

But the first and second scenarios are rare while the third one is now popularising.

The main aim of this review is to see the different possible sources of neutron star formation, their difficulties with the observations, how new born neutron stars are different from usual cold ones, to what extend they are spun up by the contraction in the subsequent cooling stages evolving to cold star.

2. BIRTH OF A STAR

It is believed that stars are born from the contraction

of condensed matter of cloud of gas and dust found in galaxy. Typical densities in such regions are around 10^{-19} kg.m^{-3} (i.e. about 10^{8} hydrogen atoms per cubic meter), and infact predominantly made of neutral hydrogen. For our simplification, we assume that a cloud of gas is large enough to induce contraction. In these initial stages the force of gravitation between different constituents of the objects is so strong as to cause a rapid collapse of the object as a whole. But this does not occur smoothly. It is rather catastrophic [15,16] . When the radius of the protostaris not too large (R ~ 10^{5} $R_{\odot}$, $R_{\odot}$ being the solar radius), the density ~ 10^{-15} g.cm^{-3} , the collapse is rather rapid (~ 500 years), and the 'Protostar' becomes very luminous [17] . Due to compression, heat is generated and as a result, a strong internal pressure builds up in the star, which tends to slow down the compression ---- until the object settles down to a more or less static states.

When the proto star has been contracting for about 20 million years, and at the same time, the temperature at the centre of the protostar has risen to 10 million degrees kelvin, a critical event occurs. At this temperature, for the first time, the hydrogen nnuclei (more precisely protons) at the centre of the protostar collide and stick together in a nuclear fusion reactions, i.e. the first nuclear reaction sets in and hydrogen burns, and converted to helium.

3. STELLAR EVOLUTION

During stellar evolution a series of stellar nucleosynthetic processes occur and they are as follows:

a) Hydrogen burning (conversion of hydrogen to helium)
   Temperature > 10^{7} K and duration $\approx 10^{10}$ years
b) Helium burning (conversion of helium to carbon, oxygen etc)
   Temperature T $\gtrsim 10^{8}$ K and duration $\approx 10^{7}$ years

c) Carbon burning and Oxygen burning (production of $16 \leq A \leq 28$)

Temperature T $\gtrsim$ 6×10^8 K (for Carbon burning)

Temperature T $\gtrsim$ 10^9 K (for Oxygen burning)

Duration $\approx$ 10^5 years unless nucleosynthesis is explosive

d) Silicon burning (production of $28 \leq A \leq 60$)

Temperature T $>$ 3 to 4 $\times 10^9$ K

Duration for the quasiequilibrium and 'e' process $\approx$ 1s

e) The s-process (production of theabundance proton rich $A \geq 60$)

heavy nuclei)

Temperature $T > 10^8$ K

Duration $\approx$ 10^3 - 10^7 years

f) The p-process (production of the $A \geq 60$)

Temperature $T > 10^{10}$ K

Duration $\approx$ 10 - 100 s (uncertain)

g) The p-process (production of low abundance proton rich heavy nuclei)
Temperature $T > 2$ or 3×10^9 K , Duration $\approx$ 10-100s.

3.1 Main Sequence Stage

Hydrogen burning : The element synthesis begins with the primeval hydrogen condensed in the star. This process of converting hydrogen to helium takes place in one of the two processes (p-p) and (C-N-O) cycles. The proton -proton (p-p) chain reaction operates in low mass stars (in the range of $1.5M_\odot$ - $2M_\odot$ or less) while carbon nitrogen oxygen (C-N-O) cycle operates in more massive stars. These nuclear reactions take a long time (~ thousands million of years). The long time duration which the star is steadily burning its nuclear fuel is called main sequence stage in the life of the star. The generation of energy by hydrogen burning develops internal pressure which opposes gravitational contraction and the star stabilized on the main sequence at the point appropriate to its mass. In these processes no neutron is available in the product.

3.2 Red Giant Stage

Helium burning : When hydrogen burning in a star's main sequence stage leads eventually to hydrogen exhaustion i.e. about 10% of the hydrogen has been transformed into helium, a core remains at the star's centre and the nuclear energy is no more sufficient to compensate the energy losses. There is first a short phase of overall contraction, during which the temperature increases inside the star. When the temperature is high enough for H to burn outside the stellar core i.e. shell burning (see fig1) the outer zone expands while the core goes on contraction. This contraction leads to increase the star's central temperature and when the central temperature becomes high enough ($\sim$ 2 x 10^8 K) for helium to burn into C and O, the star then goes to red giant stage.

For M $>$ $3M_\odot$: During the core hydrogen burning (C-N cycle) the core temperature was constant at about 10^7 K. Since the shell will ignite at 2 x 10^7 K, the star has a good deal of collapsing to do before the regions outside a core become hot enough for ignition to take place. The result is a turn toward smaller radii.

For M $<$ $3M_\odot$: The core temperature (continuously rises through p-p reaction). Then, when exhaustion occurs, the regions outside the core are close to the ignition temperature. There is thus a smooth transition to shell burning without the necessity of the whole star collapsing.

Now the consequences of the hydrogen shell burning :

i) for less massive star, the shell will be the sole source of the star's luminosity

ii) the shell will be the cause of the density gradient that the star so desperately needs to support envelope outside the core

iii) the shell will supply the push that sends the star on its way toward the red giant destiny.

The rate of energy production will depend upon the speed with which hot gases rise to the surface. With energy now reaching the surface, the temperature of the surface, which was decreasing, remains

almost constant. At this point, the temperature of the surface is about 4000K and the star is now red and very very large. It has become a red giant.

As the star moves into the red giant phase, the star has a hydrogen burning shell that was causing its non-degenerate hydrogen envelope to expand and cool. The mass of the core will remain approximately the same but the core of He will be compressed and slowly heated. The core is then composed of both He nuclei and electrons. Although the size of the red giant core is not fully kown in the compressed state, there is a great deal of uncertainty concerning the evolution of the star for $M > 3M_\odot$. We shall now try to give a general qualitatively picture of the development of massive stars :

i) $0.8M_\odot \lesssim M \lesssim 3M_\odot$: The Helium Flash

When M is greater than $0.8M_\odot$, the degenerate pressure of the electron gas is not high enough to support the envelope, so the core contracts and heats up. This heating, of course, affects only the He core and when the temperature reaches 10^8 K, the reaction assigned to the tripple alpha process begins :

$$^4He + {}^4He \longrightarrow {}^8Be ,$$

$$^8Be + {}^4He \longrightarrow {}^{12}C + \gamma ,$$

$$\text{Or } 3\ He \longrightarrow {}^{12}C + \gamma + 7.274\ \text{MeV} \qquad (1)$$

The reaction releases energy but the core cannot expand. The core explodes within a few hours after the reaction $3\alpha \longrightarrow C$ stars. This is helium flash.

The explosive release of energy finally produces enough luminosity to expand the core and lower its temperature. The core expansion soon damps out — the pull of gravity within the core overcoming the momentum created by the explosion. The explosion, thus, is confined and the star does not repture or eject material. The

expanded core is once again a gas composed mostly of He withn some C. Eventually the temperature at the centre of the star rises to 10^8 K as the star collapses. Again He burning begins, but now the core is a non-degenerate gas. So the energy production rate is controlled. Once a again the moment will come when core has used up its fuel He and can no longer produce energy. The same sequence of events now takes place as took place when the hydrogen was exhausted and the core become He. The isothermal core i.e. the layers above it will begin to collapse untill the released gravitational energy starts helium burning in a shell around the carbon core. Carbon will not burn until temperature is around 10^9 K. But with a mass in the 0.8M. - 3M. range, the electron degenerate core will support the envelope enough so that core temperature does not rise to the next fusion state.

ii) $3M_\odot \lesssim M \lesssim 10M_\odot$: The Carbon Flash

If the initial mass of the star is in this range, the electron degeneracy will not support the envelope and the core will ciontinue to contract and heat up. When the temperature of the core reaches ~ 10^9 K carbon burning takes place.

$$
\begin{aligned}
^{12}C + {}^{12}C &\longrightarrow {}^{24}Mg + \gamma + 13.930 \text{ MeV}, \\
&\longrightarrow {}^{23}Na + p + 2.238 \text{ MeV}, \\
&\longrightarrow {}^{20}Ne + He + 4.616 \text{ MeV}, \qquad (2) \\
&\longrightarrow {}^{23}Mg + n - 2.605 \text{ MeV}, \\
&\longrightarrow {}^{16}O + 2\,{}^{4}He - 0.114 \text{ MeV}
\end{aligned}
$$

Since by this the core is a lattice of solid carbon, the reaction rate is uncontrollable and the core explodes —— a 'Carbon Flash'. Then what happens after the carbon flash ?

According to one set of calculations, gravitational collapse of stars in the $8M_\odot \lesssim M \lesssim 10M_\odot$ mass range grows a core made of O+Ne+Mg through shell C burning. Gravitational collapse ensued as soon as the electron captures made the Chandrasekhar mass lower than the actual mass of the core. A conductive burning front should however start from

the centre. Burning propagation would later accelerate due to the growth of hydrodynamic instabilities. The result is that only extremelyslow deflagrations would induce collapse to a neutron star [18-23]. While other theories suggest that the O+Ne+Mg cores most likely undergo central non-explosive Ne-O ignition. The exact values depend on the amount of mixing in the semiconvective region. Stars would non-explosively burn in flashes, and later produced through the O-burning and Si-burning stages just as the more massive stars [23-24].

iii) Above $10M_\odot$:

It is believed that helium burning results in the production of approximately equal amounts of ^{12}C and ^{16}O in stars in the wide range of masses from o.5 — $50M_\odot$ [25-29]. Once ^{12}C is formed, alpha capture will become active and the reaction products of C-N-O cycle might produce neutrons [30-32] and von Weizsacker [33] predicted that when ^{13}C produced in helium burning is mixed with hydrogen at high temperature, hydrogen is converted to ^{4}He by the C-N cycle which in addition produce ^{13}C. The reaction is $^{12}C\ (p, \gamma)\ ^{13}N\ (\beta^+, \nu_+)\ ^{13}C$. That the ^{13}C formed in the C-N-O cycle can act as a source of neutrons as other particles was proposed by Greenstein [34], Cameron [35,36], Fowler etal [37] and Audouze etal [38]. Thus,

$$
\begin{aligned}
^{13}C + {}^{4}He &\longrightarrow {}^{16}O + n + 2.214\ MeV,\\
^{14}N + {}^{4}He &\longrightarrow {}^{18}F + \gamma + 4.416\ MeV,\\
^{18}F &\longrightarrow {}^{18}O + e^+ + \nu e\ ,\\
^{18}O + {}^{4}He &\longrightarrow {}^{21}Ne + n - 0.699\ MeV, \qquad (3)\\
^{18}O + {}^{4}He &\longrightarrow {}^{22}Ne + \gamma + 9.667\ MeV,\\
^{21}Ne + {}^{4}He &\longrightarrow {}^{24}Mg + n + 2.580\ MeV\\
^{22}Ne + {}^{4}He &\longrightarrow {}^{25}Mg + n - 0.481\ MeV,\\
^{22}Ne + {}^{4}He &\longrightarrow {}^{26}Mg + \gamma\ ,\\
^{25}Mg + {}^{4}He &\longrightarrow {}^{28}Si + n\ ,\\
^{26}Mg + {}^{4}He &\longrightarrow {}^{29}Si + n\ ,
\end{aligned}
$$

and the special case

$$
^{29}Si + {}^{4}He \longrightarrow {}^{32}S + n - 1.530\ MeV, \qquad (4)
$$

$$^{33}S + {}^{4}He \longrightarrow {}^{36}A + n - 2.0 \text{ MeV}$$

Concerning the alpha capture process in the red giant phase, ^{13}C and Ne take part in major reaction while very little ^{17}O remains for helium burning. Cameron emphasized the $^{13}C(\alpha, n)^{16}O$ reaction as neutron source, if it is postulated that considerable mixing between core and envelope takes place during the giant stage. The hydrogen from the envelope interacts with ^{12}C produced in the core ($3\,^{4}He \longrightarrow {}^{12}C$) and maintains constant supply of ^{13}C at such a rate that little ^{14}N is produced by the $^{13}C(p, \gamma)^{14}N$ reaction. It is also mentionable that if ^{12}C is mixed into the cooler outer regions of the core, where ^{13}C is burning, then ^{12}C captures the protons produced ffrom the reaction $^{14}N(n, p)$ and replenishes the ^{13}C. This permits all neutrons produced to be used for heavy elements synthesis just beyond ^{56}Fe.

But Fowler etal[37] proposed another reaction as an alternative source of neutrons. The reaction is $^{21}Ne(\alpha, n)^{24}Mg$. According to their proposed method ^{20}Ne, produced in the helium burning stage, is converted into ^{21}Ne in the hydrogen burning shell at about $3 - 5 \times 10^{7}$ K surrounding the helium burning cores of red giant stars. The ^{21}Ne then interacts with helium to produce neutrons which are captured by iron group nuclei to produce heavy elements. Of course, these reactions willhave to satisfy some conditions that the production of ^{21}Ne from the reaction $^{20}Ne(p, \gamma)^{21}Na(\beta^{+}, \nu_{+})^{21}Ne$ is faster than the production of ^{22}Na from the reaction $^{21}Ne(p, \gamma)^{22}Na$; the consumption of ^{21}Ne by $^{21}Ne(\alpha, n)^{24}Mg$ before helium is depleted in the core, etc.

Recent investigations[40-43] show that the $^{13}C(\alpha, n)^{16}O$ as well as $^{22}Ne(\alpha, n)^{25}Mg$ is a possible neutron source for the nucleosynthesis in this stage. To know the exact dominant role of the $^{22}Ne(\alpha, n)^{25}Mg$ reaction Parui[44] has suggested to investigate through the reaction rate measurement of it.

In this alpha process, heavier nuclei are formed by successive

fusion with more and more helium nuclei. Thus we get ^{16}O, ^{20}Ne, ^{24}Mg, ^{28}Si, ^{32}S, etc. This successive addition of an alpha particle can not go on indefinitely [30, 45, 46] because coulomb repulsion grows stronger as the nuclear charge increases. Beyond silicon or sulphu the process operates in a different manner. For stars whose mass is greater than $20M_\odot$, the core temperature can reach 3×10^9 K so that Si can burn combine with another Si to form Ni via $^{28}Si + {}^{28}Si \longrightarrow {}^{56}Ni$. This is a particular important reaction since nickel decays to cobult via $^{56}Ni \longrightarrow {}^{56}Co + e^+ + \nu$ and cobult decays to iron via $^{56}Co \rightarrow {}^{56}Fe + e^+ + \nu$. The decay chain ends since ^{56}Fe is stable. The process terminates when these three nuclei , i.e. Ni, Co, Fe of the iron group are formed.

3.3 Ca rbon Core Burning

During the helium burning phase, the predominant nuclei are ^{12}C and ^{16}O. When the temperature os greater than 10^8 K, carbon will begin to react with itself according to the reactions in eq (2). Recently Arcoragi etal [47] have investigated the core carbon burning of the massive stars having masses $15M_\odot$ and $30M_\odot$ respectively. According to them, during central C burning, the neutron capture nucleosynthesis develops upon the seed nuclei left by the previous core He burning. The neutrons in the C-burning core of $15M_\odot$ and $30M_\odot$ stars are essentially produced by $^{22}Ne\ (\alpha, n)\ ^{25}Mg$, the corresponding flux being shown in figs. 2 and 3. Their result may appear somewhat surprising in the light of the analysis by Arnett and Thielemann [48], Cameron [36] who identify $^{13}C\ (\alpha, n)\ ^{16}O$ as the dominant neutron producer in the relevant conditions. They also noted that the neutron production efficiency of $^{13}C\ (\alpha, n)\ ^{16}O$ can be drastically reduced if the production of ^{13}C via $^{12}C\ (p, \gamma)\ ^{13}N\ (\beta^+)\ ^{13}C$ can be counter balanced to a large extended by $^{13}N\ (\gamma, p)\ ^{12}C$ which is the case for high temperature $T > 8 \times 10^8$ K. They found that $^{21}Ne\ (\alpha, n)\ ^{24}Mg$ can be as an efficient neutron producer as $^{22}Ne\ (\alpha, n)\ ^{25}Mg$ at

one point or another in the evolution of some of the C-burning layers. The last potentially important neutron source $^{25}Mg\ (\alpha, n)\ ^{28}Si$, is by far least active.

They also found that in both $15M_\odot$ and $30M_\odot$ stars sequences, the neutrons produced in the central C-burning regions are mainly captured by ^{20}Ne, which is one of the main direct products of C-burning [49] and by ^{25}Mg, which is mainly built up for $^{22}Ne\ (\alpha, n)\ ^{25}Mg$.

3.4 Helium Shell Burning

After central He exhaustion, the stellar core contracts rapidly and as a consequence, layers above the He exhausted core heat up, and a He burning shell develops. That shell comprises two regions -- inner zone and outer zone which are seperated by a composition discontinuity. The chemical compositions of the inner zone of the He burning shell is almost identical to the composition at the end of He burning. The involving neutron sources are $^{13}C\ (\alpha, n)\ ^{16}O$, $^{21}Ne\ (\alpha, n)\ ^{24}Mg$, $^{22}Ne\ (\alpha, n)\ ^{25}Mg$ and $^{25}Mg\ (\alpha, n)\ ^{28}Si$. Arcoragi etal have also investigated the He-burning shell for the star of masses $15M_\odot$ and $30M_\odot$ respectively. During central C-burning the case of shell He burning is somewahat more complicated, since some of the He burning layers were part of the He burning core that receded at the end of central He burning, and left small amount of unburning He and a non-negligible enhancement of heavy elements. It appears in their result that $^{22}Ne\ (\alpha, n)\ ^{25}Mg$ reaction fails badly to produce a significant amount of neutrons. They also evaluate the role of $^{22}Ne(\alpha, n)\ ^{25}Mg$, $^{13}C\ (\alpha, n)\ ^{16}O$ in the He burning shell qualitative ground. Their result shows that the region of the He burning shell, of both $15M_\odot$ and $30M_\odot$ stars, where noticable neutron fluxes are ontained does not contain more than $0.1M_\odot$ of material.

3.5 Oxygen Burning

At about 2×10^9 K, oxygen will also react with itself acco-

rding to the reactions :

$$
\begin{aligned}
{}^{16}O + {}^{16}O &\longrightarrow {}^{32}S + \gamma + 16.539\ \text{MeV},\\
&\longrightarrow {}^{31}P + p + 7.676\ \text{MeV},\\
&\longrightarrow {}^{31}S + n + 1.459\ \text{MeV},\\
&\longrightarrow {}^{28}Si + {}^{4}He + 9.593\ \text{MeV},\\
&\longrightarrow {}^{24}Mg + 2\,{}^{4}He - 0.393\ \text{MeV}
\end{aligned}
\qquad (5)
$$

Thus we see that neutrons are produced when reaction yields are ^{22}Mg and ^{31}S.

3.6 Silicon Burning

At the end of carbon and oxygen burning, the most abundant nuclei will be ^{32}S and ^{28}Si with significant amount of ^{24}Mg. Because of the binding energies for protons, neutrons and alpha particles in ^{32}S are smaller than those in ^{28}Si, the nucleus ^{32}S will be the first to photo-disintegrate according to the reactions :

$$
\begin{aligned}
{}^{32}S + \gamma &\longrightarrow {}^{31}P + p - 8.864\ \text{MeV},\\
{}^{31}P + \gamma &\longrightarrow {}^{30}Si + n - 7.287\ \text{MeV},\\
{}^{30}Si + \gamma &\longrightarrow {}^{29}Si + n\ ,\\
{}^{29}Si + \gamma &\longrightarrow {}^{28}Si + n
\end{aligned}
\qquad (6)
$$

The resulting reactions will leave a little amount of Si. Most nuclear species between ^{28}Si and ^{59}Co (except neutron rich species ^{36}S, ^{40}Ar, ^{43}Ca, ^{46}Ca, ^{48}Ca, ^{51}Ti, ^{54}Cr, ^{58}Fe) are generated by quasi-equilibrium processes in which the only important thermonuclear reaction rates are thought to be those of the bottleneck nuclei ^{44}Ca, ^{45}Sc, ^{45}Ti.

4. PRESUPERNOVA COMPOSITION STRUCTURE

Fig. 4 illustrates the evolution of the internal structure of the $20M_{\odot}$ star [50] . The locus of the points where the maxima of nuclear energy generation by C-burning and Ne-photodisintegration

occur are indicated by the hatched lines. The composition structure at the presupernova stage [51,52] with the central density $\rho_c = 2 \times 10^{10}$ g cm^{-3} shown in fig. 6 is as follows :

i) Fe core of Mr $\leq 1.40 M_\odot$, which is composed of nuclear statistical equilibrium elements, i.e. iron peak elements and a trace of ^{4}He, free proton and neutron.

ii) Fe-Si layer at $1.40 M_\odot <$ Mr $\leq 1.48 M_\odot$ composed of two quasi-statistical equilibrium clusters, i.e. a Fe cluster and a Si cluster. The neutron excess is $\eta = 0.012$

iii) Si rich layer at $1.48 M_\odot <$ Mr $\leq 1.67 M_\odot$ composed of a Si quasi statistical equilibrium cluster. (mainly ^{28}Si, ^{32}S, ^{34}S, ^{38}Ar) where $\eta = 0.012$ for Mr $\leq 1.63 M_\odot$ and $\eta = 0.0026$ from $1.63 M_\odot <$ Mr $\leq 1.67 M_\odot$. The neutron excess in this layer is important for the synthesis of neutron rich iron peak elements but subject to uncertainties involved in the electron capture rates and the time scale of mixing of neutron rich species from the bottom of the convective Oxygen and Silicon burning layers.

iv) Oxygen rich layer at 1.67M. < Mr < 3.66M. composed of ^{16}O, ^{20}Ne, ^{24}Mg and a trace of Si, Al,Mg and Na isotopes with $\eta = 0.0016$.

v) Carbon and OXygen layer at $3.66 M_\odot <$ Mr $< 3.76 M_\odot$ with a trace of Na, Mg, and Ne isotopes.

vi) Helium rich layer at $3.76 M_\odot \lesssim$ Mr $\leq 5.71 M_\odot$ which includes ^{12}C, ^{16}O, ^{18}O, ^{22}Ne and ^{25}Mg. These elements are produced from alpha capture reactions in the $^{12}C(\alpha,\gamma)^{16}O$ and $^{14}N(\alpha,\gamma)^{18}F(\beta^+)^{18}O(\alpha,\gamma)^{22}Ne(\alpha,n)^{25}Mg$. reactions in the convective helium burning layers. More investigation needs to know the role of last reaction leading to s-process nucleosynthesis [53] .

vii) Helium layer at $5.71 M_\odot <$ Mr $\leq 6.0 M_\odot$ composed of ^{4}He and ^{14}N.

5. SUPERNOVA STAGE

Towards the end of the Si burning process, the core of the star has reached a temperature in excess of 10^9 K and iron group nuclei are available. These heavy elements are known as product of stellar

death. When the core has exhausted its supply of Si, the Si + Si ⟶ Ni shuts off and the core of the star contracts until we get burning in a ring about the Fe core. Again when the temperature further increases in the iron core, the iron core can only decomposed into elements of lower average binding energy which means a net absorption of energy and ultimately collapse of the core. Now the question arises --- what does the collapse lead to ? Some suggest a violent explosion, a supernova with a neutron star left behind. Other argu that no such explosion can take place and that a blackhole must result when the iron dissociates. Thus, when a massive star has reached the end of its nuclear fuel, it can become a supernova. A supernova arises when the core of a star collapses under its own gravitational contraction, releasing energy which causes the outer envelope to explode, i.e. the inner part of a star undergoes an implosion, while the outer part undergoes an explosion.

6. SUPERNOVA PROGENITOR TYPE THAT MIGHT LEAVE NEUTRON STAR

There is a general understanding that massive stars explode as supernova (SN), at least those do not collapse directly to make black-hole. Supernovae are classified into two main groups type I and type II.

i) Type I : Two subclasses of type I supernova are commonly believed to arise from core collapse explosions in massive stars. They are spectr-oscopically characterised near maximum light by the presence (called type Ib) or absence (called type Ic) of strong optical helium lines. Their late time light curve indicates a range of progenitor masses from ~ 5 to 10$M_\odot$ [54-60].

Type Ib: The presence of helium and the lack of hydrogen implies SN Ib progenitors are helium cores of massive stars that have lost their entire hydrogen envelopes. Allowing for a neutron star remnant, the SNIb light curves suggest the core masses range from ~ 5 to 10 $M_\odot$ corresponding to main sequence masses of ~ 15 to 30$M_\odot$. Such stars would be expected to explode following Fe core collapse to form a neutron star (and, for the most massive progenitors, probably a blackhole) [61] .

Type Ic : Based on the narrow peak and rapid post-maximum decline of the

SNIc light curves, Shigeyama etal [62] argued that SNIc are the low mass versions of the helium star while Swartz etal [63] and Swartz [64] showed that SNIc's must be helium deficient and SNIc explosions are therefore low mass metal rich events. The helium layers of a massive star can be lost in wind in single star evolution, but the initial star must be extremely massive and the resulting oxygen core may be to massive to reproduce the SNIc light curve [65].

The estimated mass of the immediate progenitor, presumed to be a bare C-O core of ~ 2 to 3 $M_\odot$, corresponds to main sequence masses of again about 10 to 15$M_\odot$, or perhaps a little larger. Thus, the main sequence mass of SNIc progenitors could be comparable to those for SNIb [66,67] i.e. the process of loss of the helium envelope is important. Two cases arise:

a) The process of loss of the helium envelope by mass transfer through Rochelobe overflow could occur in either the primary or the secondary. In this case, SNIc events could have either an unevolved or a compact companion. If the mass transfer from the helium core of the secondary takes place, the secondary's explosion may leave two neutron stars [66,68] (i.e. may be involved in the production of binary pulsars)

b) Tidal instability : Instead of helium envelope Roche lobe overflow tidal instability may remove helium from the core. This occurs through a common envelope phase [69] followed by mass and angular momentum loss from the system. To account for SNIc, for low mass helium cores, this tendency of the radius to expand may lead the common envelope process continues until the oxygen core is exposed i.e. a comon envelope process may be thorough in removing an extended envelope than the Roche lobe overflow process. If this is the primary route to SNIc, then the progenitors should all have neutron star companion and two neutron stars, either bound or unbound, should be left after explosion [61].

ii) Type II : Supernova type II (SNII) exhibit a wide range of spectral and photometric properties but by definition, all display hydrogen Balmer lines in their spectra. Two distinct subtypes can be identified bas based on the observed B light curve morphology : those with a phase of

nearly constant luminosity following maximum light (SNIIP — P for Plateau) and those showing a linear decline (SNII-L).

a) Type IIP : The generic SNIIp light curve is well understood [70-73] as the result of the explosion of a moderately massive red (spectral type M) supergiant. The plateau phase lasts weeks to months implying a progenitor mass of 10 to 20$M_\odot$ (and larger if moderate mass lass precedes the explosion). Stars within mass range grow Fe cores which collapse to form neutron stars or , perhaps, blackholes. At the low end of this mass range degenerate O-Ne-Mg cores may form. These probably collapse to for neutron stars [74-76] .

b) Type II L : The emperical evidence for homogeneity among most SNIIL is probably the most straight constraint on the progenitor mass, radius and previous evolution. Light curve calculations [77,78] require a regul- relatively low hydrogen mass at the time of explosion to prevent the plateau phase characteristic of the SN II P events.

For typical SN II L, the light curve can be fit with an O+Ne+Mg core collapse ejecting a helium enhanced envelope of 3-5 $M_\odot$ (hydrogen mass ~ 1$M_\odot$) and of initial radius R ~ 400Km $R_\odot$ [77] . Such a radius is comparable to that deduced for SN1993J [78] and implies that the progenitors may have been G or K, rather than M, supergiant. The progenitor envisioned would envelope as a single star from an initial mass of ~ 8 to 10$M_\odot$, experience some mass loss (consistent with the radio, UV, etc) and explode at the tip of the asymptotic giant branch after its surface layers have been helium enhanced. It is not clear whether such stars are sufficiently helium enriched, though standard evolution suggests that convective core contraction on the main sequence and dredged up by the convective envelope will increase the helium abundance while hydrogen will be depleted by mass lass. [79-80]

7. SUPERNOVA EXPLOSION

In case of supernova explosion, the temperature becomes so hig -h ($T > 4 - 5 \times 10^9$ K) during a short time scale (~ 1sec) that many nuclear reactions do occur and usually transfer the final abundances

of the ejected mass. Thus, the explosion of supernova does not only lead to a strong outburst of energy but also to the formation of a remnant which remains energetic for a rather long time 10^4 to 10^5 years [81].

The hypothetical mechanisms which trigger the supernova explosions are

i) Fe-Photodisintegration (or prompt mechanism)

ii) the neutrino transport (or delayed mechanism)

iii) the rotation energy transfer from the central pulsar

iv) the C-detonation

The C-detonation in principle can take place in stars of mass 4 to 8 $M_\odot$ which end up their evolution at the stage of C-burning. The explosive burning of C in a degenerate core can trigger a supernova type explosion but in this case a remnant can not servive. This explosive process also induces a large production of Fe which is in disagreement with the observations [82]. As we are interested on neutron star formation, so we shall not discuss each mechanism in details. Only we shall discuss about the current picture of supernova explosion mechanism which can occur in the case of stars more massive than $8M_\odot$.

7.1 Prompt Explosion Model

Massive stars ($M \gtrsim 8M_\odot$) develop iron cores of masses close to the Chandrasekhar mass $M_{ch} \approx 5.814\, Y_e^2\, M_\odot$ where Ye being the electron number fraction) by burning hydrogen to increasingly heavier elements (He, Ne, Mg, C, O, Si etc). The generated energy prevents the star from gravitational contraction. At the end of these successive, quiet burning stages the appearence of elements of the iron group, the most tightly bound nuclei, does not allow for any further energy release by nuclear fusion reactions in the core of the star. Therefore, the core cannot escape instability when its mass exceeds the Chandrasekhar limit. As soon as the central density reaches values high enough for neutron decays not being able to compete with electron capture any longer, the central pressure, dominated by degenerate electrons, is reduced significantly and contraction turns into a

collapse dynamical time scale i.e. essentially on the free fall time scale i.e. essentially on the free fall tim escale about a hundred milliseconds. At this point the central values of temperature, density and lepton concentration are typically $T \approx 10^{10}$ K, $\rho_c \approx 10^{10}$ g cm^{-3} and $Y_e \approx 0.42$ respectively. The core extends to a radius of roughly 100Km.

Fig.7 represents the picture of the innermost $15M_\odot$ of $25M_\odot$ presupernova model. These four $25M_\odot$ presupernova models are calculated with the help of different values of the semi convective diffusion parameter and rate for the $^{12}C(\alpha,\gamma)^{16}O$ reaction rate. In fig.5 we see that most of the differences can be traced to the smaller C-O core obtained when semiconvection is restricted. This gives less heavy element production and smaller iron core (see table 1)[86-91]. Woosley etal[85] have raised a possibility that very massive stars endowed with large mass loss rates may lose, not only all of their hydrogen envelope, but a portion of their helium and carbon-oxygen core as well.

In 1987 Arnett[44] also argued same possibilities. Density (fig.8a) and chemical composition (fig.8b) vs mass for the inner most stellar model of Arnett[92] are shown in fig.8. This model has a $4M_\odot$ helium core, a $1.5M_\odot$ oxygen core , and a metallicity $z = z_\odot/4$. The density profile shows two steep drops, which occur at the H/He and at the He/C-O interface. Muller etal[93] have suggested that these regions will become unstable due to the passage of the shock. When rotation is unimportant, the collapse, triggered by increasingly faster electron captures and additional photodisintegration of heavy nuclei, proceeds until nuclear matter density is reached. When the inner part of the collapsing core decelerates and bounces, a shockwave is generated and driven into the supersonically falling outer part of the iron core. According to the current picture, this shock wave is expected to give rise to the supernova explosion, if it survives the grave energy losses by disintegration of heavy nuclei and neutrino emission and eventually reaches the edge of the iron core and runs down the steep density gradient in the outer shells of the evolved massive star.

As the shock wave propagates through the Si and O rich layers, explosive nucleosynthesis takes place behind the shock [83, 94-96].

i) Explosive Silicon burning --- Explosive Si burning takes place at $T > 4\text{-}5 \times 10^9$ K and can be divided into three different regions: complete Si burning with either a normal or alpha rich freeze out, incomplete Si burning [97].

Complete Si exhaustion at $T > 5 \times 10^9$ K produces only Fe group nuclei. The most abundant nucleus in the normal and alpha rich freezeout is ^{56}Ni if Ye > 0.49. For the less abundant nuclei the final alpha capture plays a dominant role transforming nuclei such as ^{56}Ni, ^{57}Ni, and ^{58}Ni into ^{60}Zn, ^{61}Zn, and ^{62}Zn in an alpha rich freezeout where also trace abundances of ^{40}Ca, ^{44}Ti, ^{48}Cr and ^{52}Fe are obtained (see fig.9a).

In complete Si burning takes place at $T \sim 4\text{-}5 \times 10^9$ K. Besides the dominant fuel nuclei ^{28}Si and ^{32}S, the alpha nuclei ^{36}Ar and ^{40}Ca are most abundant. Partial leakage through baottleneck above Z=20 produces ^{56}Ni and ^{54}Fe as dominant abundances in the Fe group. Smaller amounts of ^{52}Fe, ^{58}Ni, ^{55}Co, and ^{57}Ni are also produced.

ii) Explosive Oxygen burning : At temperature $T > 3.3 \times 10^9$ K, a quasi-equilibrium is established among nuclei in the range $28 < A < 45$. The main burning products are ^{28}Si, ^{32}S, ^{36}Ar, ^{40}Ca, ^{38}Ar and ^{34}S. ^{33}S, ^{39}K, ^{35}Cl, ^{42}Ca and ^{37}Ar are also produced (mass fraction is less than 10^{-2}) In zones with $T \sim 4 \times 10^9$ K there exists still a contamination by the Fe group nuclei ^{54}Fe, ^{56}Ni, ^{52}Fe, ^{58}Ni, ^{55}Co and ^{57}Ni.

iii) Explosive Ne and C burning : Zones with temperature $T > 2.1 \times 10^9$ K undergo a combined version of explosive Ne and C burning. The main burning products are ^{16}O, ^{24}Mg and ^{28}Si. Besides the major abundances, Ne burning supplies also substantial amounts of ^{27}Al, ^{29}Si, ^{32}S, ^{30}Si and ^{31}P and C-burning contributes in addition the nuclei ^{20}Ne, ^{23}Na, ^{24}Mg, ^{25}Mg, and ^{26}Mg (see fig.10).[52]

As the shock wave propagates through the surface , the shocked layers undergo acceleration and deceleration. In particular, the composition interfaces of hydrogen/helium and helium/C+O are strongly Rayleigh-

Taylor (RT) unstable which induces mixing of material before the shock breakout at the surface. In fig.11, the velocity distribution for the homologous expansion is shown for typical hydrodynamical simulation models 14E1 and 11E0.6 [98,99]. 14E1 model denotes the model with ejected mass Mej= 14.6M. and the final kinetic energy of explosion E= 1 x 10^{51} erg, while for 11E0.6 model Mej = 11.4$M_\odot$ and E= 0.6 x 10^{51} ergs. The velocity gradient with respect to the enclosed mass, Mr, is very steep near the surface, while it is almost flat in the helium layer and the heavy element core. This is because the core materials are decelerates and form a dense shell due to the reverse shock when the expanding core hits the hydrogen rich envelope. The kinetic energy of the helium and heavy element layers is only 10% of the total kinetic energy.

Fig.12 a) and b) show the evolution of the pressure profile and the density profile of the exploding star, respectively, based on the analysis of the explosion for model 14E1 perfomed by Ebisuzaki etal [100]. Before the explosion, pressure gradient is negetive being balanced with gravitational attraction (stage 0). After the blast shock passed, the layer expands to decrease the pressure rapidly. When the blast shock is propagating through the hydrogen rich envelope with a much less steep pressure gradient, an inwardly propagating reverse shock forms (stage 2-4). The layer between the blast wave and the reverse shock is decelerated and thus has a pressure gradient, an inward-moving rarefaction wave forms and produces a negetive pressure gradient that accelerates the matter outward (stage 5). As a result, the H/He interface is first accelerated, then decelerated, and finally accelerated again; i.e., the pressure gradient changes its sign twice. The He/Metal interface also experiences similar acceleration and deceleration.

Similarly, in case of density profile (fig.12b) near the H/He and the He/metal interfaces (dashed line), the density steeply decreases with radius because of the changes in the mean molecular weight (μ) and the specific entropy (s). During the hydrodynamical stages of explosion, the sign of the gradients of 'μ' and 's' and , hence of the density near the composition interface donot change. It is also clearly seen that

(from the above figs) the pressure gradient is positive during the deceleration phase (stage 2-4 for the H/He interface), while the density gradient remains negetive near the H/He and He/metal interfaces. These layers are also Rayleigh-Taylor unstable.

In the two dimensional (2-D) hydrodynamical simulation a large nonlinear growth of the R-T instability are found around the He/C+O interface, but only a limited growth around the H/He interface [101-109]. Hachisu etal [101] found that the instability grows much more extensively at the H/He interface rather than at the He/C+O interface (see fig 13a). In their 2-D calculation 5% perturbation is applied to the velocity field just after the blast shock hits the hydrogen rich envelope (~ 10 s after the explosion). The R-T instability sets in at the H/He interface and continues to grow until the blast shock breaks out of the hydrogen rich envelope. The growth time to nonlinear regime is about t = 1000s and the mushroom structures become apparent at time t=2000s. The R-T instability, being initiated first at the H/He interface, induces the mixing between the core and the envelope. Fig.14 clearly shows that the heavy elements (core material) are mixing upto the middle of the hydrogen rich envelope. The abundance distribution after mixing is a function of mass and the expansion velocity (as shown in fig.15). The core materials composed of C+O and silicon rich elements are mixed upto the layers having expansion velocity ~ 2200 km/s. At the same time, hydrogen is mixed down to the core of expansion velocities as low as ~ 800 km/s [52]. These velocities are close to the terminal values, since the shock has already broken out of the hydrogen rich envelope at this time.

After the initial explosion energy is put into the star, the central temperature is extremely high. As a result, the time step required for stability is very small. In the beginning the neutrinos produced by electron captures onto protons and nuclei can escape nearly unhindered due to their small cross sections of the order of 10^{-44} cm^2. As the collapse proceeds and the average density in the core rises, the opacity for neutrinos increases, too, and eventually neutrinos become 'trapped'

inside the core when their diffusion time scale exceeds the time scale of dynamical changes. It is not earlier that the lepton fraction in the matter frozen in and the created neutrinos are able to come into local chemical and thermodynamicalequilibrium with the stellar material. As long as this is not the case, deleptonization and moderate entropy generation influence the collapse behaviour of the iron core, the position where the shock wave will be formed and the initial energy of the shock. According to Cooperstein [111] this prompt explosion model is operating for small progenitor masses ($10M_\odot \lesssim M \lesssim 15M_\odot$) with the iron core mass $\lesssim 1.35M_\odot$. The shock is expected to proceed without stalling and would reach the core envelope boundary in a few tens of milliseconds. Recent computations [112-125] exhibit a tendency that for stars with masses larger than about 10M. the shock wave is not energetic enough to overcome the strong energy losses in the iron material and stalls on its wayout, becoming an accretion shock at a mass position of 1.2 - $1.3M_\odot$ i.e. significantly inside the edge of the iron core.

7.2 Delayed Explosion Model

In the above discussion we see that the shock is not successful in propagating out on dynamical time scales, and 'this prompt' mechanism appears to fail to answer the collapse events during the first 20ms (sound crossing time for the core), the propagation and initial death of the shock which set the stage for what follows. An alternative picutre, called Delayed Explosion by neutrino heating, originally proposed by Colgate and White [126], newly proposed by Wilson [127] and Bethe and Wilson [128], extended by Goodman etal [129] and numerially tested by Wilson and Mayle [130] Mayle and Wilson [131]. Here the shock stalls at a radius of a few hundred km, having lost energy in dissociating nuclei and in radiating neutrino pairs that escape from the star. But over time scales of the order of a second, the shock is revived through the heating action of a small fraction of the neutrinos streating out from the neutrino sphere [128, 132]. However, the heating rate depends sensitively on the nuclear statistical equilibrium of the matter behind and this is to be handled in a self-consistent way [133].

Not only that the 'success' of this delayed mechanism depends sensitively on the neutrino luminosity and temperature.

As this Delayed model involves star of larger masses, the inclusion of rotation may , therefore, be the crucial for the correct modelling of a type II supernova explosion. Because
i) stars and specially massive stars rotate in general [134] , and because of ii) angular momentum conservation and the increasing centrifugal forces already small initial rotational energies may change the standard collapse picture completely [135] . So we shall fist discuss about the core collapse with rotation and then neutrino heating.

7.2.1 Expected Effect due to rotation

i) Core Stabilization : The collapse of stellar iron cores is initiated by electron captures on nuclei and free protons and by nuclear photo-disintegration process. Both effects lower the pressure and the index $\Gamma = (D \ln P / D \ln \rho) / M$ defined for a mass element M along its trajectory. In the absence of rotation, the core becomes dynamically unstable if $\Gamma < 4/3$.

The collapse of a non-rotating core is characterized by the formation of a subsonically and homogeneously contracting inner core and supersonically falling outer core. During collapse the mass of the inner core is roughly equal to the Chandrasekhar mass which itself depends on the mean diminishing lepton concentration of the inner core. The collapse of the inner core cannot be stopped before nuclear matter densities are reached. At this stage, the adiabatic index rises sharply, which leads to the 'bounce' of the inner core. A shock wave is formed near the edge of the inner core and propagates outwards through the iron core. The shock wave either turns into an accretion shock inside the iron core or reaches the stellar mantle causing a supernova explosion. In massive iron cores the shock suffers from severe energy losses mainly due to photo-disintegration of nuclei and stalls inside the core about 10ms after core bounce [6, 136] .

The main difference between the collapse of rotating and non-

rotating cores is that in rotating cores centrifugal forces may stop the collapse before nuclear matter densities are reached [137-142]. van Ripper etal [143], Cooperstein and Baron [6], Monchmeyer [125] showed that the stability and hydrodynamical evolution of a collapsing iron core are not determined by the adiabatic index $\gamma = (\partial \ln P / \partial \ln \rho) |_{s,Ye}$ [at fixed entropy 's' and electron concentration 'Ye') [144] but instead by an effective index $\Gamma = (D \ln P / D \ln \rho) |_{M}$ calculated along a collapse trajectory of a given Langrangian mass elements M, i.e. the stability is influenced by electron capture and non-adiabatic processes. In addition, they have also shown that even a small amount of initial rotational energy can be sufficient to stabilize a core at densities less than nuclear matter density, provided that angular momentum is conserved during the collapse and that Γ has a value close to 4/3.

ii) Collapse Time Scale

Due to conservation of angular momentum and the resulting increase of the centrifugal forces matter willnot fall in on radial trajectories. In addition, matter in the equatorial plane will not fall towards the centre as fast as matter at the polar axis. Especially this last effect leads to a progressive flattening of the core. In comparison to a spherically symmetric configuration the collapse time scale is longer in rotating model.

iii) Core Oscillations

In contrast to spherically symmetric cores, which come to rest soon after boounce, the kinetic infall energy of a rotating core bouncing due to centrifugal forces will be converted into oscillations, which are damped by non-spherical pressure waves. Therefore, after bounce a rotating core will oscillate with a superposition of various axisymmetric radial and surface modes whose frequency is determined by the average density of the inner core. It is observed through simulations and analytical considerations that the radial oscillations will become layer and nonlinear, if the collapse is stopped just before nuclear matter densities are reached [125, 145].

iv) Convective Mixing

One dimensional simulations show that a negetive entropy gradient is established behind the shock after photo-disintegration losses have been weakened if significantly and this region of decreasing entropy is unstable against convection provided that the stabilizing lepton gradient is not too large [146]. Arnett [147] has first pointed out the possible importance of convection for type II supernova explosion but it is still debated whether convection indeed helps the propagation of the shock or not [148,149]. The important point is that for rotating cores mixing of high and low entropy matter may be enhanced, if convectional currents are supported by vortices resulting from rotation in regions, where deformed surfaces of constant pressure do not coinside with isopycnic surfaces. On the other hand, it has been argued that rotation may have a stabilizing effect on certain types of convective instability modes [134]. However, the interaction or rotation and convection for centrally condensed and differentially rotating objects is not yet fully understood.

v) Shock Propagation

The propagation of the shock wave is influenced by rotation because of several effects [136, 142, 150].

a) Rotation can lead to a bounce at low densities than in the non-rotating case, which means that the kinetic infall energy of the inner core and consequently the initial shock energy of rotating cores is reduced.

b) Rotation on the other side tends to enlarge the mass of the inner core, because it changes the velocity profile and stops the collapse before (due to electron captures) the mass of the inner core can shrink to values found for spherical models at bounce. Numerical results show that the mass of the inner core increases by roughly 10 - 20 % for initial values of $0.01 < \beta < 0.02$ (where β = the ratio of rotational energy to potential energy).

c) In the outer core the binding energy gained during collapse is transferred both into rotational and kinetic infall energy. According to the Virial theorem rotation acts like a $\gamma = 5/3$ gas [135]. It therefore helps to stabilize the shock heated matter in the gravitational potential

i.e., a large part of the dissicipated kinetic infall energy can support the expansion of the heated matter behind the shock front until equilibrium is reached at larger radii and at low potential energy. The resulting compressional work adds upoto the work of the expanding inner core and strengthens the shock.

d) Centrifugal forces considerably reduce the ram pressure of the supersonic flow in comparison to one dimensional model.

e) The asymmetry of the supersonic flow gives rise to an angular dependent propagation speed of the shock wave. This effect will be evident in the dissipation rates of kinetic energy and in the maximum entropy values obtained behind the shock front. Combined action of these effects will strengthen or weaken the propagation of the shock wave depending upon the amount and distribution of the angular momentum of the core.

vi) Tri-axial Instabilities

Due to conservation of angular momentum it cannot excluded that configurations may form during core collapse, which are unstable against triaxial deformations on secular or even dynamical time scales[134,138,139], if $\beta \geq 0.14$ and ≥ 0.27 respectively. Whether these instabilities indeed do occur is a nontrivial question : If the equation of state at sub-nuclear densities is stiff, i.e., if the adiabatic index is very close to 4/3, the core may be stabilized before its rotational energy exceeds the critical value $\gamma_{crit} = (2/3)\ (2 - 5B)\ /\ (1 - 2B)$ or

$$\beta_{crit} = (1/2)\ (4 - 3\gamma)\ /\ (5 - 3\gamma). \qquad (7)$$

If on the otherhand the intial amount of rotation is small enough for the collapse to proceed to nuclear densities, $\beta > 0.14$ may not be reached before bounce (see fig. 17).

7.2.2 Core Collapse

i) Core collapse with rotation : Shapiro and Lightman[137] first give the idea that the properties of the core at the end point of its collapse can be estimated without performing a detailed collapse calculation They used a Virial relation to determine global properties of rotating equilibria and examined these properties over a wide range of paramters

so that guide lines could be established for more detailed hydrodynamical simulations, which have to be restricted in parameter space. This approach was later extended by Tohline [138] and Eriguchi and Muller [139] (hereafter EM).

Following Tohline let us assume that the adiabatic index of a rotating core ($\beta = \beta_i$) in a stable equilibrium condition suddenly decreases to a certain value smaller than 4/3 due to electron capture processes and due to photo-disintegration of heavy nuclei. The equilibrium parameter F_{EM} defines a function $F_{EM}(\beta, \gamma)$ which is very useful for a qualitative description of rotational core collapse and can be written as (for details see ref. 135, 138, 139)

$$F_{EM} = (\alpha \beta^{4-3\gamma}) / (f_\alpha f_\beta^{4-3\gamma} f_M^{14-10\gamma} f_J^{6\gamma-8})$$

Where

$$\alpha \equiv \left| \frac{E_{th}}{E_{pot}} \right| = \frac{c^2 R}{GM} f_\alpha$$

$$\beta \equiv \left| \frac{E_{rot}}{E_{pot}} \right| = \frac{v^2 R}{GM} f_\beta \qquad (8)$$

f_α, f_β, f_M, f_J are dimensionless factors depending on the details of the structure of the rigidly and differentially rotating polytropes considered by Eriguchi and Muller.

c = the average sound speed in the core

v= the rotational velocity at the surface of the core

M, R are the spherical core mass and radius respectively. Eth, Erot, Epot are the thermal energy, rotational energy and gravitational potential energy of the core.

Fig. 16 shows the equilibrium parameter F_{EM} as a function of β for various values of the adiabatic index. We see from the fig.16 that the collapse must proceed along a horizontal line since F_{EM} is constant during collapse, if as assumed the mass and the total angular momentum of the core are conserved during collapse. It is immediately obvious that

there exists only one equilibrium state for $\gamma \geq 4/3$, because F_{EM} is a monotonic function of β in this case. For $\gamma < 4/3$, there exists two equilibrium states with the same mass and the same angular momentum, one of which is dynamically unstable, and the other of which is dynamically stable against radial modes (i.e. collapse). For a given adiabatic index the unstable (stable) equilibria correspond to all points to the left (right) of the maximum of F_{EM} (β) at $\beta = \beta_{max}$. So the drop in the adiabatic index can be envisaged by a shift down along a vertical line, i.e F_{EM} decreases with $\beta = \beta_i$ being constant. If β_i is smaller than β_{max}, the core is in an unstable equilibrium configuration with the same value of F_{EM} but with a different value of β, say β_f. Two constraints arise:

1) the first constraint has to do with the fact that stellar cores typically start collapsing from a density of a few times 10^9 g/cm^3, and that therefore a density change of a factor of 10^5 will lead to neutron star densities in the core. Consequently the basic assumption of γ being roughly constant and smaller than 4/3 is no longer valid, because the equation of state drastically stiffens ($\gamma > 2$) beyond nuclear matter density.

2) The second constraint follows from stability consideration. We know that MacLaurin spheroids are secularly and dynamically stable w.r.t. non-axisymmetric perturbations, with angular dependence $e^{im\phi}$ ($m = 2$) if β doesnot exceed a value of about 0.14 and 0.27, respectively [151]. If we consider differentially rotating ploytropes, the critical values of β change slightly [129, 152-154]. Later Imamura etal [155] and Managan [156] showed for instabilities caused by gravitational radiation reaction that in contrast to the m=2 bar mode, the secular stability limits for higher modes ($m > 2$) are quite sensitive to the compressibility and angular momentum distribution of the polytrope. They found that the critical values for higher modes ($m > 2$) decrease. Even in the presence of viscosity these gravitational radiation reaction modes are more strongly damped [157, 158].

Considering all the above discripansies, Eriguchi and Mullar[139] were able to predict that the fate of a collapsing, rotating core depends

on the initial state (denoted by γ) and the equation of state (denoted by) as shown in fig.17. Initial models in the upper right part of the diagram (above the upper hatched curve) cannot collapse at all, while for those situated below the lower hatched curve the increase in density will be more than a factor 10^5 during collapse. Thus only initial models with parameters between these two critical curves are able to reach a final equilibrium state, which is stable against radial modes (i.e., further collapse), and which has a density interm ediate to white dwarf and neutron star densities. The equilibrium states can be divided into three categories :

a) states which are secularly and dynamically stable against non-axisymmetric perturbations
b) states which are dynamically stable but secularly unstable against non-axisymmetric perturbations
c) states which are both dynamically and secularly unstable against non-axisymmetric perturbations.

Initial models belongs to the category (c) will probably fission, whereas initial models belongs to category (b) and probably to category (a) will become so called fizzlers [135] and collapse to neutron star densities on a secular time scale only.

ii) Hydrodynamical Simulations : Recently Monchmeyer and Mullar (hence after MM) [125, 136, 142, 145, 150] have performed an elaborate axisymmetric simulation. They performed four two dimensional numerical simulations of the hydrodynamical evolution of axisymmetrically collapsing rotating $1.36 M_\odot$ stellar iron core. They have taken into account

a) equation of state (EOS) data based on nuclear statistical equilibrium and Hartree-Fock calculations performed by Wolff [159] in the density regime $10^6 \text{ g/cm}^3 \leq \rho \leq 4 \times 10^{14} \text{ g/cm}^3$,
b) electron captures on free protons and neutrino captures on free neutrons
c) neutrino trapping at densities $\rho \gtrsim 3 \times 10^{11} \text{ g/cm}^3$,
d) local angular momentum conservation.

The hydrodynamical equations were solved using a conservative, explicit

numerical code of second order accurate differencing [160]. This code is an improved version of the numerical scheme of Rozyczka [161], Tscharnuter and Winkler [162].

Common to all modes of MM is the formation of a subsonically falling inner core during collapse. About 10 - 20 ms before bounce this inner core begins contracting rapidly, whereby it significantly flattens due to angular momentum conservation. At bounce the ratio of its polar to equatorial radius is roughly 1/2 in each model. The profile of the infall velocity is asymmetric during collapse, especially in the supersonic flow region. At bounce the ratio of the maximum polar infall velocity typically ranges from 1.8 to 2.5 , and the maximum compression of the inner core in polar direction occurs before the equatorial contraction is stopped completely. Model A of MM is a more slowly rotating model with $\beta_i = 0.005$. The bounce of model A is , therefore, dominated by the stiffness of the EOS beyond nuclear saturation density ($2.75 < \gamma < 3$). As a consequence most of the kinetic infall energy of the inner core is at bounce directly transfered to the shock within 0.3 ms, only. The average oscillation period of the inner core within an equilibrium central density of $2.6 \times 10^{14} g/cm^3$ is 2.5 ms. The stiffness of the EOS prevents large oscillation amplitude of the inner core. Despite a rather small initial shock energy of only 3.6×10^{51} erg the shock reaches a mass coordinate of ~ $1.3 M_\odot$ before it stalls, because of the stabilizing effect of rotation on the shocked matter. In contrast to one dimensional models a R-T instability develops behind the shock front (see fig.18) . However the evolution of a R-T instability due to a large negative entropy gradient behind the shock and the mixing of low with high entropy matter do not strengthen the shock [146].

Model B is decelerated by centrifugal forces over an initial of 5ms after the weak reaction rates have come into equilibrium in the centre of the core. Despite $\gamma \approx 1.35$ and a low compressibility of the matter (with an initial value of $\beta_i = 0.02$) the small amount of kinetic energy of the inner core doesnot allow for large amplitude oscillations after bounce, when a maximum central density of $2.6 \times 10^{13} g/cm^3$ is reached

[i.e., this model is a fizzeler . The high ram pressure of the infalling matter prevents a core expansion into polar direction. In the equatorial plane a weak shock reaches a distance of 250 Km. There it turns into an accretion shock, which eventually reaches the edge of the iron core. The small kinetic energy of the centrifugally decelerated matter in the equatorial plane causes a small entropuy production in the shock. Therefore, matter is not disintegrated and γ remains close to the value of 4/3. No explosion is found., Behind a rather weak shock front a secularly stable rotating equilibrium configuration is formed (see fig.19). The further secular evolutioni of this configuration, which occurs due to neutrino cooling on a time scale of the order 0.1s, has not yet been investigated.

The third model (model D of MM) with $\beta_i = 0.01$ is the intermediate to the above two discussed models and bounces at a central density of 1.5×10^{14} g/cm^3. Because of its relatively large gravitational and kinetic energy the inner core oscillates around its equilibrium density of 7×10^{13} g/cm^3 with large amplitudes (see fig.22). For roughly 8ms after bounce the inner core expands behind the shock with an average velocity around $1.0 - 1.5 \times 10^9$ cm/s. The polar and equatorial diameters of the inner core increase from 50km to 215 km and from 100km to 300km, respectively. Therefore, the kinetic infall energy of the inner core is only 1.6×10^{51} ergs. But due to the small adiabatic index of matter at sub-nuclear densities the inner core exerts compressional work on the surrounding shock heated matter and drives the shock outward. In this model the kinetic infall energy of the innercore is not directly transferred to the shock but powers a large scale post bounce expansion of the inner core, which pushes the shock like an expanding piston (see fig.20). The shock passes the $1.3 M_\odot$ mass shell already 5ms after bounce with a matter velocity of 1.6×10^9 cm./s. Afterwards, the shock is weakened due to neutrino losses [163] . The polar entropy blobs cool down, and a region of almost homogeneous specific entropy is produced behind the shock. A second contraction of the inner core sets in 228ms after the begins of the collapse. The resulting second bounce at 235ms leads to a

the formation of a 'jet' like flow pattern confined to a diameter of 250km around the axis. The jet propagates through the shock heated and disintegrated matter with velocities ~ 2 x 10^9cm/s. After a third bounce at 244ms the calculation was stopped and the mass sorrounded by the shock surface is 1.42 $M_\odot$ i.e. the shock reaches and even penetrates the silicon shell with a positive (radial) velocity indicating a weak explosion (fig.21).

7.2.3 Neutrino Heating and Nuclear Dissociation

When the shock stalls and ultimately recedes towards the centre of the star, the rate of neutrino heating for material behind the shock increases. This established a strong pressure gradient, which may be sufficient to overcome gravitational potential barrier and give rise to an outward acceleration and velocity. Bethe and Wilson[128] investigated the circumstances under which this can occur and they included (electron) neutrino absorption on free nucleous and neutrino-electron scattering [both charged and neutral current contributions . Domogatskii and Nadyozhin[164] and later Haxton[165] pointed out that the nuclear contribution comes primarily because of the participation of 'mu' and 'tau' neutrinos. However, as the matter behind the shock is heated by neutrinos coming from deep inside the core, its temperature rises and in turn, this leads to a radiation of neutrinos. Nuclei heated by neutrinos dissociate through reactions like $^{56}Fe \longrightarrow 13\,\alpha + 4\,n$ and $\alpha \longrightarrow 2\,p + 2\,n$. Thus neutrino emission depends on the progenitor star structure as well as how fast the shock moved out of the core. The evolution in effect breaks up into two phases:

a) the eraly phase lasting upto about ~ 500ms involves the collapse and compression of the outer mantle as it cools and undergoes neutronization.

b) the long term diffusion cooling phase of the inner core which lasts more than 10seconds.

During the early phase, the electron neutrino luminosity is ~ 10^{52}erg/s. In the diffusion cooling phase, the neutrino luminosity is ~ 10^{51} erg/s. Figs. 23 & 24 show the results of the delayed heating for two iron core

masses 1.37 $M_\odot$ and 1.33 $M_\odot$ with stellar masses 25 $M_\odot$ and 18 $M_\odot$, respectively. In fig.23a the fraction of alpha particles (X_α), neutrons (X_n) and proton (X p) for the star 25 $M_\odot$ plotted against time for the standard case with $L_{\nu_e} = 4 \times 10^{52}$ ergs/s. Core bounce is taken as the origin of time. By the time t = 0.417 s , iron is completely dissociated. Initially the dissociation of alpha particles is slow because the heat absorbed is small due to a small free nucleon fraction, as the total nucleon fraction becomes larger, heating increases fast and by t = 0.477s the alpha's dissociate completely. Fig.23a also gives the total entropy of the system as a function of time. Fig.23b represents the total internal energy $\mathcal{E}_{int}$ for the three values of luminosity L_{ν_e} = 2, 4,and 5 x 10^{52}ergs (solid lines) and compared the final values with the critical internal energy $\mathcal{E}_{cr}$ = G Mc /Rc = 14.1 (where Mc = 1.665 $M_\odot$ and Rc = 150 km) . It is also seen from the above figure that the position of the shock front changing with time. We also see that all three cases have enough energy for expulsion of matter, although with L_{ν_e} = 2 x 10^{52} ergs/s the energy inparted is barely above the critical value. The dependence of this internal energy on the luminosity is still strong but we find a substantial increase in its final vlue using the new heating rate [166]. Even the alpha particles take slightly more time in dissociating and rise in entropy is also some what less.

Fig.24 deals with the effect of the stalled shock for the 18 $M_\odot$. Fig.24a represents the baryon fraction X Fe, X_α , X n , and Xp as a function of time for $\dot{M}$ = 0.1 $M_\odot$ / s . Around t= 0.262 s, iron completely dissociate the alpha particles while Xn and Xp always stay lower than 0.15. The reason is that once the shock starts moving out again at t = 0.287 s some recombination takes place reducing Xn and Xp even further. The internal energy per nucleon for two cases with accretion rate $\dot{M}$ = 0.1 $M_\odot$ / s and $\dot{M}$ = 0 respectively are shown in fig. 24b. This alos shows the position of the shock as a function of time. We see that for both cases the maximum $\mathcal{E}_{int}$ is much less than the critical value $\mathcal{E}_{cr}$ of 8.7 MeV (where Mc = 1.64 $M_\odot$ and Rc = 240 Km). Not only

that even with the extra heating through the inelastic scattering of nuclei, the energy im parted is insufficient to revive the shock to go further into the phase II heating required to produce explosion. The alpha particles were only partially dissociated and the total internal energy always remained considerably below $\mathcal{E}_{cr}$.

Thus neutrino energy deposition plays a crucial role to restart the shock front and to power the final explosion of the star in the type II supernova event. Fig.25 shows a graphical summary and overview of physical events occuring in the centre of a massive star between the onset of core collapse and the formation of the young neutron star on the one side, and the start of the explosion and later ejection of the mantle and envelope of the star on the other side. This shows particular radial positions in the star's central region as they evolve in time. Time is measured in seconds from the beginning of core collapse. The evolution can be divided into the collapse phase, the phase of prompt shock propagation, the matter accretion phase and the protoneutron star cooling phase. The thick solid line (R Fe) marks the surface of the stellar iron core, while (Ric) indicates an inner part , which falls coherently (homologously). Initially this part grows as well in mass as in radius, containing the region where sound waves are able to communicate that the centre has started to collapse i.e. for $^{10}\log(t) < -1$ the line Ric marks the size of the subsonically collapsing inner part of the stellar core, at later times it encompasses the settled, compact inner region of the nascent neutron star. The maximum mass of this region is always close to the Chandrasekhar mass (~ 5.8 Ye^{2} $M_{\odot}$ ~ 1.2 ... 1.5 $M_{\odot}$, Ye being the electron concentration) determined by the average value of electron concentration Ye in the core. Since emission of electron neutrinos continously reduces Ye, there is a point when this inner part of the core will begin to shrink in mass. This Ric also seperates the subsonically infalling inner layers from the supersonically collapsing outer regio n. Therefore it gives the approximate position where the shock wave is formed at the core bounce. During collapse the neutrino emission is by far dominated by electron neutrinos, copiously produced

in electron captures ($e^- + p \longrightarrow \nu_e + n$) on free protons and nuclei. The region where most neutrino stem form is roughly indicated by the shaded area. It is bounded at the lower side by an inner zone where the high densities let the matter be opaque to neutrinos on collapse time scale (in general) . The transition region between neutrino opaque core or neutrino diffusion region and the neutrino transparent layers above is called " neutrino sphere" and marked by R_ν . In the outer region of the stellar iron core the neutrino emission becomes negligible, because of long capture time scale for electrons at low densities. The supernova shock is formed at core bounce, stagnates for several hundred milliseconds, and is revived by neutrino heating to propagate outwards into the stellar mantle with some time delay. The shock position as a function of time is marked by the line R sh. The corresponding variation of neutrino luminosities during the different phases of the evolution as discriminated in fig.25 is shown in fig.26. Right after formation the shock front propagates quickly outward, transforms into a standing accretion shock at about 100 - 200 km soon after it posses the neutrino sphere and an out burst of electron neutrinos (see fig. 2) from the hot matter behind the shock yields a significant energy sink and causes a pressure reduction in the shocked matter. Over time scales of several 10 to 100 milliseconds neutrino emission from post shock layers dominates and the burst phase is followed by a plateau phase in the neutrino luminosities. Different phases of neutrino emission are :

1) Collapse Phase --- During collapse the average lepton fraction in the inner 1 $M_\odot$ of the iron core drops from the initial value of 0.42 to about 0.36 - 0.38 at trapping . As the collapse proceeds, the luminosity increases steadily. From the onset of instability upto core bounce about (5 - 7) x 10^{55} electron neutrinos are set free, each of which carries away an energy of 6 - 10 MeV i.e. during the roughly 100 ms duration of this phase energy released less than 10^{51} erg which gives corresponding to an upper limit of 10^{52} erg/s of the luminosity.

2) Shock Breakout Phase —— This is the second significant phase. The

effective propagation peed of neutrinos is around 1/10 of the speed of light. During a short interval of 2 - 10 ms more than 10^{56} electrton neutrinos are emitted from captures of electrons onto free protons in the dissociated, shock heated material and on the average each electron neutrino leaves the star with 10 - 12 MeV. This ' neutronization burst' rediates away approximately 2 x 10^{51} ergs of energy with a peak luminosity of several times 10^{53} ergs/s upto nearly 10^{54} ergs/s . Only minor contributions to the emission stem from thermally produced neutrinos of all flavours during this time.

3) Accretion and Hot Mantle Cooling Phase ---- The decay from the above luminosity spike levels out into a plateau-like phase lasting for several hundred miliseconds. It is associated with the cooling of the hot (temperature between 4 - 10 MeV), shocked mantle material and the deleptonization of continuously accreted lepton rich matter. Thermal energy of about 1.5 x 10^{52} erg is emitted mainly in electron type neutrinos and anti neutrinos. However, local thermal production as well as slowly increasing diffusion fluxes from deeper inside the hot proto-neutron star add neutrinos of all other kinds (mu and tau neutrinos and antineutrinos)[119,149,167,168] . With cooling , and contraction of the surface layers of the newly born neutron star going on, diffusion fluxes of all kinds of neutrino leaking out from deeper regions start to dominate more and more.

4) Kelvin-Helmholtz Cooling Phase ---- This is where the transition to cooling phase of the protoneutron star is to be located. During this phase the newly born neutron star with a radius of 10 - 15 km looses most of its gravitational binding energies,

$$\Delta E \approx (3/5)\,(G M^2 / R) \sim 1.6 \times 10^{53}\,(M / M_\odot)^2\,(R / 10\ \mathrm{Km})^{-1}$$

ergs which is initially stored as internal energy in the degenerate lepton gases. More than 60 - 70 % of the 2 - 4 x 10^{53} ergs of energy release accompanying the birth of a neutron star [169,170]. Typicaly, starting of with luminosities of about 10^{52} ergs/s approximately 70% of the energy is rediated away within 5 seconds. Upto 90% after 10 seconds, being overtaken by the nearly complete deleptoniztion of the object [171] .

The luminosities are as small as several 10^{50} ergs/s.

The intermediate period of high neutrino luminosities must also be the time of shock revivbl [168]. If the neutrino energy deposition below the shock is sufficiently high, the post shock material starts to expand and develops positive velocities. This causes the end of the matter accretion onto newly formed neutron star and naturally shut down when the supernova explosion goes off. The protoneutron star deleptonizes cools, and shrinks in the quasi static Kelvin-Helmholtz phase, accompanied by roughly exponentially decaying neutrino luminosities, which are dominated by neutrinos diffusing out from successively deeper layers of the young remnant.

7.2.4 The Problem of Neutrino Transport

In the above , we see that neutrinos play important roles during all stages of the supernova and protoneutron star evpolution. They trigger core collapse and decide about the size of deleptonization and entropy generation, sink of energy during shock propagation and probably the key to successful explosions, cooling and , finally neutronization process -es leading to the cold neutron star remnant. Even the problem of nucleosynthesis in supernova explosions is affected by the huge flux of neutrinos traversing the stellar mantle and envelope [172-177].

The time evolution of the supernova neutrinos is divided into two stages : a dynamicl stage of core bounce and explosion and a quasi-static cooling stage of the proto-neutron star just born. So far many numerical simulations and various methods [178 - 210] have been used but still unsolved. Neither it is clear to which fraction the different neutrino species contributed to the release of the gravitational binding energy stored as internal energy in the collapsed stellar core nor is reliable and satisfactory information about spectral and temporal strucures of the neutrino luminosities available upto this moment.

a) Neutrino Spectra

The energetic distribution of neutrinos emitted from supernovae and protoneutron stars are important for the investigztion of neutrino

induced nucleosynthesis processes in the mantle and envelope layers of the exploding star. During the phase of the collapsed stellar core, where the matter is still rich of free protons besides of free neutrons, the nucleonic absorption process is the dominant contribution to transport opacity k_t (= $1/\lambda t$, λt the transport mean free path) and also to the opacity for energy exchange k_ϵ for electron neutrinos and antineutrinos. In the case of heavy lepton neutrinos as well as for electron antineutrinos during the later, neutronized stages of the post bounce evolution kt is determined by the convective scattering matter is governed by the scattering of charged leptons. This results in different transport properties of electron type neutrinos compared to muon and tauon neutrinos and in an increasing similarity of the behaviour of electron antineutrinos and heavy lepton neutrinos during the later stages of the protoneutron star cooling. Very roughly, neutrino opacities vary likely the square of the neutrino energy ϵ [i.e. $k \propto \epsilon^2$]. This quite strong energy dependence immediately implies that in general neutrinos will not be emitted from well defined surface but will decouple from the stellar gas within a radially extended region, where gradients of the state variables T, ρ, μ_e, etc are present., High energy neutrinos, having larger reaction cross sections, will interact with the stellar gas until far out in the star, while low energy neutrinos should decouple from the stellar surroundings deeper inside the star. This means that the emitted neutrino spectra will in genral not be thermal. Figs. 27 a - d show spectra of ν_e , $\bar{\nu}_e$, ν_x for the neutrino emission from a supernova at times between 10 and several hundred milliseconds after core bounce. The spectra computed with the Monte Carlo transport (solid lines) are compared with 'thermal' spectra [performed by Janka and Hillebrandt[211]]. The pinched shape of the real spectra relative to the thermal distributions (dashed linees) is clearly visible. Figs. 28 a - c give spectra for all types of neutrinos at three different times during the protoneutron star cooling phase (about 3.3, 5.8, and 7.8 seconds after core bounce)[212] . They also show the suppression in the high energy tails. In figs.27a - c the corresponding fits are shown by the dotted lines.

Of course, the neutrino temperature varies with time as the energies of the emitted neutrinos do and depends on the particular structure of the supernova model (density, temperature, etc) and on the phase of the supernova evolution. Also the suppression of the high energy tail of the spectra has consequences for the interpretation of supernova neutrino observations as well as for neutrino induced nucleo synthesis processes in the outer layers of the progenitor star. Therefore, neutrino luminosity and the average energy of the emitted neutrinos raise a question -- how does the neutrino-matter interaction differ, when the spectra have an effective degeneracy instead of being blackbody spectra ?

During the phase of matter accretion, lasting for several hundred milliseconds after core bounce, material is falling through the standing accretion shock. Initially cooling processes dominate in this material, which radiates away its gravitational binding energy by neutrinos, and settles onto the protoneutron star. As the neutron star becomes more and more compact and the accretion rate shrinks with the decreasing density of the infalling layers of the progenitor star, there is a moment, when net heating by neutrino energy deposition must win against neutrino cooling. In this context the most important neutrino processes in the hot, dissociated post shock material during the accretion phase, electron / positron absorption on protons/neutrons and the inverse reactions are :

$$e^- + p \longleftrightarrow \nu_e + n \; ; \qquad e^+ + n \longleftrightarrow \bar{\nu}_e + p \qquad (9)$$

This processes ultimately give a net energy deposition in the region close to the newly formed neutron star which is unavoidable.

As an alternative source of energy transfer to the stellar gas around the protoneutron star Tubbs and Schramm [213] suggested neutrino-electron/positron scattering.

$$\nu + \begin{Bmatrix} e^- \\ e^+ \end{Bmatrix} \longleftrightarrow \nu + \begin{Bmatrix} e^- \\ e^+ \end{Bmatrix} \qquad (10)$$

In this process energy deposition becomes important only when the

density gets low ; the gas temperature stays around or above 0.5 MeV. Here Goodman etal [129, 212] claimed the importance of neutrino pair annihilation

$$\nu + \bar{\nu} \longrightarrow e^- + e^+ \qquad (11)$$

in the close vacinity of the young neutron star, just outside of the neutrino sphere. The detailed calculations [213 - 215], however, give the previous result i.e. the total energy transfer to the stellar gas is given as sum of the contributions for all flavours of neutrino. Even the careful analysis of the heating using Monte Carlo results of neutrino transport in protoneutron stars [215] could not confirm the proposal given by Goodman [129]. So it remains contraversial whether reaction (11) is really relevant. But it is ascertain that the inverse reaction, electron-positron annihilation into neutrino/antineutrino paris, however, takes part in the cooling of the hot material near the neutron star surface.

b) Numerical Simulations

In the above discussion it is understood that absorption of electron neutrinos and antineutrinos can deposit enough energy in the matter between protoneutron star and stalled shock to slow down the infall of the post shock material and to drive the shock outwards. Bethe and Wilson [128] suggested that a 'hot buble' (a region of low density, but temperatures above and around 0.5 MeV), starts to form and expands. The energy transfered to the stellar material in that buble region during the subsequent evolution will decide about the final energy of the supernova explosion. The detailed study [216] of the cooling time of the protoneutron star (together with contributions by the other heating reactions like neutrino electron/positron scattering) [using hot buble], suggests that explosion energy of the order of several 10^{50} ergs, which is quite close to typical energies of type II supernova events of 1 - 2 x 10^{51} ergs. But it doesnot tell anything about how much of the deposited energy will finally endup as

kinetic energy of the explosion. It is crucial to know it.

In order to clearify this, Janka and Muller [217,218] performed numerical studies of the neutrino heating phase after core bounce. Fig. 29 shows the radial positions of selected mass shells in the star as functions of time during the first second and the first three seconds respectively, of the evolution. In the lower parts of the figure the protoneutron star is located. It is also seen that it is loosing its gravitational binding energies of 2.7×10^{53} erg by radiating neutrinos with an exponentially decaying luminosity on a time scale of about 45 seconds. A part of this energy is deposited in the sorrounding gas and driving a rapid expansion, which leads to a clear separation of the neutron star from the stellar mantle far out. On a time scale of about 100 - 200 ms (beginning at about 0.075 seconds after the start of simulation) an energy of 1.5×10^{52} erg (a fraction of just 5% of the gravitational energy lost by the protoneutron star, thus unobservable in SN 1987A) is radiated away by neutrinos ν_e, $\bar{\nu}_e$, ν_x ($x \equiv \mu, \bar{\mu}, \tau, \bar{\tau}$) of average energies around 25 - 30 MeV i.e. it needs a high thermal neutrino pulse. Colgate etal [219] have suggested that such kind of thermal neutrino pulse might originate from aspherical accretion flows onto the protoneutron star . This causes strong neutrino heating on time scales of the order of the sound crossing time through the buble region (i.e. $\tau \sim 0.1$ s). Since the energy deposition happens on a dynamical time scale, the matter in the hot buble region is not radiation dominated, and thus the temperature in the buble region can reach higher values, which leads to a powerful supernova explosion with an energy of 1.33×10^{51} erg (comparable with $1.2 - 1.6 \times 10^{51}$ erg for SN 1987A) [220] . It is obvious that neutrino driven supernova explosion takes place. But to work, one needs a violent, efficient neutrino heating phase within about one second after core bounce. So the question naturally comes --- which physical mechanism (s) can yield that ? Recent investigtions [221-223] suggest that it is due to convection process inside the protoneutron star and/or between the protoneutron star and the shock. Convection may yield an

efficient mechanism for energy transfer and imply significant enhancement of the neutrino emission from the neutron star or from matter accreted onto the newly born neutron star.

c) Convection in and around the pro-neutron star

In the 'hot buble' model the rapid expansion of the material between the shock (at about 2000km) and protoneutron star (with a radius of roughly 25km) has produced a nearly isentropic buble region between about 150 km and the shock with a nearly negative entropy gradient. The inner part of this region is slightly unstable against convection and indeed some mixing takes. Fig.30 shows the electron concentration Ye in a region of 376 km radial extension at 193 ms after the start of the computation. Since difference in the lepton concentration are very small initially, the Rayleigh-Taylor instabilities comprise variations of Ye between 0.475 and 0.485 only. Figs. 31 and 32 show the convection in a protoneutron star some ten milliseconds after core bounce and time evolution of the electron, respectively, and the entropy in a region between 20km and roughly 220 km at four different times 16 ms, 21 ms, 26 ms, and 31 ms after the start of the 2 - D simulation. In fig.32 one can clearly see how first the inner layer becomes unstable and develop R-T fingers penetrating inward. A little later zones with negative entropy gradients farther out begin to break up, too, while the structures deeper inside merge to successively larger blobs. After another 10 ms the inner region is completely mixed and homogenized. The convective velocities are near and beyond the local speed of sound, therefore significant overshooting at the outer and inner boundaries of the initially unstable regions occurs. These convective processes behind the supernova shock cannot prevent the failure of the prompt explosion mechanism, although the shock gets an additional boost, which helps to bring it out to larger radii (see fig.32). Because pressure waves are generated by the turbulent motions and catch up with the shock, during it faster out. Since leptons are removed from deeper layers, the pressure is reduced

there, and the inner region below about 60 km settles and becomes more compact. The corresponding release of gravitational binding energy leads to an explosion of the out layers and supplies the shock with new energy. The gain in energy from both effects, however, is moderate [168] and by it self will not convert a failed explosion into a successful one. So further investigation needs by including

i) neutrino transport in subsequent simulations

ii) how enhancement of the neutrino losses will influence the shock propagation on one side and the neutron star formation otherside.

8. FORMATION OF NEUTRON STAR THROUGH WHITE DWARFS

This the second route for the formation of neutron stars through white dwarf. In this route there are three possible scenarios. The important one is accretion induced collapse of a white dwarf in a binary. The other two scenarios are

i) the collapse of a white dwarf more massive then the Chandrasekhar limit [225,226] and

ii) Coalescence of an extremely tight binary consisting of two white dwarfs.

But these two scenarios are very rare. So we shall deal with the scenario accretion induced collapse.

8.1 Accretion Induced Collapse

The possibility that accretion at certain rates onto a white white dwarf may lead directly to neutron star formation has been studied by many groups [227-232]. It is found that only possible model for the white dwarf collapse are :

i) C+O white dwarf (in which carbon and oxygen may or may not have chemically seperated)

ii) O+Ne+Mg white dwarf

For a wide range of mass accretion rates and initial white dwarf masses, the O+Ne+Mg white dwarfs collapse due to electron capture on ^{24}Mg and ^{20}Ne . On the other hand, the C+O white dwarfs could either explode or collapse depending on the conditions of the white

dwarfs and binary systems in which they are formed [233, 234]. Therefore, chemical separation in such objects is crucial. This is still hypothetical an in any case could not be complete before Carbon burning starts [235]. Now we shall see how degenerate C+O and O-Ne-Mg cores arise from stellar evolution.

Depending on mass M, the stellar evolution can be classified as follows : [236]

a) for $M < 0.08\ M_\odot$, the star will become a planet like black dwarf without igniting hydrogen burning

b) for $0.08\ M_\odot < M < 0.45\ M_\odot$, the star will endup as a helium white dwarf, though such a single star has not evolved off the main sequence in a Hubble time.

c) For $0.45\ M_\odot < M < 8\ M_\odot$ the star forms a C+O core of mass smaller than $1.06\ M_\odot$, which then become strongly degenerate. Most of them will become a C+O white dwarf by losing their hydrogen rich envelope but some of them ($\sim 6 - 8\ M_\odot$) could reach a supernova stage by increasing the C+O core mass to the Chandrasekhar mass and ignites a carbon deflagration .

d) for $8\ M_\odot < M < 10\ M_\odot$: The star forms an O+Ne+Mg core. The core mass is smaller than $1.37\ M_\odot$ and becomes a strongly degenerate.

e) for $10\ M_\odot < M < 13\ M_\odot$, neon is ginited in a semi-degenerate O+Ne+Mg core. Whether subsequent evolution leads to a non-degenerate configuration depends on the neutronization during oxygen burning and crucial for the final fate.

f) for $M > 13\ M_\odot$: The star undergoes non-degenerate burning to form an iron core.

8.1.1 Accreting of degenerate C+O core

The ultimate fate of accreting C+O white dwarfs depends on $\dot{M}$, the growth rate of the C+O white dwarf mass, and the initial mass of the white dwarf Mco. The detailed evolution of the C+O white dwarfs has been studied by Nomoto and Iben [237] , Kawai etal [238]

, Saio and Nomoto [239] , Woosley etal [240] . They found that for $\dot{M} > 2.7 \times 10^{-6} M_{\odot}$ / year, center carbon burning is ignited by rapid compressional heating. Though this off centre carbon burning the C+O white dwarf is peacefully changed into an O+Ne+Mg white dwarf. The resulting O+Ne+Mg white dwarf will collapse to form a neutron star due to electron capture on ^{24}Mg and ^{20}Ne, if the Chandrasekhar mass is reached (see fig. 33a).

For a relatively high accretion rates ($2.7 \times 10^{-6} M_{\odot}$ / yr $> \dot{M} > 4 \times 10^{-8} M_{\odot}$ / year) a carbon deflagration starts in the white dwarf's centre at low density $\rho_c \sim 3 \times 10^9$ g/cm^3 [241,242]. The convective deflagration wave then propagates outward at a subsonic velocity. Recently Timmes etal [243] and Woosley [244] have examined the details of flame propagation, the dynamics of the collapse and the first second of the neutron star's life and found that a critical central density at nuclear ignition which is about 6×10^9 g/cm^3 for C+O dwarfs. For larger densities, electron capture behind the flame leads to its stabilization aginst R-T modes. There are two scenarios arise in which a carbon deflagration is initiated in the center when the central density is as high as 10^{10} g/cm^3. i) At such densities, the carbon deflagration may not lead to an explosion since electron capture is much faster at these high densities than at the lower densities encountered in the models of SNIa. ii) if the central part of the white dwarf is in the solid state, the propagation mode of the burning front could be different. If the solid is strong enough, convection will be suppressed and the burning front will propagate as a conductive deflagration wave [227,245] . Even for fluid layers, conductive deflagration could dominate convective deflagration in the central region [246] . Even for solid core, propagation of the deflagration wave is not necessarily due to conduction alone since convection could influence the melting of the solid core [247] . However, if the propagation velocity of a conductive deflagration wave is low (high) enough and /or the central density is high (low) enough, a carbon deflagration will lead to

collapse (explosion) . So the outcome is rather sensitive to the propagation velocity and the central density . More study is needed in this point.

8.1.2 Collapse of O+Ne+Mg White dwarf

The star in the mass range 8 - 10 $M_\odot$ undergoes non-degenerate carbon burning and forms an O-Ne-Mg core. The advance of the carbon burning shell stops near the helium burning shell at Mr = 1.28 $M_\odot$ (M_α = 2.2 $M_\odot$) and 1.34 $M_\odot$ (M_α = 2.4 $M_\odot$) [248] . Hence the oxygen-Neon core mass does not exceed the critical mass of 1.37 $M_\odot$ and , therefore, neon is never ignited. After attaining the maximum temperature, which is far below the ignition temperature of Ne, core temperature Tc decreases due to neutrino emission. Afterwards, the core becomes strongly degenerate. If the core mass stays constant (~ 1.3 $M_\odot$) , the degenerate core will simply continue to cool like a white dwarf. In a red giant, the core mass interior to the helium burning shell grows because hydrogen and helium shell burning processes the material of the He rich envelope into carbon-oxygen. When the core mass grows to 1.38 $M_\odot$, core density ρ_c reaches 4 x 10^9 g/cm^3 i.e. the electron captures ^{24}Mg, ^{24}Na, ^{24}Ne, and later for ^{20}Na, ^{20}F, ^{20}O . Electron captures produce entropy by distorting the Fermi distribution function and emitting gamma rays [249, 250] . This electron captures occur only in the nuclear statistical equilibrium (NSE) layer behind the burning front and, therefore, the region of small Ye is confined to a central region which grows gradually. But the O-Ne-Mg core contains nuclear fuel which ignites during infall. It is found that heating due to $^{24}Na\ (e^-, \nu)\ ^{24}Ne$ is slower than the plasmon neutrino cooling but electron capture on Ne and ^{20}F leads to the ignition of oxygen at ρ_c ~ 10^{10} g/cm^3 [234, 251, 252] . However, this oxygen deflagration does not lead to explosion because the decrease in Ye due to electron capture behind the burning front is fast enough to induce collapse.

Hillebrandt etal [253] found that this collapse is slower than the collapse of the iron core of a massive star until the burning front has propagated to roughly ~ 8 $M_\odot$. Afterwards, the collapse accelerates quickly. As Ye in the NSE region of the O+Ne+Mg core is smaller than in iron core, the entropy at the burning front is higher and thus proton fraction is larger. These two effects result in a homologous core whose mass is smaller and an outer infalling layer which is less dense than that in iron core collapse. These produces two effects on the bounce shock : a) the binding energy of the rebouncing core is smaller and , hence, the shock wave is weaker [254, 255] b) the low density in the outer layers makes the shock propagation easier. However, the outcome of the accretion induced collapse for a O+Ne+Mg core depends on the initial mass of the white dwarf and explosion energy which are still uncertain. In many cases it is found that mass of the O-Ne-Mg core is very close to the Chandrasekhar mass i.e. only a small mass increase is enough to trigger collapse [236] . Recentl examination on the details of flame propagation determines a critical central density at nuclear ignition, 8×10^9 g/cm^3 for a O-Ne_Mg core , above which collapse to a neutron star is likely.

9. CONCLUSION

Type II supernova events is thought to be a consequence of the gravitational collapse of the central region of massive evolved star after elements of the iron group have been produced there in a sequence of successive nuclear burning phases. The collapse of the roughly 1.4 $M_\odot$ iron core, giving rise to the ejection of the star's mantle and envelope in a supernova explosion of type II and to the birth of a neutron star or blackhole; associated with the emission of huge amounts of energy in form of neutrinos. Neutrinos obviously play an important role during all stages of the Supernova and protoneutron star evolution. In particular, trigger core collapse, decide about the size of deleptonization, energy generation, sink of energy during shock propagation

etc.

In our above discussion we see that there are several phases with clear distinct neutrino emission such as core collapse , prompt shock propagation and shock break out, matter accretion onto the nascent neutron star, Kelvin-Helmholtz cooling of the protoneutron star, etc. So, neutrinos certainly may open an important and useful windows to observe the physics happening deep inside the supernova core and to learn about the mechanism which leads to the explosion of the star , and formation of neutron star. This needs a thorough study iin the following areas :

i) the exact reason of the failure of the prompt shock mechanism to explode type II supernovae. Although several numerical description of the hydrodynamics have been performed, but still it is unknown. Possibly, there must have another physical reasons.

ii) The success or failure of the core bounce / prompt shock mechanism depends on the position where the shock is formed and on the energetics of the shock wave. As the position of shock formation and the energy balance of the shock both are intrinsically coupled, this needs a detailed hydrodynamical evolution and numerical simulation during collapse, bounce and shock creation.

iii) The currently most promising model to explain the explosion of massive stars in type II supernovae is the "delayed mechanism" by neutrino heating particularly, hot buble model. Neutrino transport in the supernova context, which is dependence on the energy of the propagating particle is vital i.e. a suitable description of neutrino transport (see fig.33)

iv) How and to which extent does the use of flux-limiting techniques affect the neutrino transpoft and what are the consequenecs for the picture of core collapse, shock propagation and proto neutron star cooling ?

v) Which influence on the transport and emission of neutrino does

neutrino-electron scattering have ?

vi) To which extent does a thorough description of neutrino transfer in the semitransparent outer layer of the newly formed hot protoneutron star change the neutrino heating that acts as the source of energy for the late time shock revival ?

vii) Which spectral (and temporal) signature does the neutrino emission from supernovae and hot protoneutron stars have and what are the implications for theevlution and interpretation of detections of neutrinos from stellar core collapse events ?

viii) More investigtion on the large scale aspherical accretion flows down to the protoneutron star which may yield another source of high energy neutrinos during convection phase.

ix) Role of magnetic field during or after the collapse .

ACKNOWLEDGEMENT

The author is grateful to Prof. A. Salam, Director, ICTP, Trieste for his kind hospitality where a part of this work has been carried out. He is also grateful to Prof. J. V. Narlikar, Director, IUCAA, for his kind hospitality which helps to complete it. He is greatly indebated to Dr. H.-Th. Janka, Petra Berkemeyer, Max Planck Institute for Astrophysics, Garching , Germany, Dr. Bhavani Srinivashan, World Scientific, Bangalore, all the library staff of IUCAA for their kind help for providing the required preprints/reprints, journals for this work. Thanks are due to staff, Computer section, IUCAA, Mrs. Tapati Parui for their help in various stages during the preparation of this paper. Lastly, the author wish to thank Prof. H. N. K. Sarma, Head, Dept. of Physics, Prof. P.S. Mazumdar, of Manipur University, staff, National Airports Authority, ACS, Imphal Airport, for their continuous encouragement.

REFERENCES

1. H.A. Bethe, G.E. Brown, J. Applegate and J.M. Lattimer, Nucl. Phys. A 324 , 847 (1979)
2. R. I. Epstein and C. J. Pethick, Astrophys. J. 243, 1003 (1981)
3. D. Z. Freedman, D.N. Schramm, D. L. Tubbs, Ann. Rev. Nucl. Sci. 27, 167 (1977)
4. J. R. Bond, Ph.D. Thesis, California Inst. Tech. CA. USA (1978)
5. J. Cooperstein, Phya. Reports. 163, 95 (1988)
6. J. Cooperstein, E. W. Baron, in Supernovae, eds. H. G. Petschek, (Springer, NY, 1990) p 213
7. A. S. Barrows, in ref. 6 pp 143
8. H. A. Bethe, Rev. Mod. Phys. 62 , 801 (1990)
9. K. Hirata etal, Phys. Rev. Lett. 58, 1490 (1987)
10. R. M. Bionta etal, Phys. Rev. Lett. 58, 1494 (1987)
11. A. Barrows, Ann. Rev. Nucl. Part. Sci. 40, 181 (1990)
12. A. Barrows and J. M. Lattimer, Astrophys. J. 307, 178 (1986)
13. T. Takatsuka, in The Structure and Evolution of Neutron Star eds. D. Pines etal.(Addison Wiley, NY, 1992) pp 257, 8
14. S. W. Bruenn and W. C. Haxton, Astrophys. J. 376, 678 (1991)
15. S. Chandrasekhar, An Introduction to the study of stellar structure (Dover, USA, 1939)
16. T. Kanjilal and K. Basu, Indian J. Phys. 65B, 299 (1991)
17. J. Audouze and S. Vonclair, Introduction to Nucl. Astrophys. (D. Riedel, Holland, 1980) pp 28
18. H. Goldberg and M. D. Scadron, Phys. Stellar Evolution and cosmology (Gordon and Breach, USA, 1981)
19. S. E. Woosley, in Nucleosynthesis and Chemical Evolution eds. B. Hauck, etal (Saas, Fee Courses, Geneva, 1986) pp1
20. S. Miyaj and K. Nomoto, Astrophys. J. 318, 307 (1987)
21. S. E. Woosley, in Supernovae, ref. 6 pp 182
22. J. Isern, R. Canal and J. Labay, Astrophys. J. Lett. (1991) Preprint
23. R. Canal, J. Isern and J. Labay, in Proc. 6th workshop on Nucl. Astrophys., eds. W. Hillebrandt and E. Mullar (Max Planck Institute, Germany, MPA/P5 , 1991) pp 88
24. M. Takahara etal, Nucl. Phys. A504, 167 (1989)
25. E. E. Salpeter, Astrophys. J. 115, 326 (1952)
26. E. E. Salpeter, Ann. Rev. Nucl. Sci. 2, 41 (1953)

27. E. J. Opik, Proc. Roy. Irish Acad. A54, 49 (1951)

28. E. J. Opik, Mem. Socy. Roy. Sci. Liege, 14, 131 (1954)

29. F. Hoyle and M. Schwarzschild, Astrophys. J. Suppl. 2, 1 (1955)

30. F. Kappeler, H. Beer, K. Wisshak, Rep. Prog. Phys. 52, 945 (1989)

31. J. Audouze and V. Vonclair, in ref 17, chapter Nucleosynthesis

32. H. Bethe, in Essays in Nucl. Astrophys. eds.: C. A. Barnes etal (Cambridge Univ. Press, UK, 1982) pp 439 - 66

33. C. A. vonWeizscher, Z. Phys. 39, 633 (1938)

34. J. L. Greenstein, Mod. Phys. for Engineers, (Mac Graw Hill, NY, 1954) pp 267

35. A. G. W. Cameron, Phys. Rev. 93, 932 (1954)

36. A. G. W. Cameron, Astron. J. 65, 485 (1960)

37. W. A. Fowler, G. R. Burbidge, E. M. Burbidge, Astrophys. J. 122, 271 (1955)

38. G. R. Burbidge, E. M. Burbidge, W. A. Fowler and F. Hoyle, 29, 547 (19570

39. J. Audouze and V. vonclair, in ref 17, pp28

40. H. W. Drotlett etal, in Proc. 5th Int. Symp. Nucl. Astrophys. MPA/4 (Max Planck Institute, Garching, 1990) pp 181

41. K. Wolke etal, Z. Phys. A334, 491 (1989)

42. H. W. Drotlett etal, in ref 23, pp 23

43. T. R. Wang etal, hys. Rev. C43, (1991) Preprint

44. R. K. Parui, Indian J. Phys. 67B, 109 (1993)

45. J. V. Narlikar, The Structure of the Universe (Oxford Univ. Press, Oxford, 1977) pp 46 -48

46. G. J. Mathews and R. A Ward, Rep. Prog. Phys. 48, 1371 (1985)

47. J. P. Arcoragi etal, Max Planck Institute Preprint 559, (1990)

48. W. D. Arnett and F. K. Thielemann, Astrophys. J. 295, 589 (1985)

49. Z. Y. Bao and F. Kappeler, At Data Nucl. Data Tables 36, 411 (1987)

50. G. Meynet, Proc. 5th Int. Workshop on Nucl. Astrophys. MPA/P1, eds: W. Hillebrandt and E. Muller (Max Planck Institute, Garching, 1991) pp 83

51. K. Nomoto and M. Hashimoto, Phys. Report, 163, 13 (1988)

52. K. Nomoto, T. Shigeyama, S. Kumagai, H. Yamaoka and T. Suzuki, Max Planck Institute Preprint No 602 (1991)

53. N. Prantzos, M. Arnold, M. Casse, Astrophys. J. Lett. 331, L15

--- (1988)

54. J. Wheeler, R.P. Harkness, Rep. Prog. Phys. 53, 1467 (1990)

55. H. P. Harkness and J. Wheeler, in ref 6, pp 1

56. A. V. Filipenko, in I. J. Danziger and K. Kjaer eds, Supernovae 1987A and other Supernovae, ESO, Garching , 343 (1991)

57. A. Clocchiatti and J. Wheeler , in preparation (1994)

58. L. M. Ensman and S. E. Woosley, Astrophys. J. 333, 754 (1988)

59. D. A. Swartz, J. C. Wheeler, Astrophys. J. 379, L 13 (1991)

60. S. D. VanDyk, R. A. Sramek, K. W. Weiler, N. Panagia, Astrophys. J. 409, 162 (1993)

61. J. C. Wheeler and D. A Swartz, The Evolution of massive stars to Explosion, Univ. of Texas at Austin Preprint No 245 (1993)

62. T. Shigeyama, K. Nomoto, T. Tsujimoto and M.A. Hashimoto, Astrophys. J. 361, L 23 (1990)

63. D. A. Swartz, A. Clocchiatti, R. Benjamin, D. F. Lester, J. C. Wheeler, Nature 365, 232 (1993)

64. D. A. Swartz, Astrophys. J. (Preprint) (1993)

65. S. E. Woosley, N. Langer, T. A. Weaver, Astrophys. J. 411, 823 --- (1993)

66. D. Bhattacharya, E.P.J. vanden Heuvel, Phys. Report, 203,1 (1991)

67. R. A. Mutter etal, Astrophys. J. 384, 29 (1992)

68. H. Yamaoka, T. Shigeyama, K. Nomoto, Astron. Astrophys. (1993) in press

69. R. W. Romani, Astrophys. J. 399,621 (1992)

70. B. Doggett and D. Branch, Astrophys. J. 90, 2303(1985)

71. R. P. Kirshner, in ref 6, pp 59

72. S. W. Falk and W. D. Arnett, Astrophys. J. Suppl. 33, 515 (1977)

73. I. Yu. Litvinova and D. K. Nadyozhin, Astrophys. Space Sci. 89 , 89 (1983)

74. M. Hashimoto, K. Iwamoto and K. Nomoto, Astrophys. J. 414, L105

75. B. P. Schmidt etal, Astron. J. 105, 2236 (1993)

76. F. Patat, R. Barbon, E. Cappelloro, M. Turatto, Astron. Astrophys. (1993) Preprint.

77. D. A. Swartz, J.C. Wheeler, R. P. Harkness, Astrophys. J. 374, 266 (1991)

78. J. C. Wheeler, A.V.Filippenko, in R.A.McCray & Z.Wang eds. Supernovae and supernovae remnants, (Cambridge Univ. Press. UK,

1994) in press

79. S.I.Blinnikov and O.S.Bartunov, Astron. Astrophys. 273, 106 --- (1993)
80. S.E.Woosley, N. Langer, T.A.Weaver, Astrophys. J. 411, 823 (1993) ---
81. J. Audouze and S.vonclair, in ref 17, pp 62
82. S.E.Woosley and T.Weaver, Ann.Rev.Astron. Astrophys. 24, 205 (1986)
83. F. K.Thielemann, M.Hashimoto, K.Nomoto, Astrophys. J. 348, 222 --- (1990)
84. S.E.Woosley, in Proc. of the Structure and Evolution of Neutron Star, eds: D. Pines etal (Addison Wiley, USA, 1992) pp 241
85. S.E.Woosley, N.Langer, T.Weaver, Astrophys.J.(1991) Preprint
86. S.E.Woosley, T.A.Weaver, in Les Houches, Session LIV: Supernovae, eds: J.Audouze etal (Elsevier, North Holland, 1991)
87. T.A Weaver, S.E.Woosley, B.A.A.S., 23, No 2, 975 (1991) --
88. T.A.Weaver, S.E.Woosley, Astrophys.J. (1992) preprint
89. S.E.Woosley, T.A.Weaver, Phys. Reports. 163, 79 (1988) ---
90. G.A.Caughlan, W.A.Fowler, Atomic Data and Nucl. Data Tables 40, 238 (1988) --
91. Z.Barkat, A.Marom, in Supernovae, vol 6 of the Jerusalem Winter School for Theor. Phys., eds: J. Wheeler etal (World Scientific, Singapore, 1990) pp 95
92. W.D.Arnett, Astrophys. J. 319, 136 (1987) ---
93. E. Muller, B.A.Fryxell, W.D.Arnett, in Proc. of the ESO/EIPC Workshop SN1987A and other Supernovae, eds: I.J.Danziger etal (ESO, Garching, 1991)
94. K.Nomoto, T.Shigeyama, S.Kumagai and M.Hashimoto, Proc. Astron. Socy. Australia 7 , 490 (1988) -
95. M.Hashimoto, K.Nomoto, T.Shigeyama, Astron.Astrophys 210, L5 (1989) ---
96. F.K.Thielemann, in ref 86 (1991)
97. K.Nomoto etal, in ref 52 pp 15
98. T.Shigeyama, K. Nomoto, Astrophys. J. 360, 242 (1990) ---
99. S.Kumagai, M.Itoh, T.Shigeyama, K.Nomoto, J.Nishimura, S.Tsuruta, Astrophys. J. 345, 412 (1989) ---
100. T.Ebisuzaki, T.Shigeyama, K.Nomoto, Astrophys. J. Lett. 344, L 65 (1989) ---
101. T.Shigeyama, Astrophys. J. Lett. 358. L57 (1990)
102. M.Den, T. Yoshida, Y.Yamada, Prog. Theor. Phys, 83, 723 (1990)
103. W.D.Arnett, A Fu, Astrophys. J. 340, 396 (1989) ---

04. W.D.Arnett, B.A.Fryxel, E.Muller, Astrophys. J. 341, 163 (1989)

05. W.D.Arnett, J.N.Bahacall, R. Kirshner, S.E.Woosley, Ann. Rev. Astron. Astrophys. 27, 629 (1989)

06. Y.Yamada, T.Nakamura, K.Oahara, Prog. Theor. Phys. 84, 436(1990)

07. M.Herant, W.Benz, Astrophys. J. 370, L81 (1991)

08. I. Hachisu, T.Matsuda, K.Nomoto, and T.Śhigeyama, Astrophys.J. (1991) Preprint

09.K.Nomoto, T.Shigeyama, S.Kumagai, H.Yamaoka, in Supernovae, eds:S.E. Woosley (Springer, Berlin, 1991) p 176

10.---------, in Supernovae and stellar evolution, eds: A.Roy & T.Velusamy (World Scientific, Singapore, 1991)

11.J.Cooperstein, in Supernovae and Stellar Evolution, eds: A.Roy and T. Velusamy (World Scientific, Singapore, 1991)

12.J.Cooperstein, A.Borons, in ref 6 p 213

13.R.L.Bowers and J.R.Wilson, Astrophys. J. 263, 366 (1982)

14.S.W.Bruenn, Astrophys. J. Suppl. 62, 331 (1986)

15.-------- , Astrophys. J. 311, L69 (1986)

16. ------- , Astrophys. J. 340, 955 (1989)

17. ------- , Astrophys. J. 341, 385 (1989)

18. A.Burrows, J.M.Lattimer, Astrophys. J. 299, L19 (1985)

19.R.W.Mayle, Ph.D. Thesis, University of California, Berkeley, UCRL report no: 53713 (1985)

20.R.W.Mayle, J.R.Wilson, D.N.Schramm, Astrophys.J. 318, 288 (1987)

21.W.Hillebrandt, in High Energy Phenomena around collapsed stars, eds: F.Pacini, NATO ASI C195 (D.Reidel, Dordrecht, 1987) p 73

22.J.R.Wilson, R.W.Mayle, S.E.Woosley, T.Weaver, Ann. NY.Acad.Sci,USA 470, 267 (1986)

23.E.S.Myra, J.M.Lattimer, A.Yahil, in Supernovae 1987A in the Large Magellanic Cloud, eds: M.Kafatos and A.Michalitsianos (Cambbridge Univ. Press, UK, 1988) p 213

24.E.S.Myra, and S.A. Bludmann, Astrophys.J. 340, 384 (1989)

125. R. Monchmeyer, Ph.D. Thesis, TU Munchen, Germany (1990)

126. S.A. Colgate, R.H.White, Astrophys.J. 143, 626 (1966)

127. J.R.Wilson, in Proc. Univ. Illinois Meeting on Numerical Astrophys. (1982)

128. H.A.Bethe, J.R.Wilson, Astrophys. J. 295, 14 (1985)

129. J. Goodman, A. Dar, S.Nussinov, Astrophys. J. 314, L 7 (1987)

130. J.R.Wilson, R.W.Mayle, M.G.Talk Australia, Aug'88 (1988)

131. R.W.Mayle, J.R.Wilson, talk at the Tenth Santa Cruz Summer Workshop on Supernovae, 10-21 July'89, Santa Cruz, CA (1989)

132. J.R.Wilson, in Numerical Astrophys. eds: J. Centrella (John and Bartlett, Boston 1985)

133. A. Roy and K. Kar, Astrophys. J. 319, 143 (1987)

134. J.-L. Tassoul, Theory of Rotating Stars, (Princeton Univ. Press, N.J., 1978)

135. E.Muller, Max Planck Institute Preprint No 573 (March 1991)

136. E. Muller, J. Phys. G. 16, 1571 (1990)

137. S.L.Shapiro, A.P.Lightman, Astrophys. J. 207, 263 (1976)

138. J.E.Tohline, Astrophys. J. 285, 721 (1984)

139. Y.Eriguchi, E.Mutter, Astron. Astrophys. 147, 161 (1985)

140. E.Mutter, M.Rozyczka, M. Hillebrandt, Astron. Astrophys. 81, 288 (1980) --

141. E. Symbalisty, Astrophys. J. 285 , 729 (1984)

142. R. Monchmeyer, E.Muller, in NATO ASI on Timing Neutron Star, eds: H.Ogelman and E. vanden Heuvel (Kluwer,Dordretch 1989) p 549

143. K.A.van Riper, J.M.Lattimer, Astrophys. J. 249, 270 (1981)

144. P.Ledoux, Astrophys. J. 102, 143 (1945)

145. R. Monchmeyer, G.Schafer, E. Muller, R. Kates, Astron. Astrophys. (1991) preprint

146. R.I.Epstein, MNRAS 188, 305 (1979)

147. W.D.Arnett, unpublished work (1985)

148. A. Burrows, Astrophys. J. Lett. 318, L 57 (1987)

149. H.a.Bethe, G.E.Brown, J.Cooperstein, Astrophys. J. 322,201 (1987)

150. R.Monchmeyer, in Proc. 5th Workshop.Nucl. Astrophys. eds: W.Hillebrandt and E. Muller, MPA/P1 (Max Planck Inst. Garching 1989) p92

151. S.L.Shapiro and S.A.Teukolsky, Blackholes, Whitedwarfs and Neutron Stars (Wiley, NY 1983) p 173

152. J.P.Ostriker, J.L.Tassoul, Astrophys. J. 155, 987 (1969)

153. J.P.Ostriker, P.Bodenheimer, Astrophys. J. 180, 171 (1973)

154. R.H.Durisen, J.N. Imamura, Astrophys. J. 243, 612 (1981)

155. J.N.Imamura, J.L.Friedman, R.H.Durisen, Astrophys.J. 294,474 (1985)

156. R.A.Managan, Astrophys. J. 294, 463 (1985)

157. ------ , Astrophys. J. 309, 598 (1986)

158. L.Lindblom,m S.L.Detweiler, Astrophys. J. 211, 565 (1977)

159. W.Hillebrandt, R.G.Wolff, in Nucloesynthesis: challanges and new Developments, eds: W.D.Arnett & J.W.Truran, (Chicago Univ. Press, USA, 1985) p 131

160. R. Monchmeyer, E.Muller, Astron. Astrophys. 271, 351 n(1989)

161. M. Rozyczka, Astron. Astrophys. 143, 59 (1985)

162. W.M.Tscharnuter, K.H.Winkler, Comp. Phys. Comn. 18, 171 (1979)

163. H.Th.Janka, R.Monchmeyer, Astron. Astrophys. (1989) Preprint

164. G.V.Domogatsky, D.K.Nadyozhin, Sov.Astron. 22, 297 (1978)

165. W.C.Haxton, Phys. Rev.Lett. 60, 1999 (1988)

166. A.Roy and K.Kar, Astrophys. Lett. Commn. 28, 276 (1992)

167. J.R.Wilson, R.W.Mayle, Phys. Reports. 163, 63 (1988)

168. H.Th.Janka, Max Planck Institute Preprint No:MPA 720 (1993)

169. T.Hecht, Diploma Thesis, TU Munchen (1989)

170. H. Suzuki, Ph.D. Thesis, Univ. of Tokyo, (1989)

171. H.Th. Janka, Max Planck Inst. ,Preprint No: MPA 587 (1991)

172. G.V.Domogatsky, R.A.Eramzkyan, D.K.Nadyozhin, Astrophys.Space Sci. 58, 273 (1978)

173. G.V.Domogatsky, D.K.Nadyozhin, MNRAS 178, 33 (1977)

174. G.V.Domgatsky, V.S.Imshennik, Sov. Astron. Lett. 8, 190 (1982)

175. R.I.Epstein,m S.A.Colgate, W.C.Haxton, Phys. Rev. Lett.61,2038 (1988

176.S.E.Woosley, W.C.Haxton, Nature 334, 45 (1988)

177. S.E.Woosley, etal , Astrophys. J. 356, 272 (1990)

178. V.S.Imshennik, D.K.Nadyozhin, Sov.Phys. JEPT, 36 , 821 (1973)

179. T.J.Mazurek, Nature 252, 287 (1974)

180. ----- , Astrophys., Space Sci. 35, 117 (1975)

181. ----- , Astrophys. J. 207, L87 (1976)

182. T.J.Mazurek, Comments Astrophys. 7, 77 (1977)

183. S.A.Bludman, K.A.van Riper, Astrophys. J. 224, 631 (1978)

184. K. Sato, Prog. Theor. Phys. 53, 595 (1975)

185. ---- , Prog. Theor. Phys. 54, 1325 (1975)

186. D.Q.Lambn, C.J.Pethick, Astrophys.J. 209, L77 (1976)

187. W.R.Yueh, J.R.Buckler, Astrophys.J., 211, L121 (1977)

188. ---- , Astrophys.J. 217, 565 (1977)

189. S.W.Bruenn, Astrophys.J. 340, 955 (1989)

190. ----- , Astrophys.J. 341, 385 (1989)

191. W.Hillebrandt, in High Energy Phenomena around collapsed stars, eds: F. Pacini, NATO ASI C 195, (D. Riedel, Dordrecht, 1987) p73

192. I.Lichtenstand, etal, Astrophys.J. 226, 222 (1978)

193. S.W.Bruenn, Astrophys. J. Suppl. 58, 771 (1985)

194. E.S.Myra etal, Astrophys. J. 318, 744 (1987)

195. E.Baron etal , Astrophys. J. 339, 978 (1989)

196. J.R. Bond, Ph.D.Thesis, Caltech, USA (1978)

197. P.J.Schinder, S.L. Shapiro, Astrophys.J. 259, 311 (1982)

198. P.J.Schinder, Astrophys. J. Suppl. 50, 23 (1982)

199. P.J.Schinder, S.L.Shapiro, Astrophys. J. 273, 330 (1983)

200. P.J.Schinder, in Radiation Hydrodynamics in stars and compact objects, eds: D. Mihalas etal, Lecture notes in Physics 255 (Springer, Berlin, 1985) p 121

201. P.J.Schinder, Phys. Review D 38, 1673 (1988)

202. D.G.Hummer, G.B.Rybicki, MNRAS 152, 1 (1971)

203. D.L.Tubbs, Astrophys. J. Suppl. 37, 287 (1978)

204. D.L.Tubbs etal, Astrophys. J. 239, 271 (1980)

205. D. Kazanas, D.C.Ellison, Proc. 17th ICRC,[Paris, 1981] p 176

206. Yu.L. Levitan etal, Sov. Astron. 26, 202 (1982)

207. D.C.Elison etal, in Supernova 1987A in the large Magellanic cloud, eds: M. Katatos etal (Cambridge Univ. Press, 1988) p 194

208. P.M.Giovanani etal, Astrophys. J. 342, 416 (1989)

209. H.Th. Janka, Diploma Thesis, TU Munchen (1987)

210. H.Th. Janka, Lecture Notes in Physics 287, (Springer, Berlin 1987) p 319

211. H.Th. Janka, W. Hillebrandt, Astron. Astrophys. 224, 49 (1989)

212. H.Th. Janka, Ph.D. Thesis, TU Munchen (1990) p 89, 90

213. D.L.Tubbs, D.N.Schramm, Astrophys. J. 201, 467 (1975)

214. J.Cooperstein, L.J.van der Horn, E.A.Baron, Astrophys.j. 321, L 129

(1987)

215. H.Th. Janka, Astron. Astrophys. 244, 378 (1991)

216. G. Mau etal, Astron. Astrophys. 266, 266 (1992)

217. H.Th.Janka, preprint (1993)

218. H.Th. Janka, E.Muller, Neutrino Driven Type II Supernova ; neutrino heating and post bounce dynamics (Univ. Acad. Press, Tokyo, 1992) in press.

219. S.A.Colgate etal, Phys. Reports (1991) preprint

220. P.Hoflich etal, Astron.Astrophys. (1992) Preprint

221. A. Burrows, Astrophys. J. 318, L57 (1987)

222. M. Herant etal, Astrophys. J. 395, 642 (1992)

223. A.Burrows, B.A.Fryxell, Science 258, 430 (1992)

224. H.Th. Janka, E. Muller, Max Planck Int. Preprint No MPA 711 (1993)

225. I.S.Shkolovsky, Sov. Astron. 22, 413 (1978)

226. J.P.Ostriker, Ann. Rev. Astron. Astrophys. 9, 353 (1971)

227. R. Canal, J. Isern, J. Labay, Astrophys.j.Lett 241, L33 (1980)

228. R. Canal etal, Ann. Rev. Astron. Astrophys. 28, 183 (1990)

229. J.Isern etal, Astrophys. J. 273, 320 (1983)

230. K. Nomoto etal, in IAU Colloquium 53, White Dwarfs and variable degenerate stars, eds: H.M. van Horn etal (Univ. Rochester, 1979) p 56

231. K.Nomoto, Y. Kondo, Astrophys. J. Lett. 367, L 19 (1991)

232. J.Isern, etal, Astrophys. J. (1991) Preprint

233. K. Nomoto, in Type I Supernovae, ed: J.C.Wheeler (Univ. of Texus, Austin, 1980) p 164

234. S.Miyaji etal, Publ. Aston. Soc. Japan 32, 303 (1980)

235. R. Mochkovitch, Thesis, Univ. of Paris, (1980)

236. K.Nomoto, in IAU Symp. 125, The Origin and Evolution of Neutron Star eds: D.J.Helfand and J.H.Huang (D.Riedel, Dordrecht, 1987) p 281

237. K.Nomoto, I. Iben. Jr, Astrophys.J. 297, 531 (1985)

238. Y. Kawai, H.Saio, K. Nomoto, Astrophys. J. (1986) Preprint

239. H.Saio, K. Nomoto, Astron. Astrophys. 150, L21 (1985)

240. S.E.Woosley, T. Weaver, in Nucleosynthesis and its implications for Nuclear and Particle Physics, eds: J. Audouze etal (D. Riedel, Dordrecht, 1986)

241. L.N. Ivanova etal, Astrophys. Space Sci. 31, 497 (1974)

FIGURE CAPTIONS :

Fig.1 : Schematic diagram of the changes in stellar structure from the pre-main sequence contraction to the onset of central helium burning.

Fig.2 : Nuclear fluxes corresponding to $^{22}Ne\ (\alpha, n)\ ^{25}Mg$ vs mass coordinate Mr/M (where M is the current stellar mass) for the star of mass 15 $M_\odot$. Model M15A corresponds to contraction phase toward C ignition, while model M15 B relates to central C exhaustion. These fluxes are defined as $\int X_4\ Xi\ N_A \langle \sigma v \rangle$ where X_4 , X_i are the mass fraction of alpha particles and of ^{13}C, ^{22}Ne or ^{21}Ne while $N_A \langle \sigma v \rangle$ designates the relevant (α, n) rate in the usual notation (see ref. 47)

Fig.3 : Nuclear fluxes corresponding to $^{22}Ne\ (\alpha, n)\ ^{25}Mg$ vs mass coordinate Mr/M for the star whose mass is 30 $M_\odot$. Notations are same as in fig. 2.

Fig.4 : Evolution of the internal structure of 20$M_\odot$ star. Cloudy regions are convective zones, heavy hatched regions indicate zones where nuclear energy rates are superior to 10^3 erg/g. sec. At the begining of the C and Ne burning phases, time has reset to zero and the scale has been changed (see ref.50)

Fig.5 : Composition profile within the 20$M_\odot$ model near the end of the O-burning phase. Abscisa, the lagrangian mass coordinate, ordinate, the logarithm of the mass fraction (see ref.50)

Fig.6. : The abundance distribution at the onset of collapse for the 6 $M_\odot$ helium core of the 20 $M_\odot$ star. "Fe" and "Si" denote iron peak elements and silicon peak elements, respectively (see ref. 52)

Fig.7 : Four 25$M_\odot$ pre supernova models calculated with different values of the semi convective diffusion parameter and rate for the $^{12}C(\alpha,\gamma)^{16}O$ reaction rate. Only the inner 15 $M_\odot$ of the 25 $M_\odot$ models are shown. The letter 'S' means much more semiconvection was employed, while letter 'N' means that a very small amount of semi convection was included in the calculation (see ref. 84)

Fig.8 : a) Density and b) Chemical composition vs mass for the innermost 7.5 $M_\odot$ of the 15 $M_\odot$ stellar model of Arnett (ref. 44). The model has a 4 $M_\odot$ helium core, a 1.5 M. oxygen core and a metallicity $z = z_\odot/4$. The density profile shows two steep drops, which occur at the H/He and at the He/C-O interface. These regions will become unstable due to the passage of the shock (ref.93)

Fig.9 : a) Detailed abundancee distributions in zones which undergo alpha rich freezeout and b) incomplete Si burnijng at Mr < 1.74 $M_\odot$ and explosive O-burning at Mr < 1.8 $M_\odot$ (ref.83)

Fig.10 : Abundance distribution after passage of the supernova shock front. Matter outside 2 $M_\odot$ is essentially unaltered. Mass zones further in experience explosive Si, O, Ne, and C-burning (ref.95)

Fig.11 : The velocity profiles at t = 100 d for model 14 E 1 (solid curve) and 11 E 0.6 (dashed curve) [see ref. 99]

Fig.12 : a) Change in the pressure profile (top) and b) change in the density profile (bottom) of the ejecta model 14E1. Stage numbers corresponds to (0) t = 0 s, (1) 9.0 s ,

(2) 167 s (3) 1060 s (4) 3330 s (5) 7460 s after the explosion [see ref. 100]

Fig.13 : Nonlinear growth of the Rayleigh-Taylor (R-T) instability for 14 E 1 with the 5 % sinusoidal perturbations on velocities [ref. 108, 109, 110]

Fig.14 : Nonlinear growth of the Rayleigh-Taylor instability for 14E1 with random perturbations shown in the density contour (left) and positions of the marker particles initially located at the H/He , He/C+O, and C+O/Si interfaces (right). The core material finally reaches the top of the mashroom head [see ref. 108 - 110]

Fig.15 : Abundance distribution (mass fraction) as a result of Rayleigh-Taylor instability. Hydrogen is mixed down to Mr ~ 1 $M_\odot$. The mean radial velocity is also shown [see.ref. 108 - 110]

Fig.16 : Equilibrium parameter F_{EM} as a function of the (absolute) value of the ratio of rotational to gravitational energy β. The number attached to each curve is the adiabatic index γ determined by the equation of state. The solid and dashed curves represent differnt rotation laws [ref. 135, 139]

Fig.17 : Possible evolutionary scenarios of collapsing rotating ploytropes as a function of the initial (absolute) value of the ratio of rotational to gravitational energy β_i, and of the adiabatic index γ determined by the equation of state [see ref. 135, 139]

Fig.18 : Profiles of the specific entropy and flow pattern about 6.5 ms after bounce showing the instability at the edge of the high entropy region. The contours covers a range from Fmin to F max with a specific Delta. The time, the central entropy and the velocity scale are given in the legend of

the fig. [see ref. 142, 150]

Fig.19 : Profiles of the density [log 10 $^{(\rho)}$] and flow patter about 84 ms after bounce showing the strongly flattened, rotationally stabilized configuration at the end of the calculation. The contour cover a range from F min to F max with a specific Delta. The time, the central density and the velocity scale are given in the legend of the figure (see ref.150)

Fig.20 : Profiles of the density [log 10 $^{(\rho)}$] and flow pattern about 3.6 ms after bounce showing the expansion movement of the inner core behind the shock front. The contours cover a range from F min to F max with a specing Delta. The time the central density and the velocity scale are given in the legent of the fig. [ref. 150]

Fig.21 : Profiles of the specific entropy and flow pattern about 45ms after bounce showing the shock front, which already penetrted the silicon shell, and the 'jet', which rapidly expands into polar direction. The contours cover a range from F min to F max with a specing of Delta.The time, the central entropy and the velocity scale are given in the legend of the fig. [ref. 142, 150]

Fig.22 : The post bounce oscillations of the rotating models are shown for different quantities. In the first figure of each column the central density ρ_c [g/cc] of each model is plotted. The second plot shows the rotational energy integrated from the core center upto selected mass zones. [see ref.150]

Fig.23 : a) Mass fraction of neutrons, protons and alpha particles in the shocked zone plotted as a function of time for the standard case with $L_{\nu_e} = 4 \times 10^{52}$ erg/s and $R_{\nu_e} = 30$ km

case. Also shown with a dashed curve is the variation of total entropy. The dot-dashed curves rerpresent the variation of the corresponding quantities in which the neutral current heating on nuclei was neglected [ref. 166]

b) Internal energy per nucleon $\mathcal{E}_{int}$ behind the shock front plotted against time for various values of the neutrino energy flux. Solid cuve I, II, III are for neutrino luminosities $L_{\nu e} = 2 \times 10^{52}$, 4×10^{52} and 5×10^{52} erg/s , respectively with $R_{\nu e} = 30$ km. Also shown on the ordinate is the gravitational potential barrier $\mathcal{E}_{cr} = GMc/Rc = 14.1$ MeV. Dashed curve denotes the position of the shock as a function of time. The dot-dashed curve (II') represents the evolution of $\mathcal{E}_{int}$ for $L_{\nu e} = 4 \times 10^{52}$ erg/s. without the neutral current heating on nuclei [see ref. 166]

Fig.24 : a) Mass fraction of neutrons, protons, alpha particles and Fe nuclei in the shocked zone plotted as a function of time with $R_{\nu e} = 55.4$ km and $L_{\nu e} = 3.28 \times 10^{52}$ erg/s for the 18 M. core. Also shown with a dashed curve is the variation of total entropy [see ref. 166]

b) Internal energy per nucleon $\mathcal{E}_{int}$ behind the shock front plotted against time with $R_{\nu e} = 55.4$ km and $L_{\nu e} = 3.28 \times 10^{52}$ erg/s. Curve I is with $\dot{M} = 0.1\ M_\odot$, and curve II with $\dot{M} = 0$. Also shown on the ordinate is the gravitational potential $\mathcal{E}_{cr} = G\,Mc / Rc = 8.7$ MeV. Dashed curve denotes the position of the shock as a function of time [ref. 166]

Fig.25 : Schematic picture of stellar core collapse, formation of the neutron star remnant and start of the supernova explosion. The shaded region indicates those layers where most of the neutrino emission comes from.

R_{Fe} = the radius of the stellar iron core

R_{ν} = the position of the 'neutrino sphere' which separates

the regions of neutrino diffusion and neutrino transparency.

R ic = the size of the subsonically collapsing innerpart of the stellar core, at later times it encompasses the settled, compact inner region of the nascent neutron star

R sh = the supernova shock which is formed at core boounce, stagnates for several hundred milliseconds and is revived by neutrino heating to propagate outwards into stellar mantle with some time delay

Details are in the text [see ref. 168]

Fig.26 : Schematic representation of neutrino ' light curves' during stellar core collapse, shock propagation and shock breakout, accretion phase and protoneutron star cooling, the different phases separated by vertical short dashed lines. The solid curve corresponds to ν_e , long dashed line marks $\bar{\nu}_e$ emission, the dashed dotted curve indicates the luminosity in each of the neutrino kinds ν_μ , $\bar{\nu}_\mu$, ν_τ , & $\bar{\nu}_\tau$. Time is measured in milliseconds with $\log_{10}(t) = 0$ positioned at the moment of core bounce [ref. 168]

Fig.27 : Spectra of neutrinos from a supernova . The figures a) and b) give results for ν_e at 12 ms and 315 ms after core bounce, respectively. c) the ν_e spectrum and d) the ν_x ($x = \mu$, $\bar{\mu}$, τ , $\bar{\tau}$) spectrum at the later stage of the supernova evolution. The spectra plotted as solid lines were obtained by Monte Carlo simulations of neutrino radiative transfer, the dashed lines show the 'thermal' or 'blackbody ' spectra (i.e. $\eta_\nu = 0$) with same average energy, the dotted lines represent fits with non-vanishing neutrino degeneracy parameter $\eta_\nu^{eff} \neq 0$. Note that the Monte Carlo spectra show significant depletion at low and high energies compared with the thermal spectra. The average spectral energies are 9.5 MeV,

8.2 MeV, 14.4 MeV, and 17.2 MeV in figs (a) — (d) respectively [see ref. 168]

Fig.28 : Spectral distributions of energy emitted in neutrinos per unit area of these surfaces of the protoneutron star models, integrated over the time intervals during which transport was followed by Monte Carlo methods.
Solid lines correspond to a model at about 3.3 s after core bounce (radius of the neutron star R ns = 16 km.). Dashed lines to a model at 5.8s after bounce R ns = 12.8 km. Dotted lines represent the emission at 7.8 s post bounce (R ns = 11.8 km). The average spectral energies are 12 - 13 MeV for ν_e , about 16 MeV for $\bar{\nu}_e$, and 24 - 27 MeV for ν_x [ref. 168]

Fig.29 : Radial position of selected mass shells as functions of time for the first three seconds of a simulation run where neutrino effects were included. Time is measured from the start of computation. The matter external to the neutron star is heated by the neutrino flows from the neutron star and a huge expansion sets in [ref. 168]

Fig.30 : Electron concentration Ye with in a region of 376 km radial extension above the newly formed neutron star at about 0.8 s after core bounce. The convection is driven by a negative entropy gradient and mixes material of lower Ye from positions close to the neutron star with matter of higher Ye farther out [se ref. 168]

Fig.31 : Convection in a protoneutron star some ten milliseconds after core bounce. The plot shows the time evolution of the electron concentration Ye in a region between 20 km and 125 km. The four pannels are arranged in counter clockwise order, starting from the right upper side, and show snapshots at 13 ms, 16 ms, 21 ms, and 26 ms after the start of the 2-D computation. The grey

levels correspond to Ye values between 0.05 and 0.5 with a linear variation from dark to bright [ref.168]

Fig.32 : Convection in a protoneutron star some ten milliseconds after core bounce. The plot shows the time evolution of the entropy (in k_B per nucleon) in a region between 20 km and 218 km. The panels are arranged in counter clockwise order, starting from the right upper side, and show snapshots at 16 ms, 21 ms, 26 ms, and 31 ms after the start of the 2-D computation. The grey levels correspond to entropy values between 2 and 9 with a linear variation from bright to dark [see ref. 224]

Fig.33 : Imagined convective overturn in the region between proto-neutron star and supernova shock during the matter accretion phase after core bounce. The matter is accreted onto the nascent neutron star in narrow flow tubes and emits high energy neutrinos, which helps to power the supernova explosion [see ref. 224]

tion

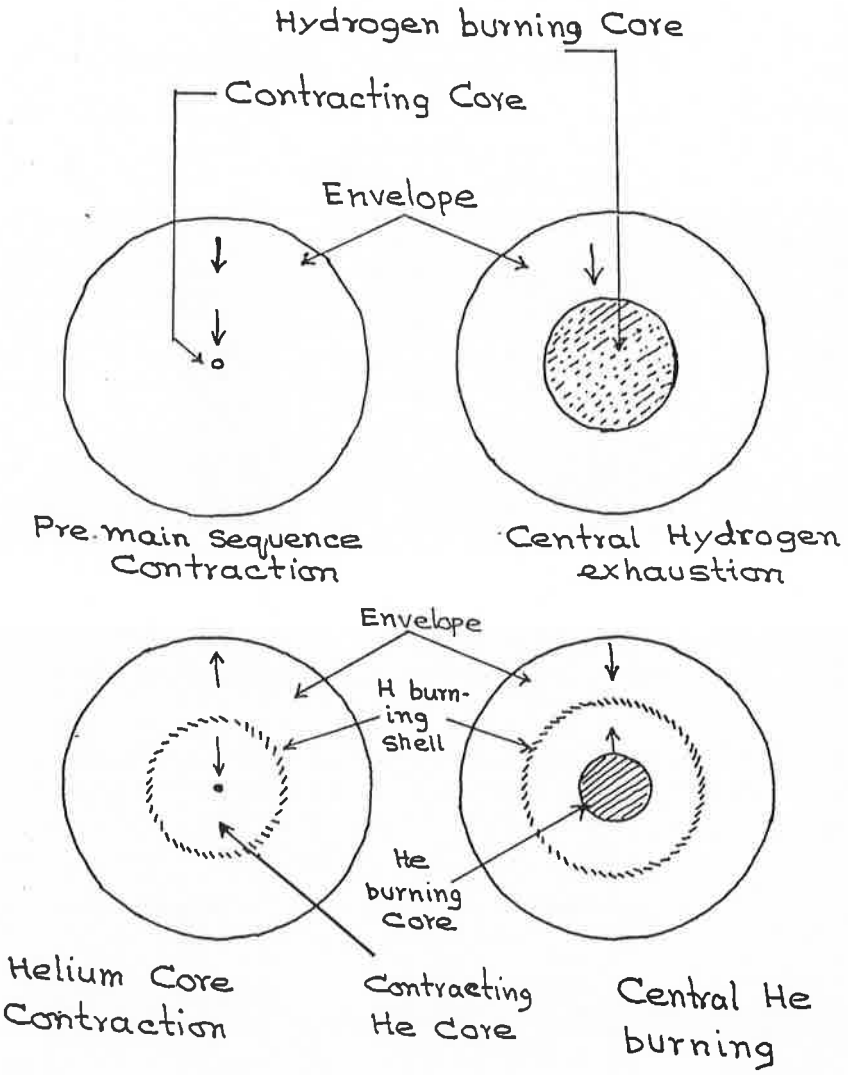
Hydrogen burning Core
Contracting Core
Envelope
Pre-main sequence Contraction
Central Hydrogen exhaustion
Envelope
H burning shell
He burning Core
Helium Core Contraction
Contracting He Core
Central He burning

Fig- 1

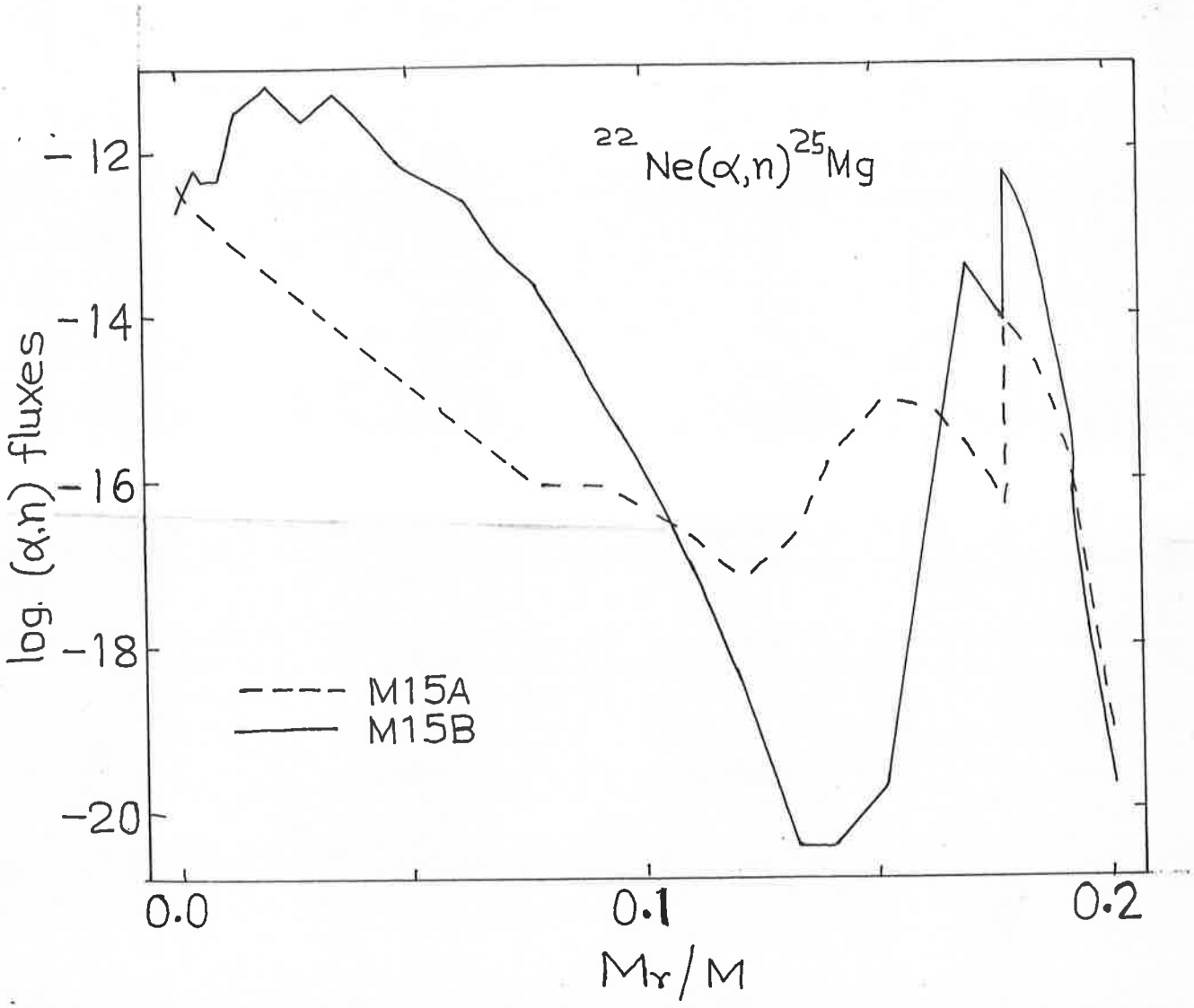
$^{22}Ne(\alpha,n)^{25}Mg$
log. (α,n) fluxes
-12
-14
-16
-18
-20
M15A
M15B
0.0
0.1
0.2
M_r/M

Fig - 2

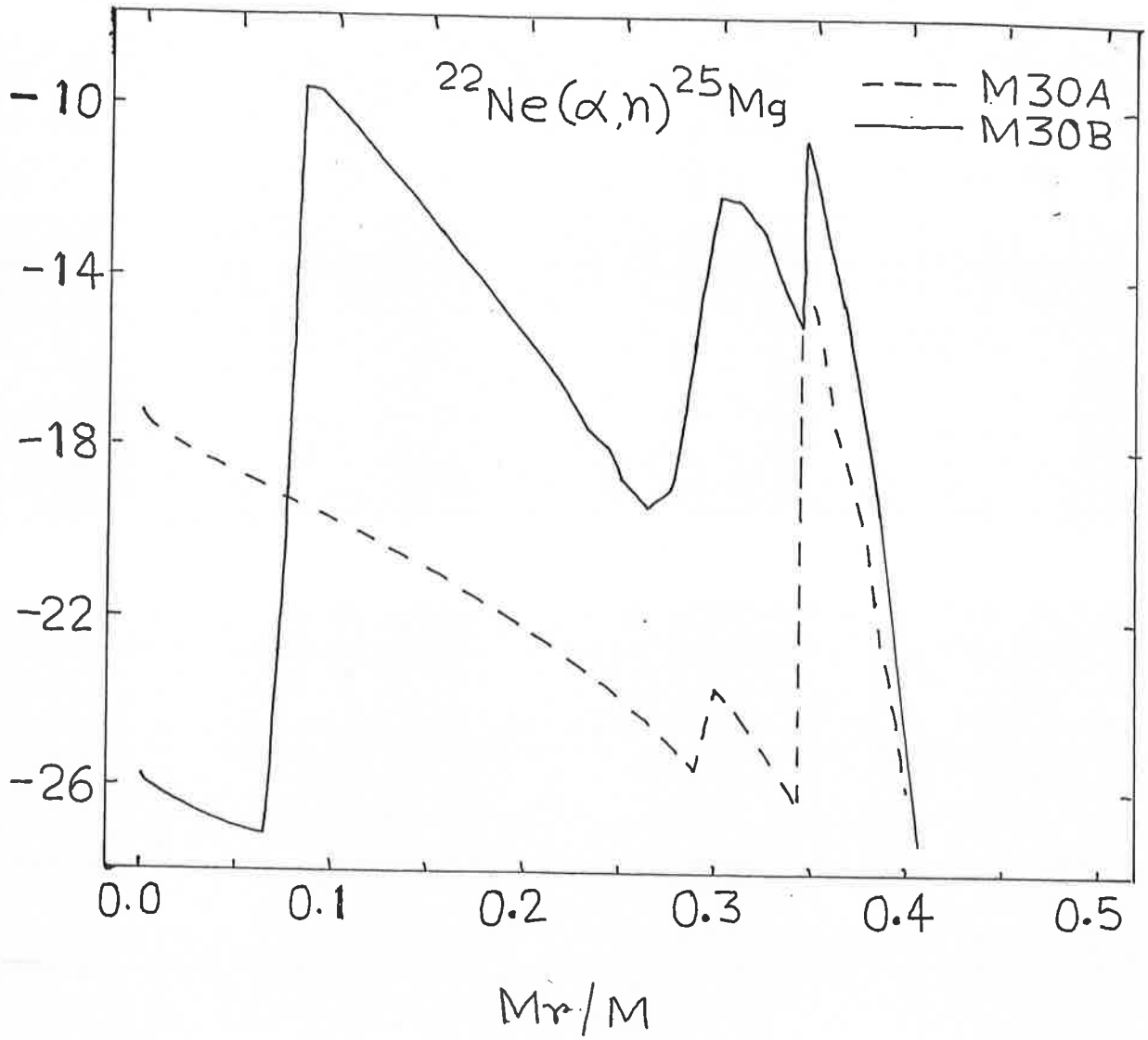

Fig-3

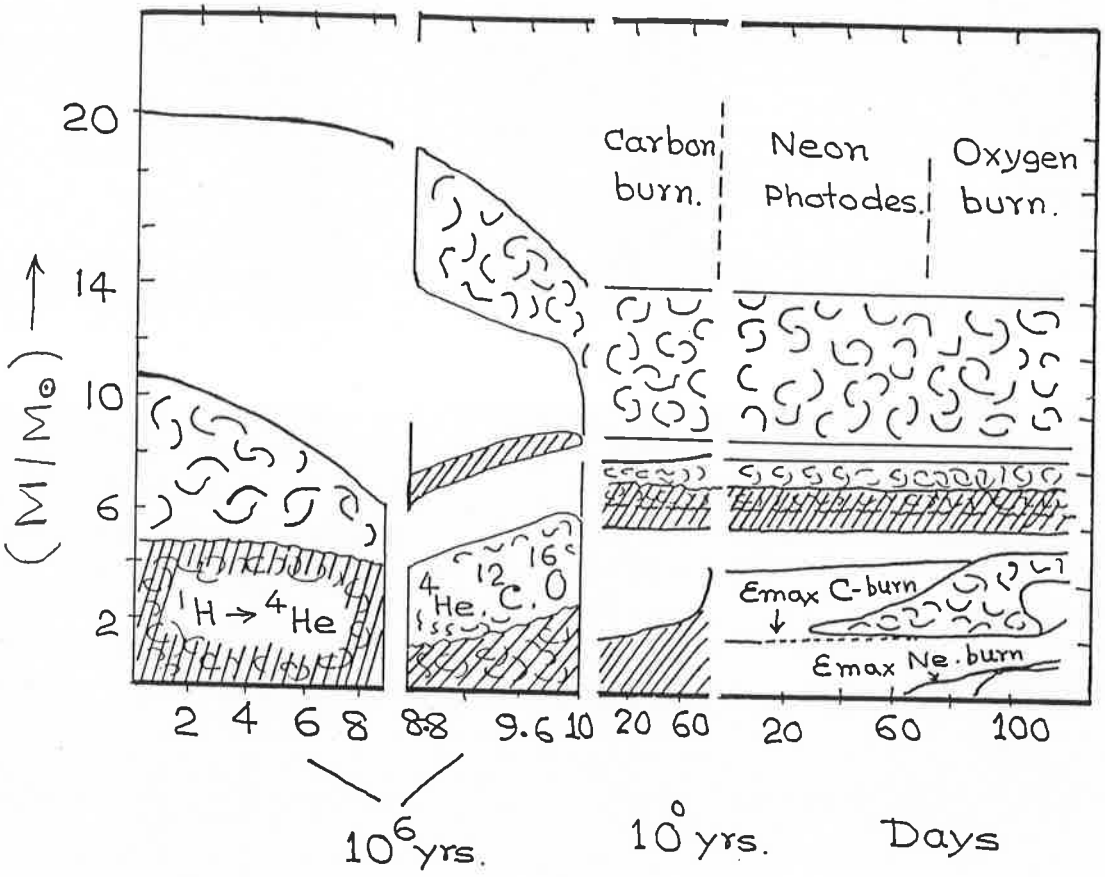
20
14
10
6
2
(M/M⊙) →
Carbon burn.
Neon Photodes.
Oxygen burn.
$^1H \rightarrow {}^4He$
^4He. ^{12}C. ^{16}O
Emax C-burn
Emax Ne. burn
2 4 6 8 8.8 9.6 10 20 60 20 60 100
10^6 yrs.
10^0 yrs.
Days

Fig. 4

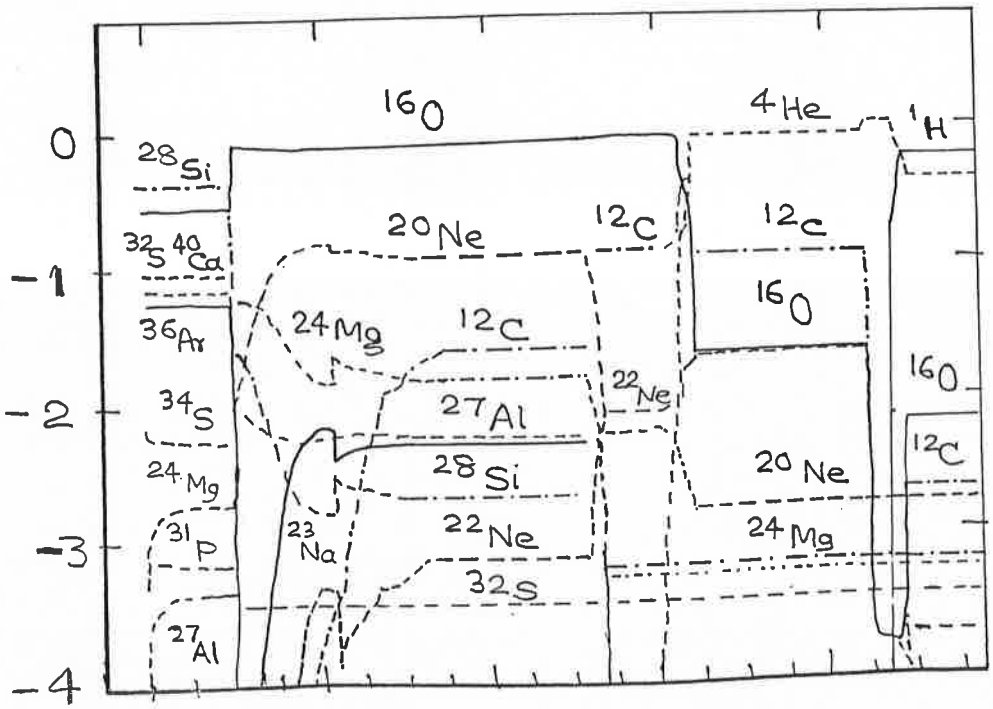
0
-1
-2
-3
-4
16O
4He
1H
28Si
20Ne
12C
12C
32S 40Ca
16O
24Mg
12C
36Ar
22Ne
27Al
34S
28Si
20Ne
24Mg
22Ne
24Mg
31P
23Na
32S
27Al

Fig. 5

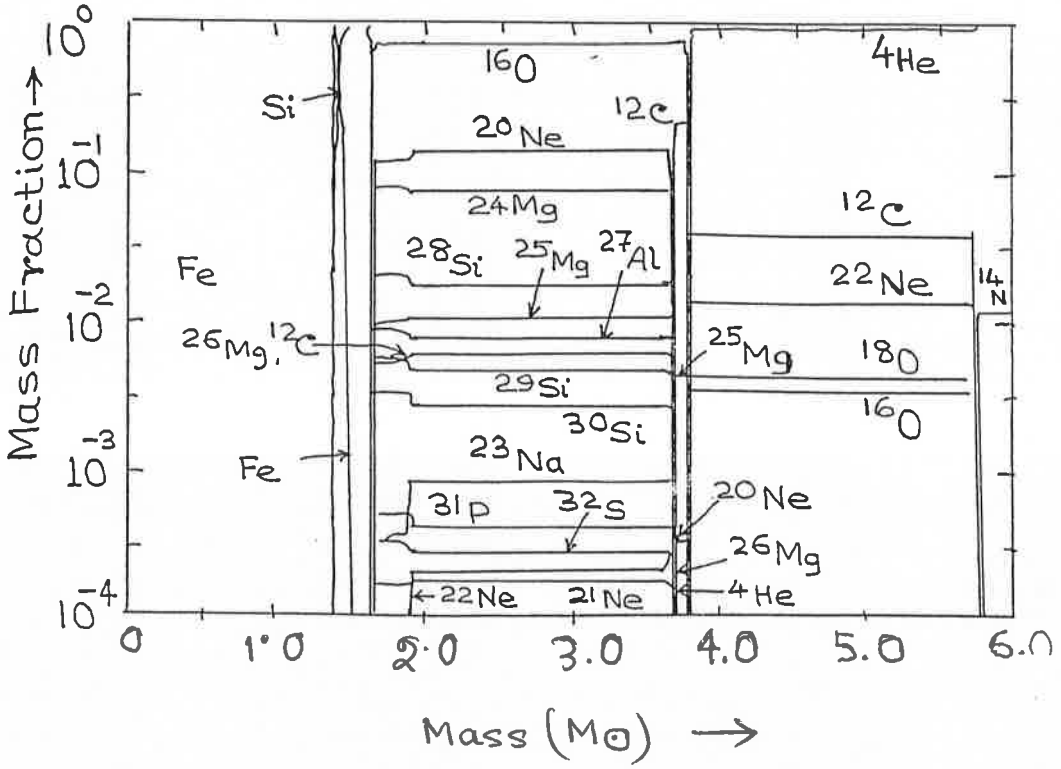
Mass Fraction →
10^{0}
10^{-1}
10^{-2}
10^{-3}
10^{-4}
Si
Fe
^{26}Mg, ^{12}C
Fe
^{16}O
^{20}Ne
^{12}C
^{24}Mg
^{28}Si
^{25}Mg
^{27}Al
^{29}Si
^{30}Si
^{23}Na
^{31}P
^{32}S
←^{22}Ne
^{21}Ne
^{4}He
^{12}C
^{22}Ne
^{14}N
^{25}Mg
^{18}O
^{16}O
^{20}Ne
^{26}Mg
←^{4}He
0
1·0
2·0
3.0
4.0
5.0
6.0
Mass (M⊙) →

Fig-6

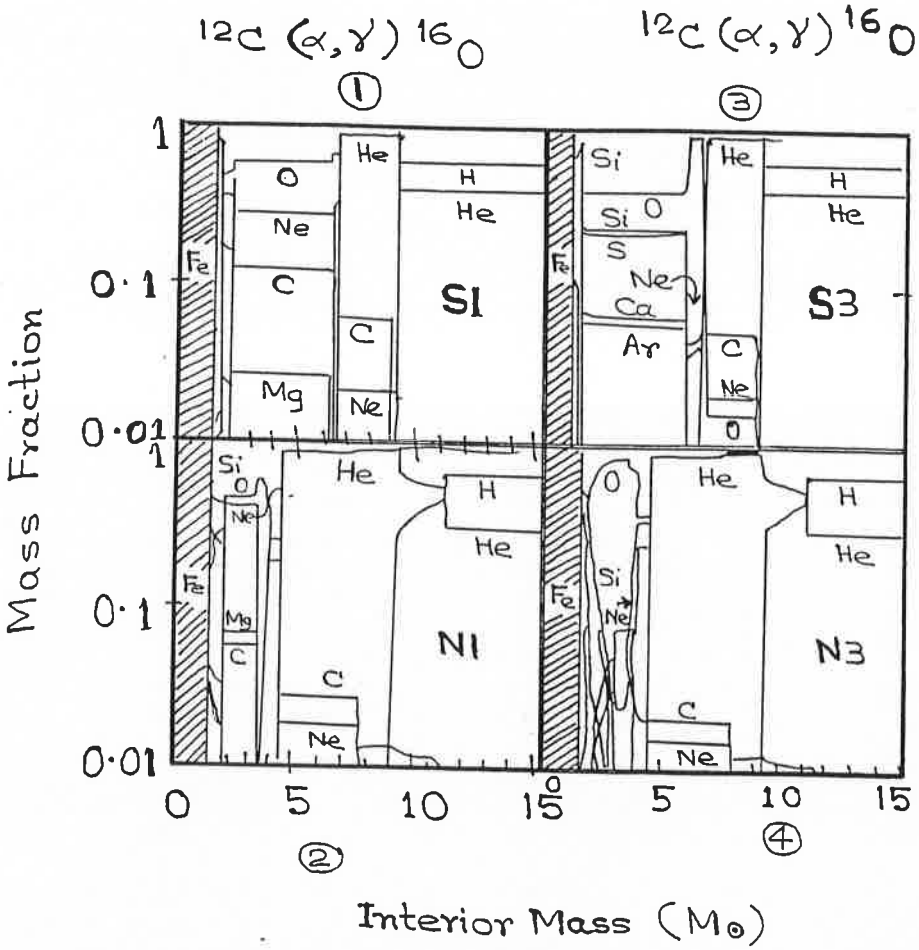
12C (α,γ) 16O
①
12C (α,γ) 16O
③
Mass Fraction
1
0·1
0·01
1
0·1
0·01
Fe
O
Ne
C
Mg
He
H
He
C
Ne
SI
Si
O
Ne
C
Mg
He
H
He
C
Ne
NI
Fe
Si
O
S
Ne
Ca
Ar
He
H
He
C
Ne
O
S3
O
He
H
He
Si
Ne
C
Ne
N3
0
5
10
15
②
0
5
10
15
④
Interior Mass (M⊙)

Fig. 7

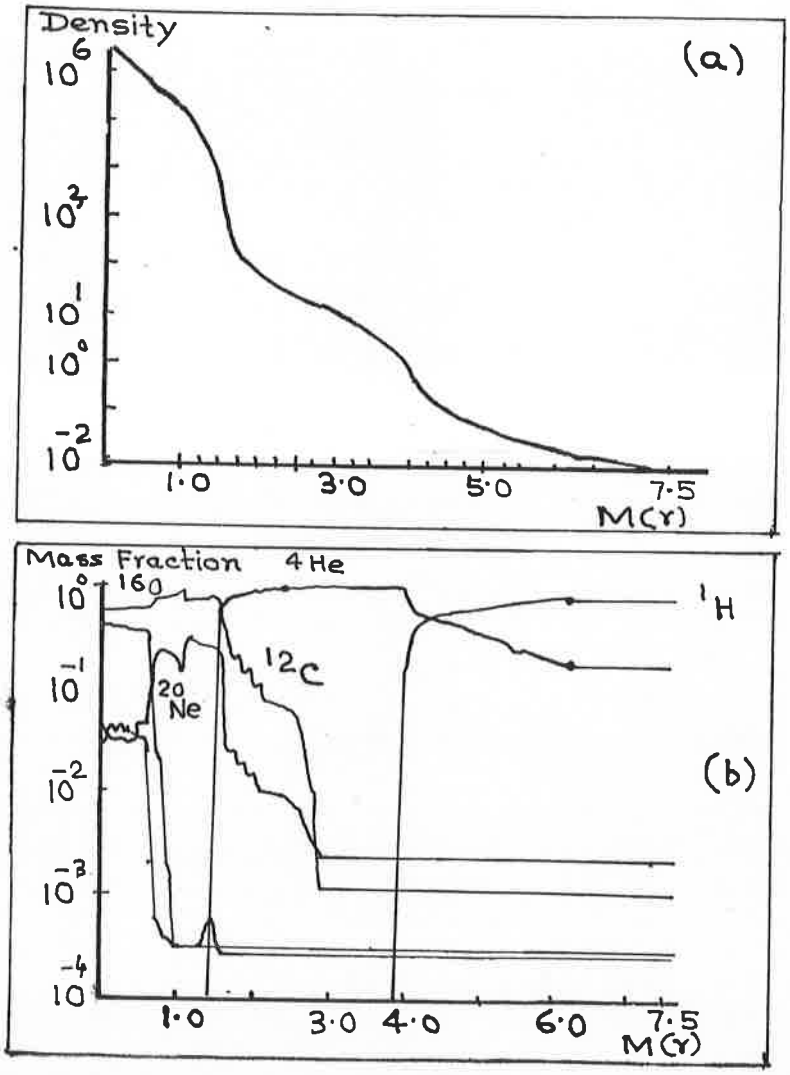
Density
(a)
10^{6}
10^{2}
10^{1}
10^{0}
10^{-2}
1·0
3·0
5·0
7·5
M(r)
Mass Fraction
4He
16O
10^{0}
10^{-1}
10^{-2}
10^{-3}
10^{-4}
20Ne
12C
1H
(b)
1·0
3·0
4·0
6·0
7·5
M(r)

Fig-8

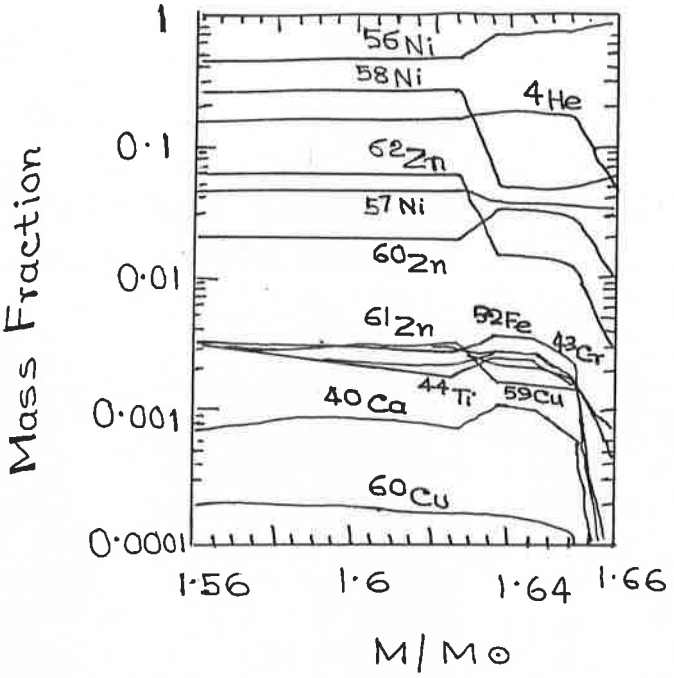
Mass Fraction
1
0·1
0·01
0·001
0·0001
56Ni
58Ni
4He
62Zn
57Ni
60Zn
61Zn
52Fe
43Cr
44Ti
59Cu
40Ca
60Cu
1·56
1·6
1·64
1·66
M/M⊙

Fig 9 (a)

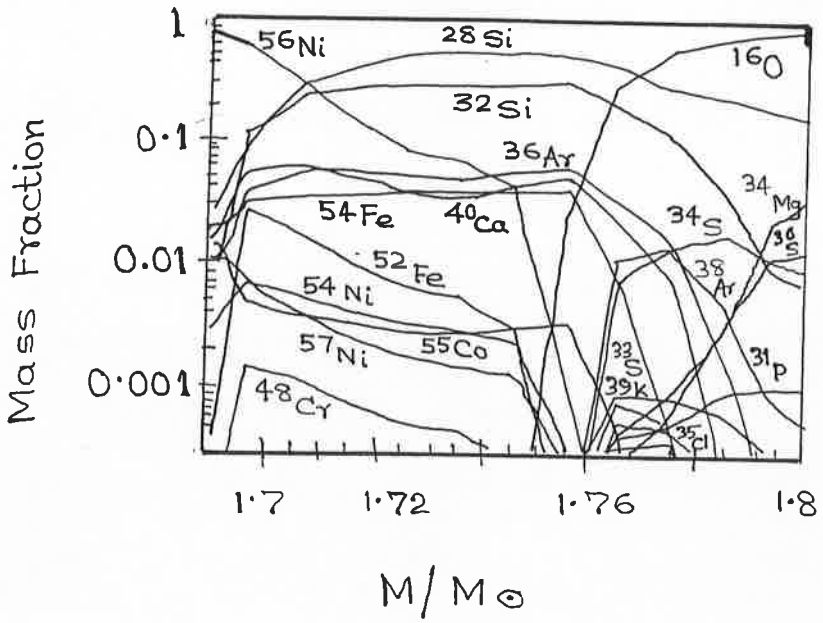
Mass Fraction
1
0·1
0.01
0·001
56Ni
28Si
16O
32Si
36Ar
34Mg
54Fe
40Ca
34S
36S
52Fe
38Ar
54Ni
57Ni
55Co
33S
31P
39K
48Cr
35Cl
1·7
1·72
1·76
1·8
M/M⊙

Fig 9 (b)

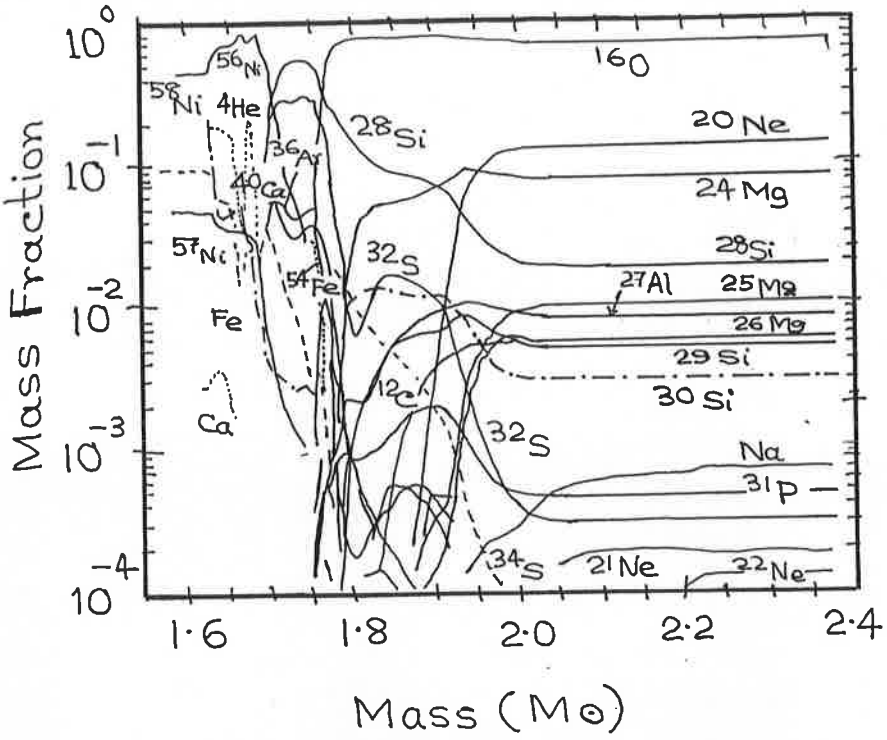
Mass Fraction
Mass (M⊙)
10^{0}
10^{-1}
10^{-2}
10^{-3}
10^{-4}
1·6
1·8
2·0
2·2
2·4
^{56}Ni
^{58}Ni
4He
^{36}Ar
^{40}Ca
^{57}Ni
^{54}Fe
Fe
Ca
^{28}Si
^{32}S
^{12}C
^{16}O
^{20}Ne
^{24}Mg
^{28}Si
^{27}Al
^{25}Mg
^{26}Mg
^{29}Si
^{30}Si
^{32}S
Na
^{31}P
^{34}S
^{21}Ne
^{22}Ne

Fig-10

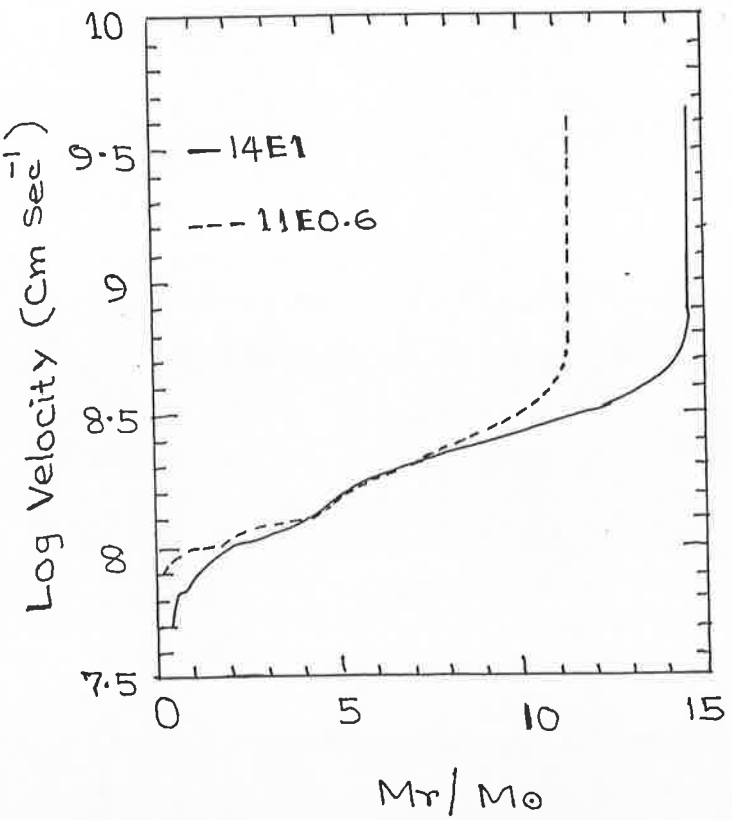
Log Velocity (Cm Sec^{-1})
Mr/ M⊙
10
9·5
9
8·5
8
7·5
0
5
10
15
—14E1
---11E0·6

Fig-11

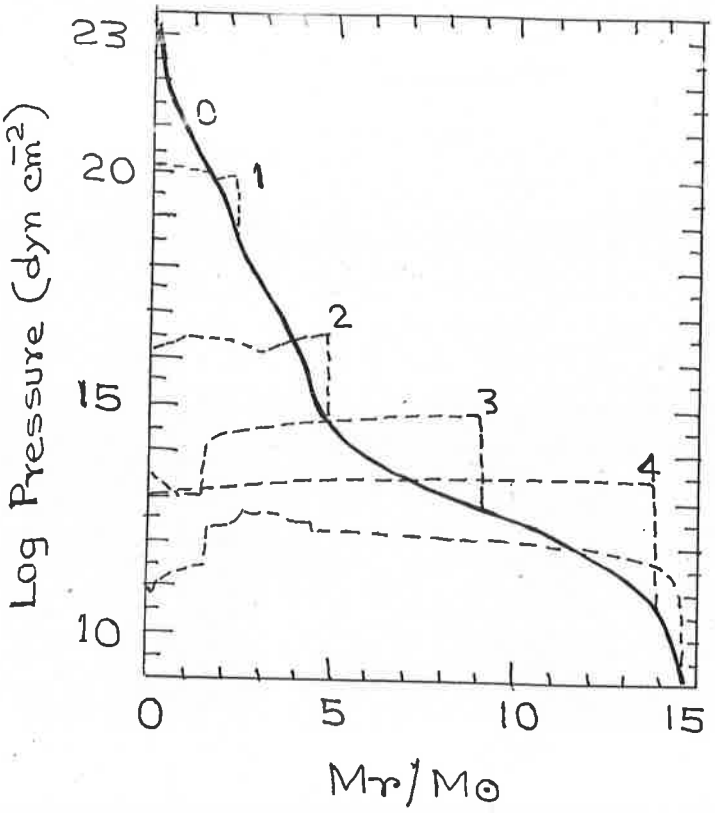

12(a)

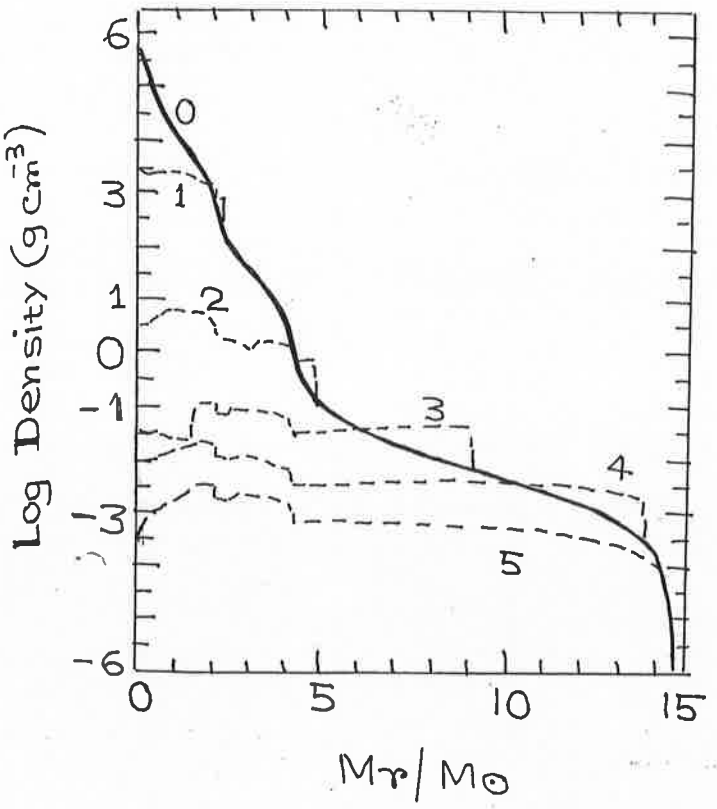

12(b)

Fig - 12

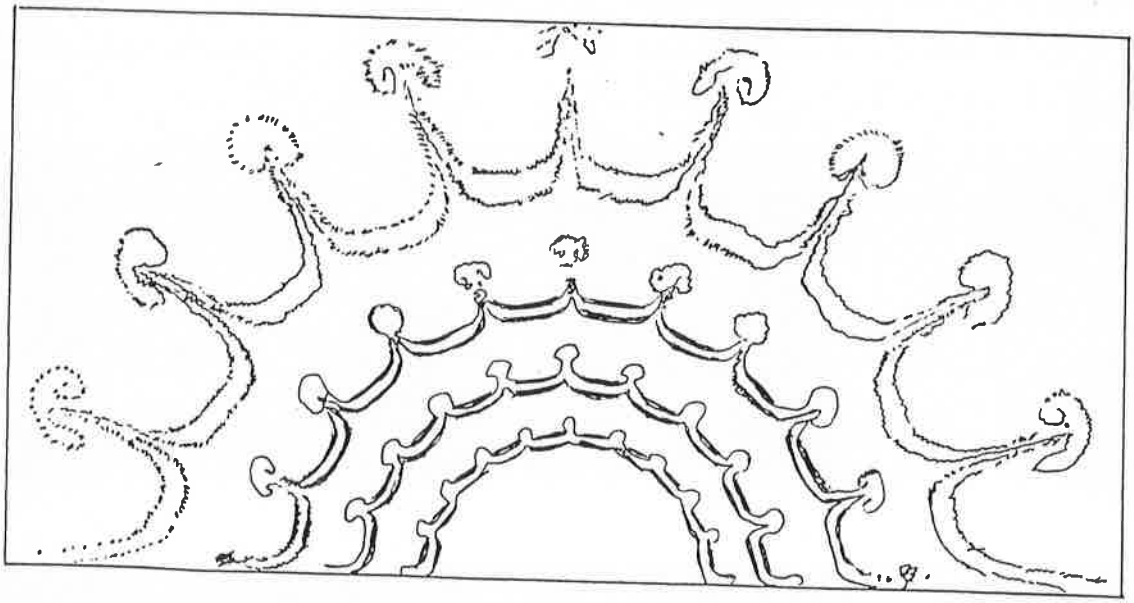

Fig. 13

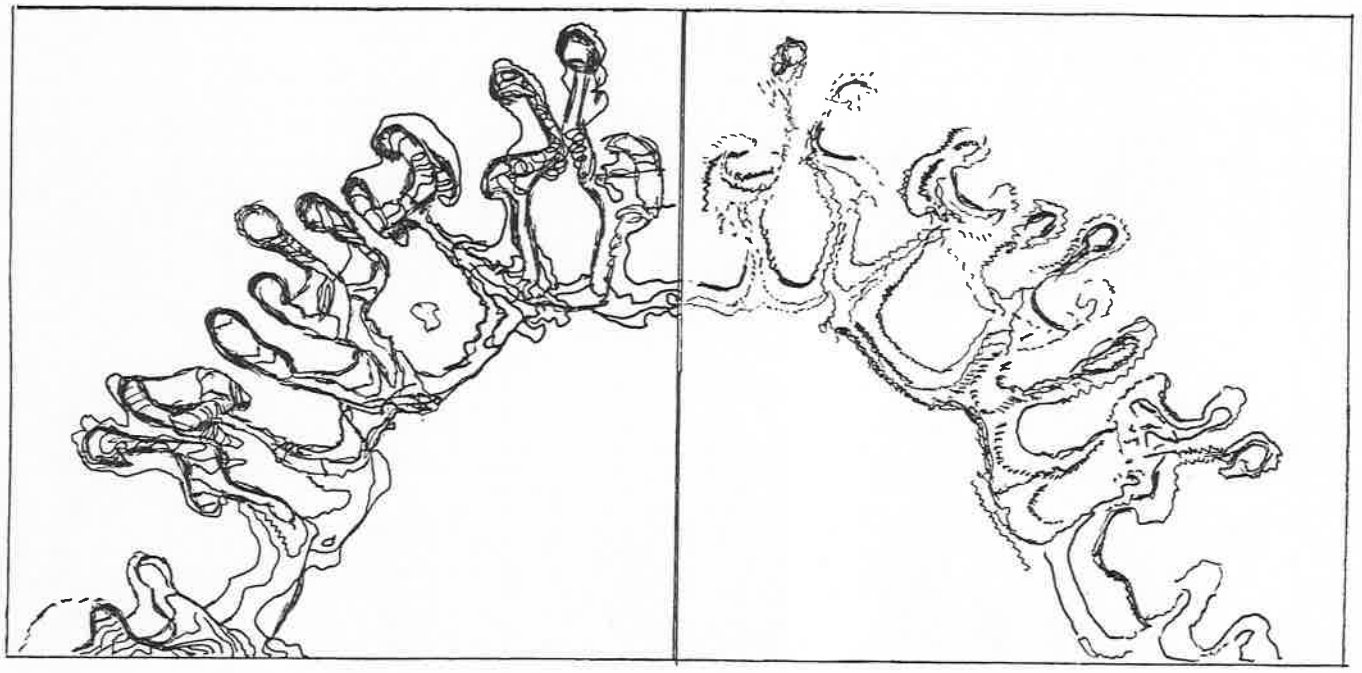

Fig - 14

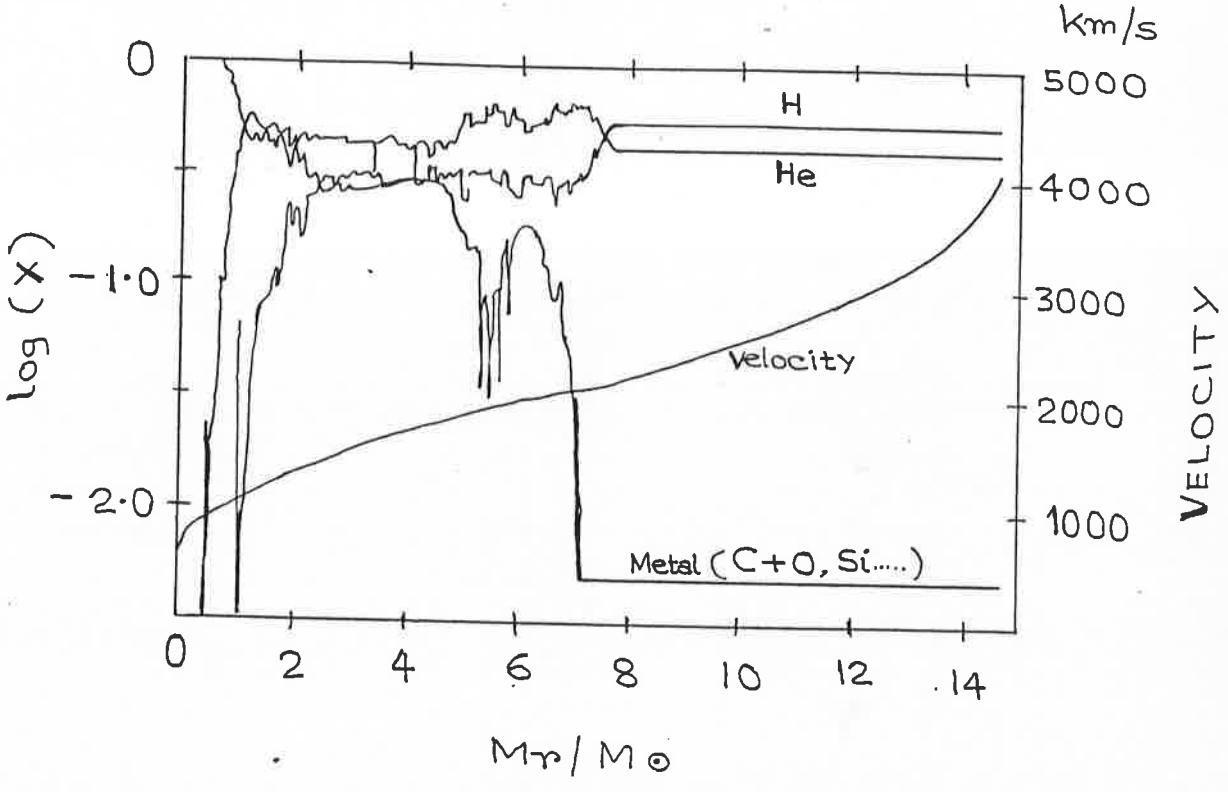
km/s
0
5000
H
He
4000
Log (X)
-1·0
3000
Velocity
2000
-2·0
1000
VELOCITY
Metal (C+O, Si.....)
0
2
4
6
8
10
12
14
Mr/M⊙

Fig - 15

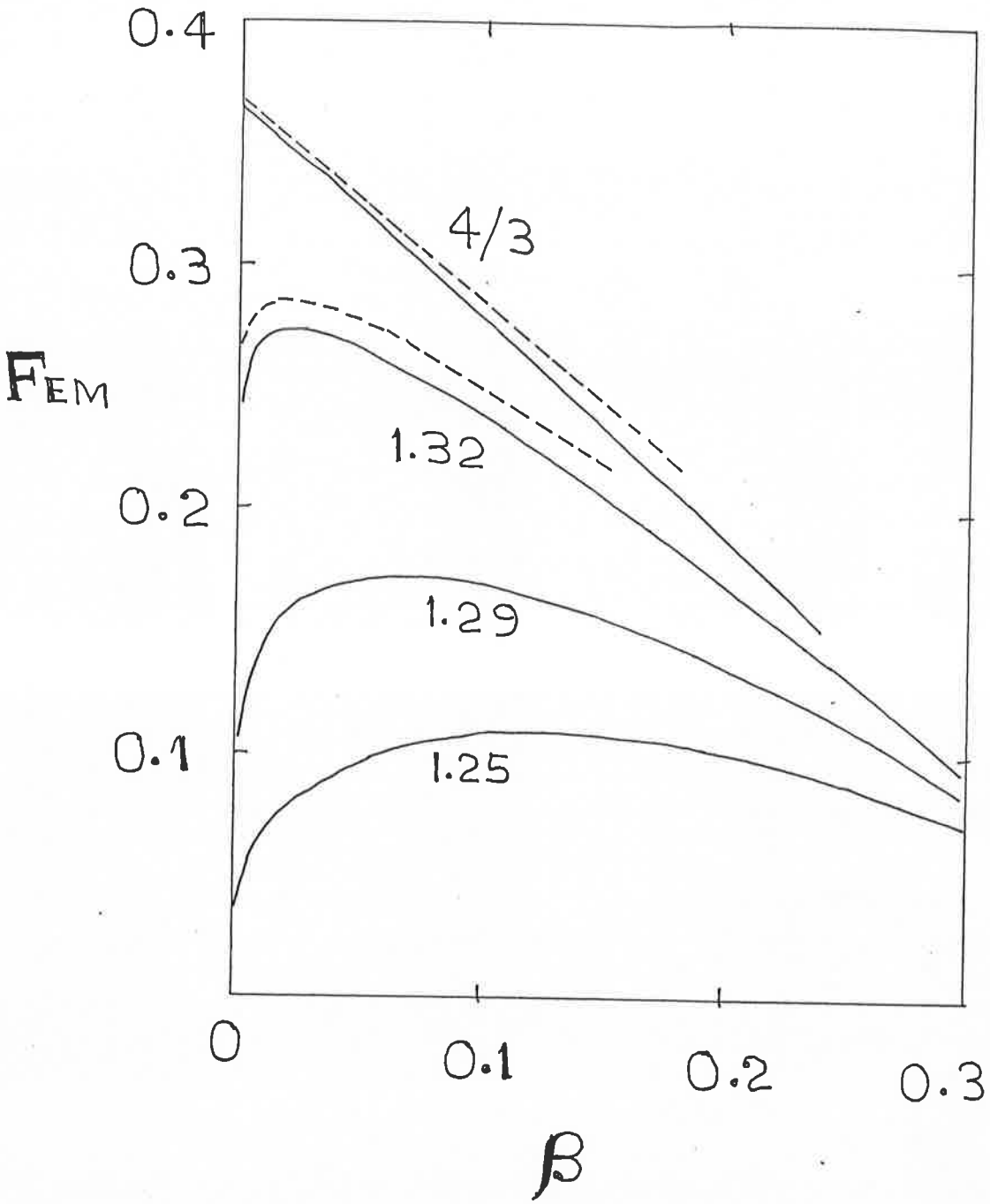

Fig 16

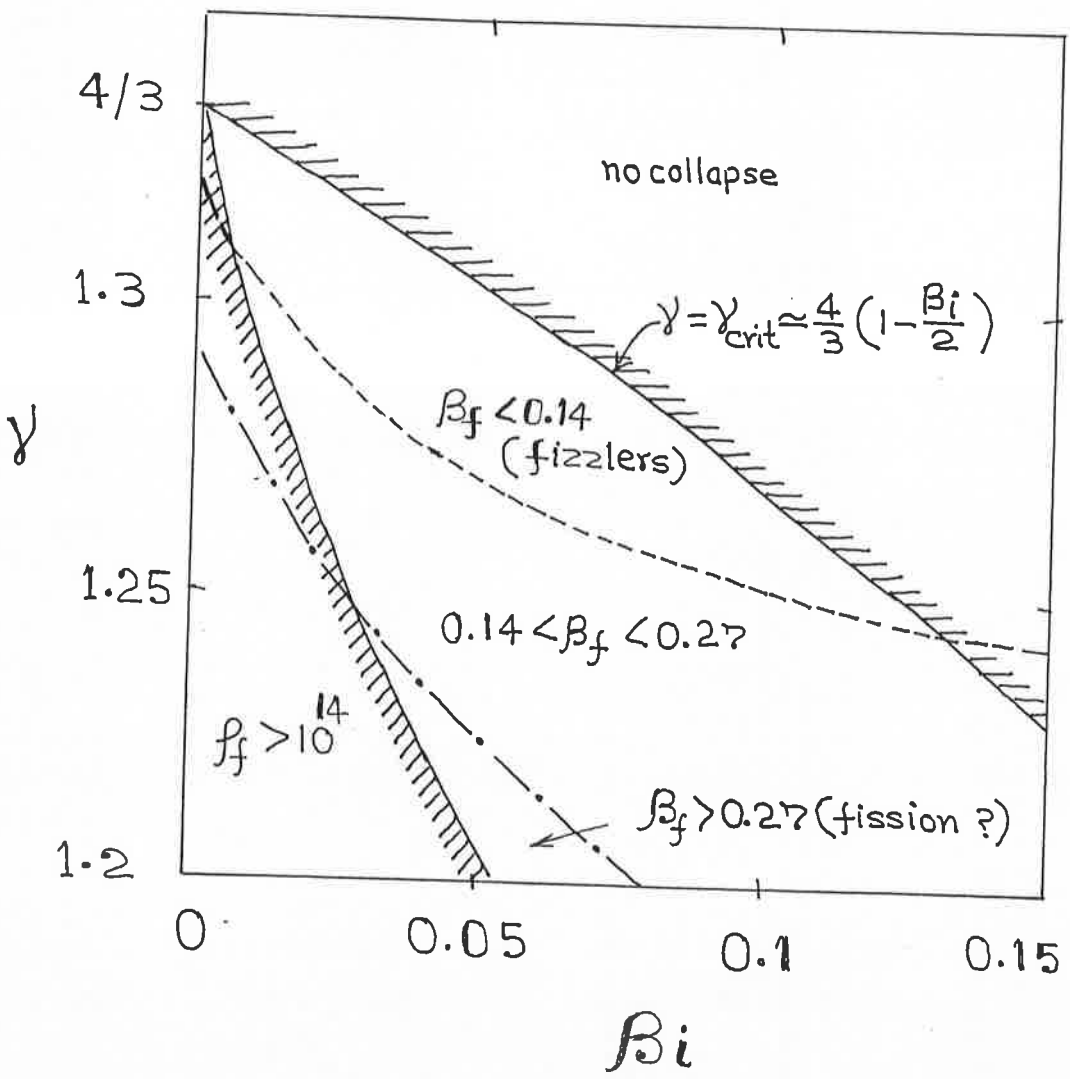
4/3
1.3
1.25
1.2
γ
no collapse
γ = γcrit ≃ 4/3 (1 − βi/2)
βf < 0.14
(fizzlers)
0.14 < βf < 0.27
βf > 10^14
βf > 0.27 (fission ?)
0
0.05
0.1
0.15
βi

Fig - 17

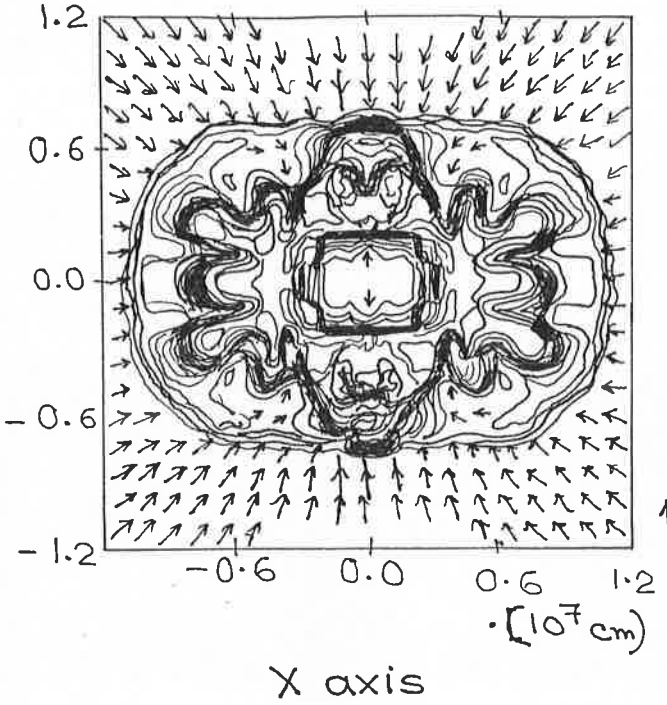

Entropy
Velocity
Model 82400
Timestep 2.16E-07
t(m.s) 195.66
Se(k/nuc) 0.991

Contours 19
Delta 4.00E-01
Fmin 1.20E+00
Fmax 8.40E+00

Center 0.0
0.0
0.0

↑ 5.0×10^9 cm/s

Fig 18

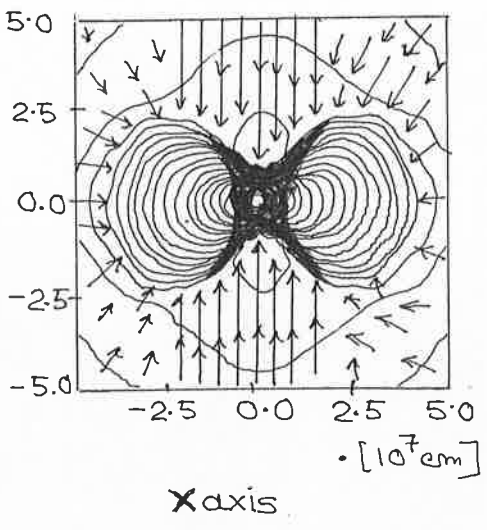

Density
Velocity
Model 167900
Timestep 7.99E-07
t (m.s.) 392.58
log(Se) 13.332
Contours 26
Delta 2.50E-01
Fmin 7.00E+00
Fmax 1.32E+01
Center 0.0
0.0
0.0

↑ 4.0×10^9 cm/s

Fig - 19

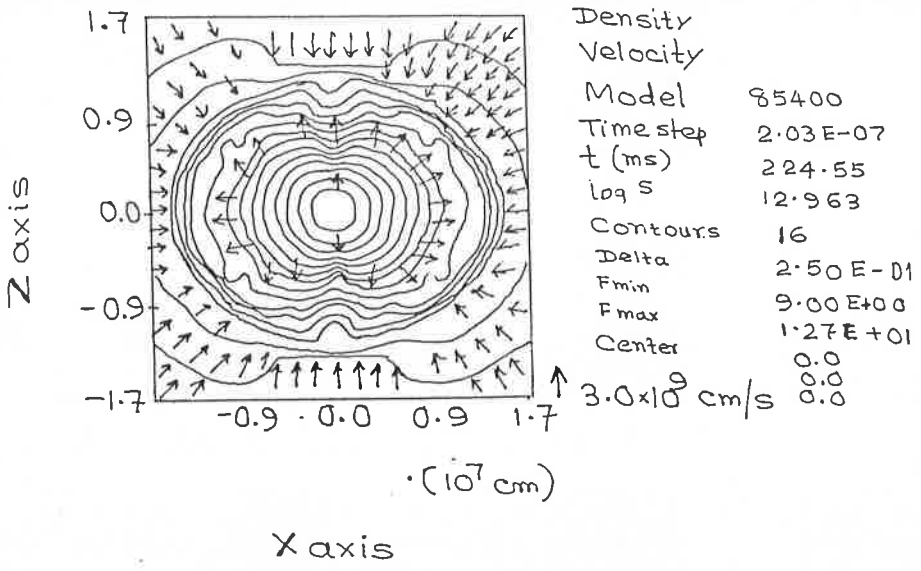
Density
Velocity
Model 85400
Time step 2.03E-07
t (ms) 224.55
log s 12.963
Contours 16
Delta 2.50E-01
Fmin 9.00E+00
Fmax 1.27E+01
Center 0.0 0.0 0.0
3.0×10^9 cm/s
1.7
0.9
0.0
-0.9
-1.7
-0.9 0.0 0.9 1.7
(10^7 cm)
Z axis
X axis

Fig 20

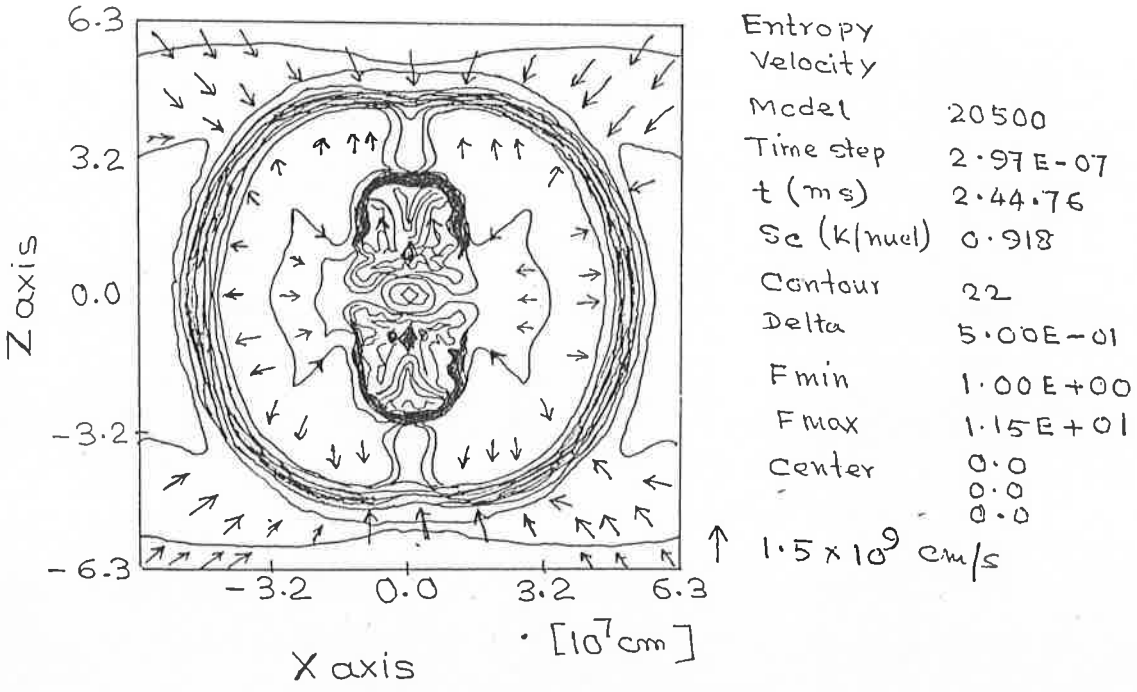
Entropy
Velocity
Model 20500
Time step 2.97E-07
t (ms) 2.44.76
Sc (k/nucl) 0.918
Contour 22
Delta 5.00E-01
Fmin 1.00E+00
Fmax 1.15E+01
Center 0.0 0.0 0.0
1.5×10^9 cm/s
6.3
3.2
0.0
-3.2
-6.3
-3.2 0.0 3.2 6.3
[10^7 cm]
Z axis
X axis

Fig-21

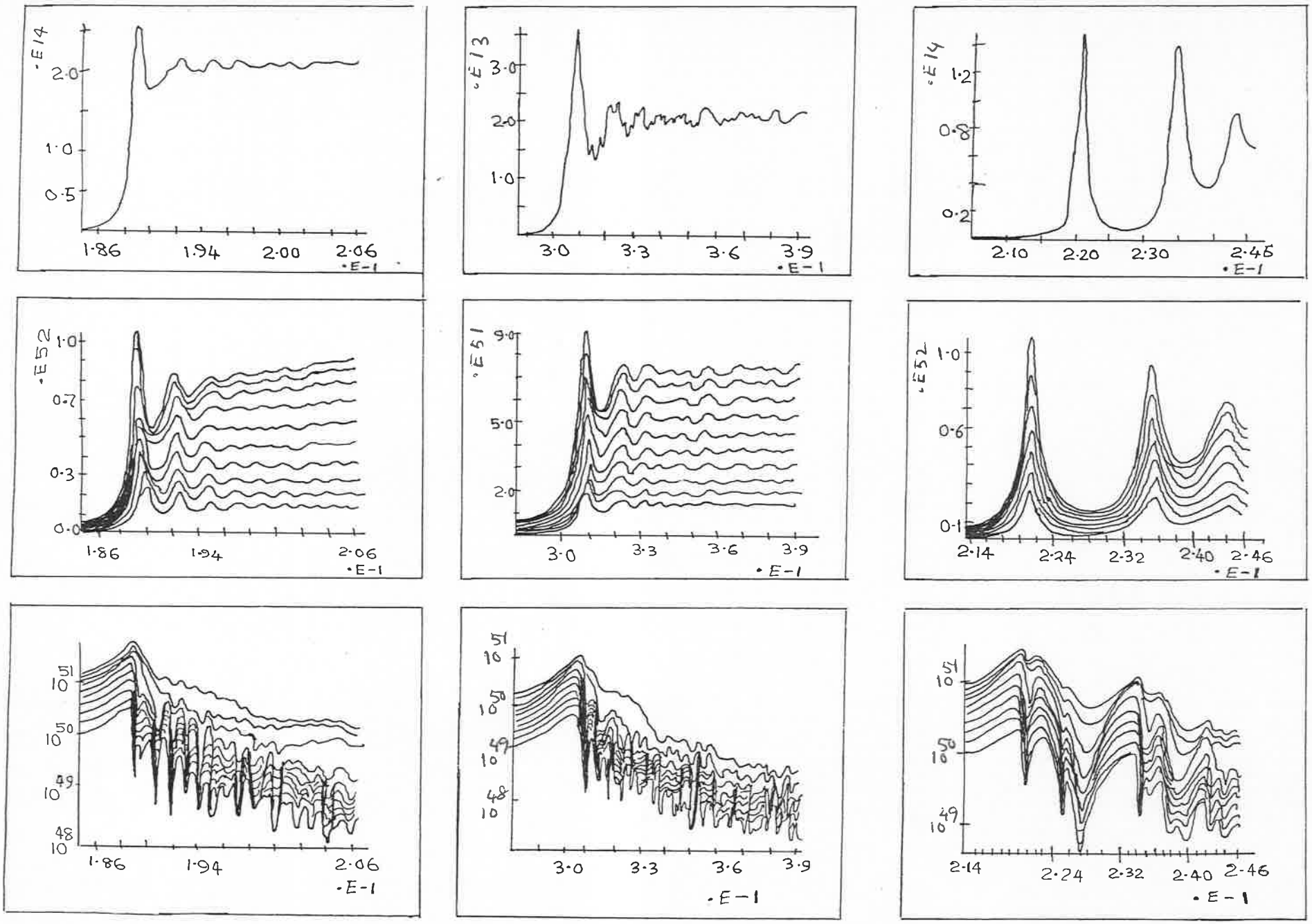
·E14
2·0
1·0
0·5
1·86
1·94
2·00
2·06
·E-1
·E13
3·0
2·0
1·0
3·0
3·3
3·6
3·9
·E-1
·E14
1·2
0·8
0·2
2·10
2·20
2·30
2·45
·E-1
·E52
1·0
0·7
0·3
0·0
1·86
1·94
2·06
·E-1
·E51
5·0
2·0
3·0
3·3
3·6
3·9
·E-1
·E52
1·0
0·6
0·1
2·14
2·24
2·32
2·40
2·46
·E-1
10^51
10^50
10^49
10^48
1·86
1·94
2·06
·E-1
10^51
10^50
10^49
10^48
3·0
3·3
3·6
3·9
·E-1
10^51
10^50
10^49
2·14
2·24
2·32
2·40
2·46
·E-1

Fig. 22

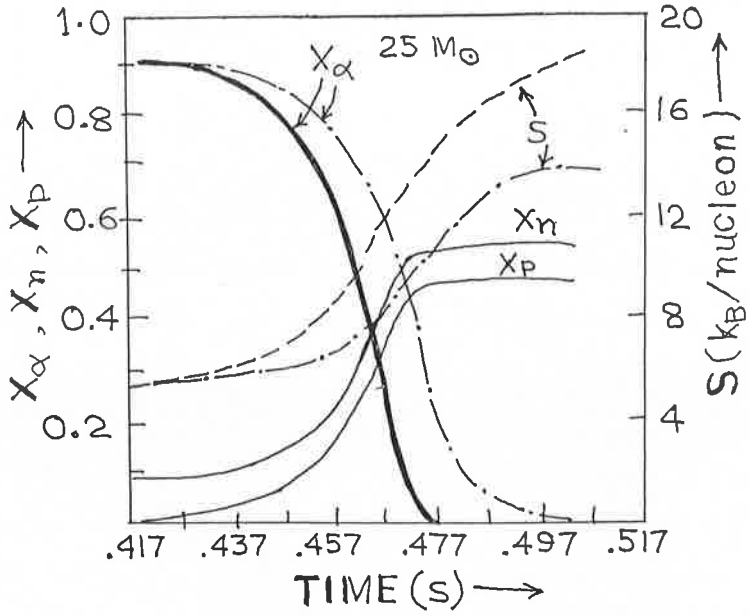

Fig-23 (a)

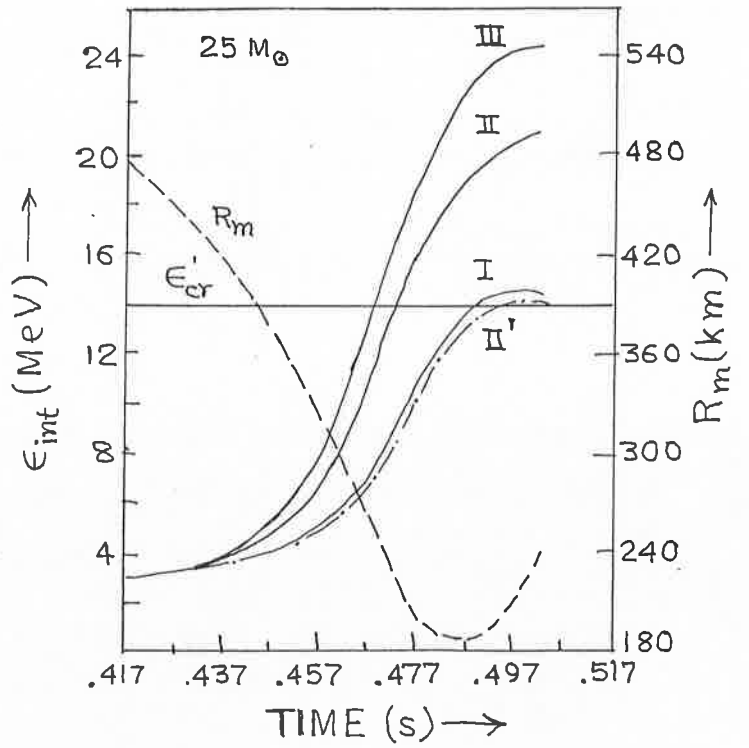

Fig-23(b)

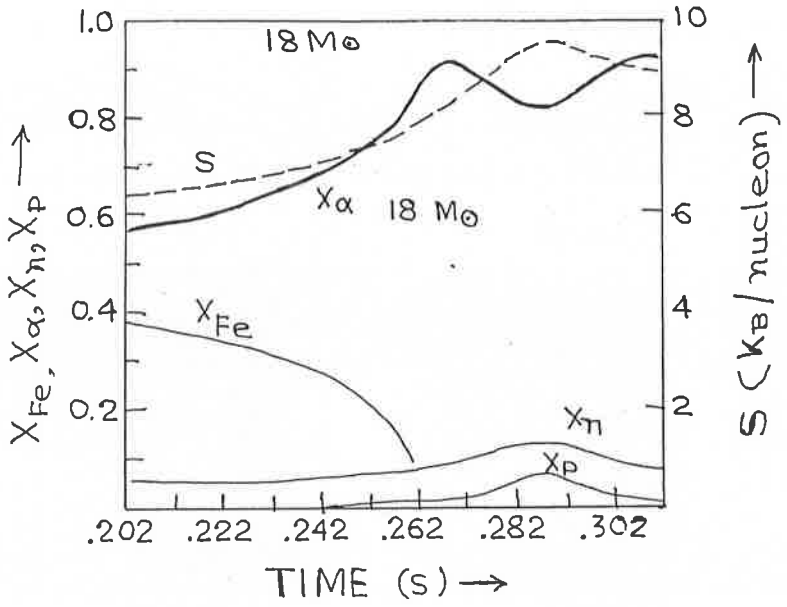
18 M⊙
S
Xα 18 M⊙
XFe
Xn
Xp
XFe, Xα, Xn, Xp →
S (KB/nucleon) →
TIME (s) →
1.0
0.8
0.6
0.4
0.2
10
8
6
4
2
.202
.222
.242
.262
.282
.302

24 (a)

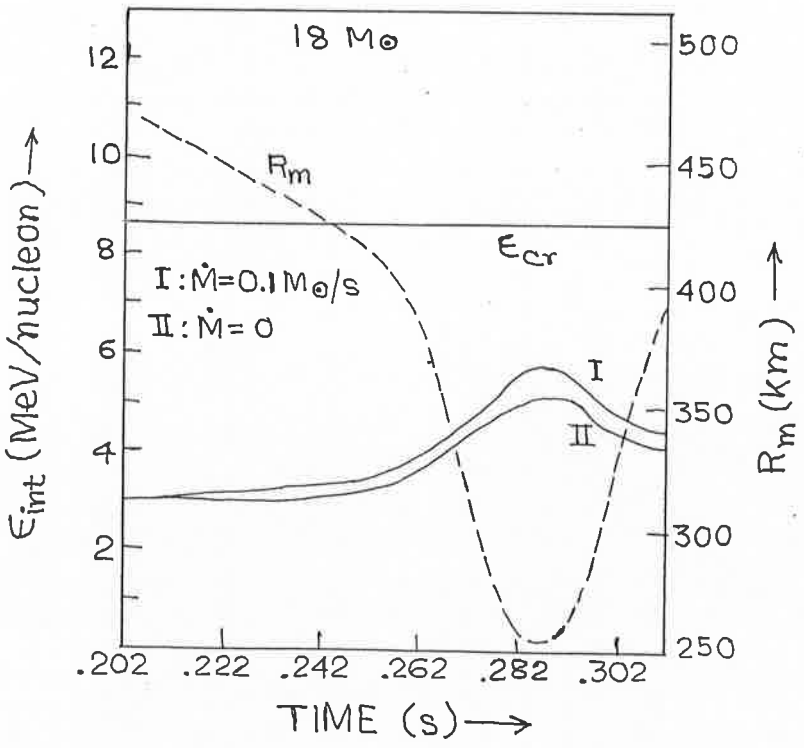
18 M⊙
Rm
Ecr
I : Ṁ = 0.1 M⊙/s
II : Ṁ = 0
I
II
εint (MeV/nucleon) →
Rm (km) →
TIME (s) →
12
10
8
6
4
2
500
450
400
350
300
250
.202
.222
.242
.262
.282
.302

(b)

Fig - 24

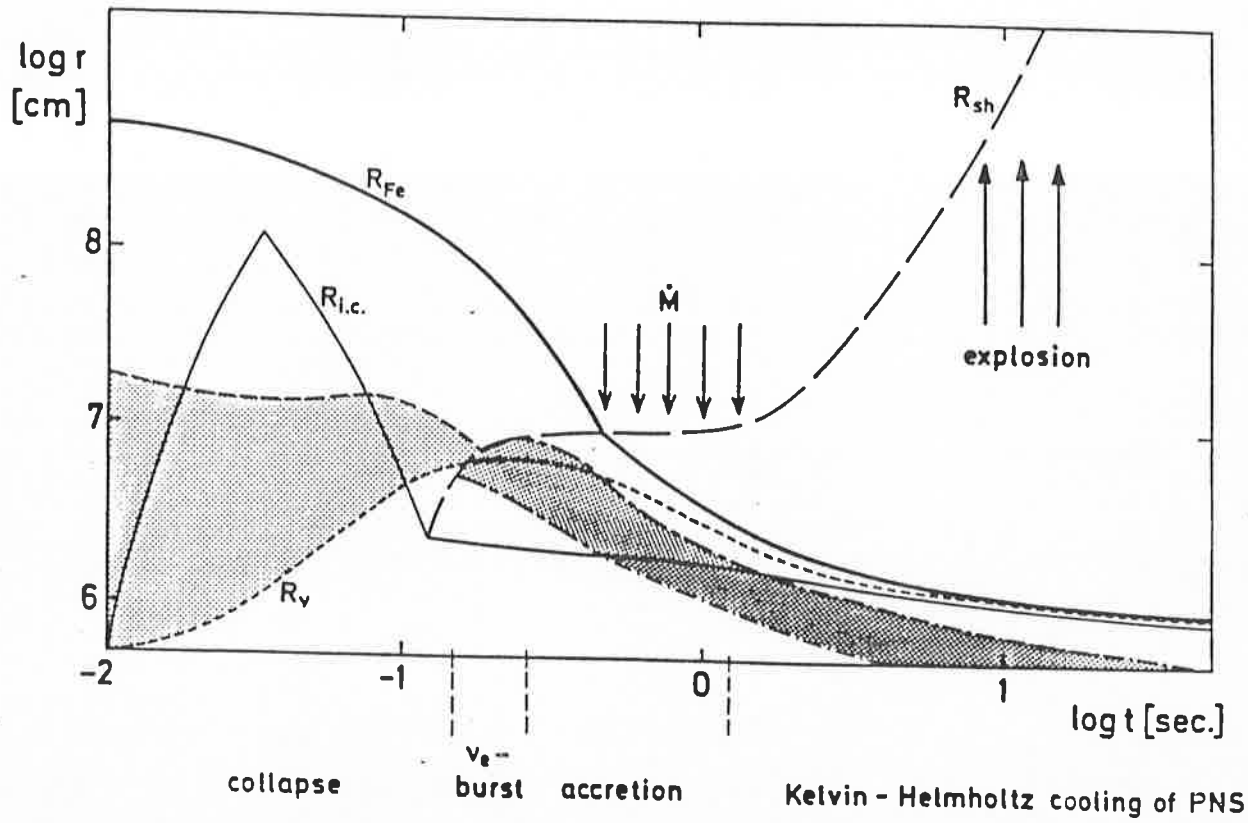
log r
[cm]
8
7
6
-2
-1
0
1
log t [sec.]
R_{Fe}
$R_{l.c.}$
R_{ν}
R_{sh}
$\dot{M}$
explosion
collapse
ν_e-burst
accretion
Kelvin - Helmholtz cooling of PNS

Fig- 25

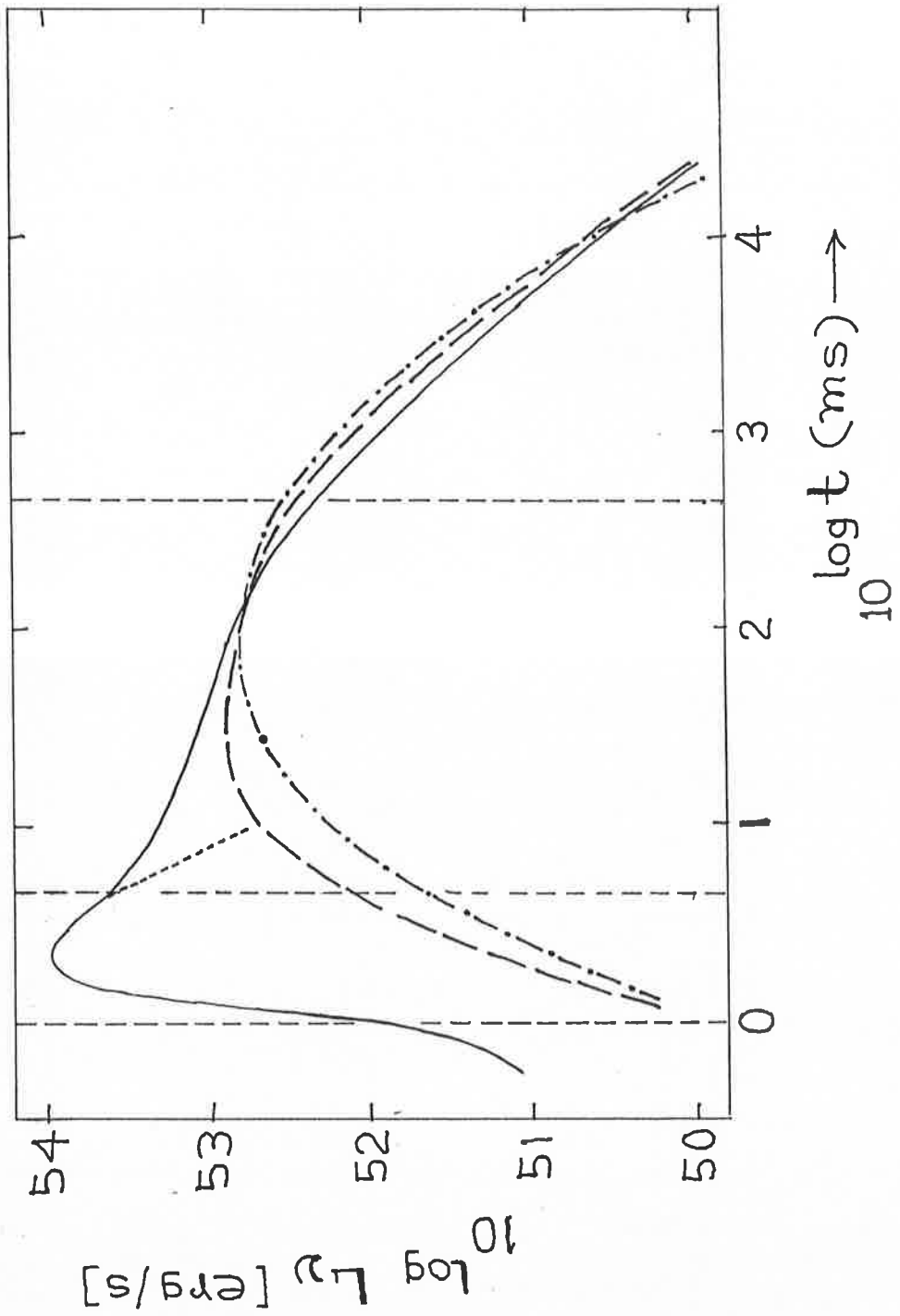

Fig- 26

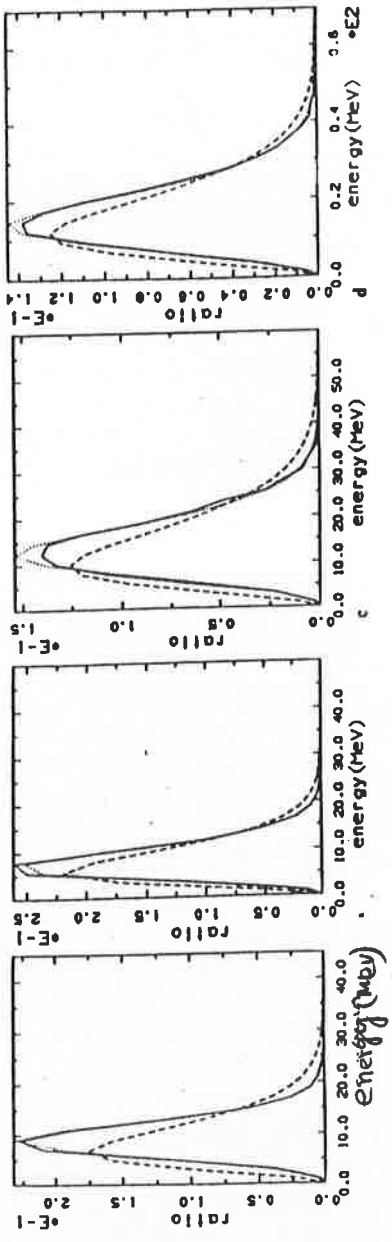

Fig- 27

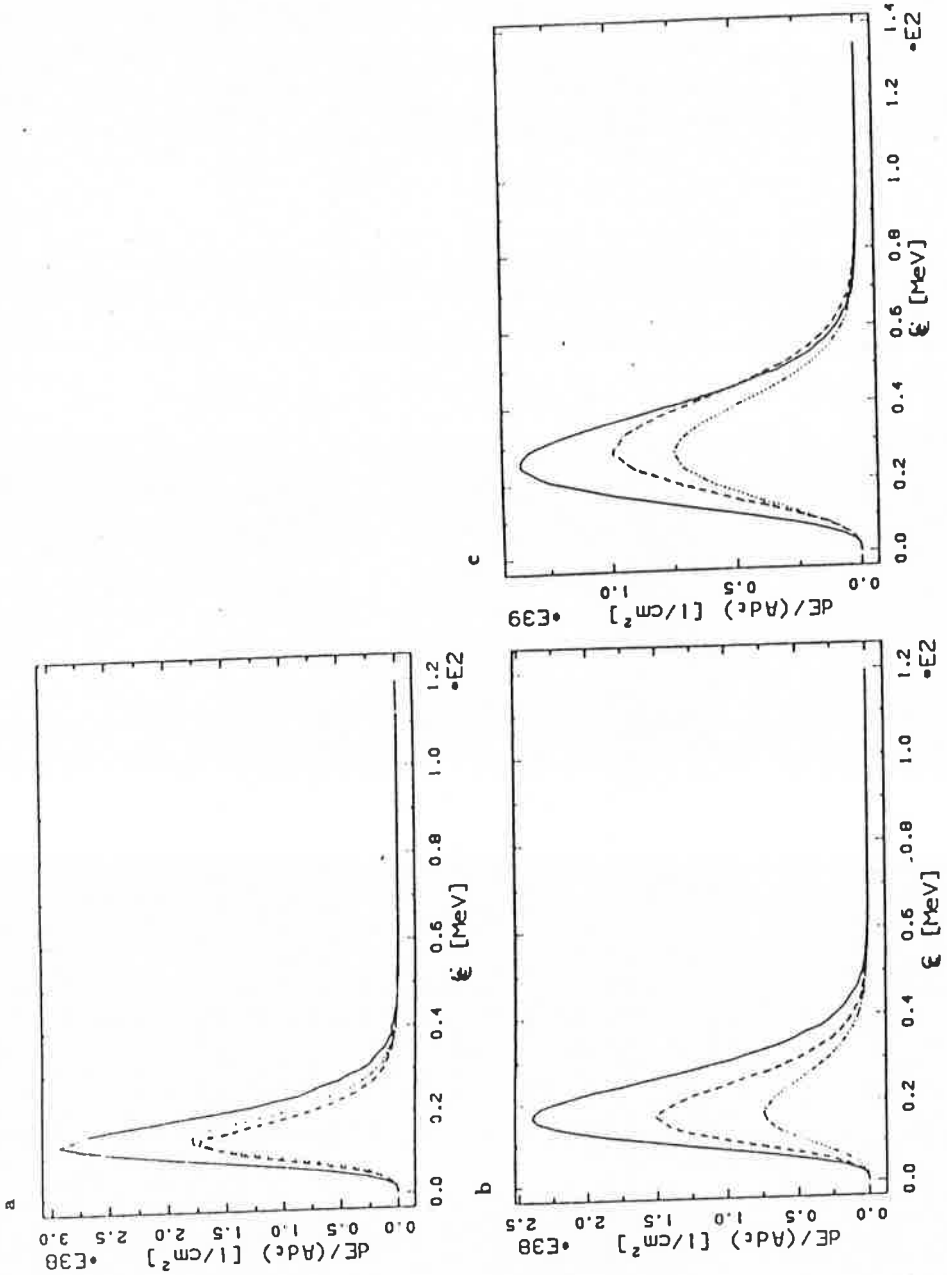

Fig - 28

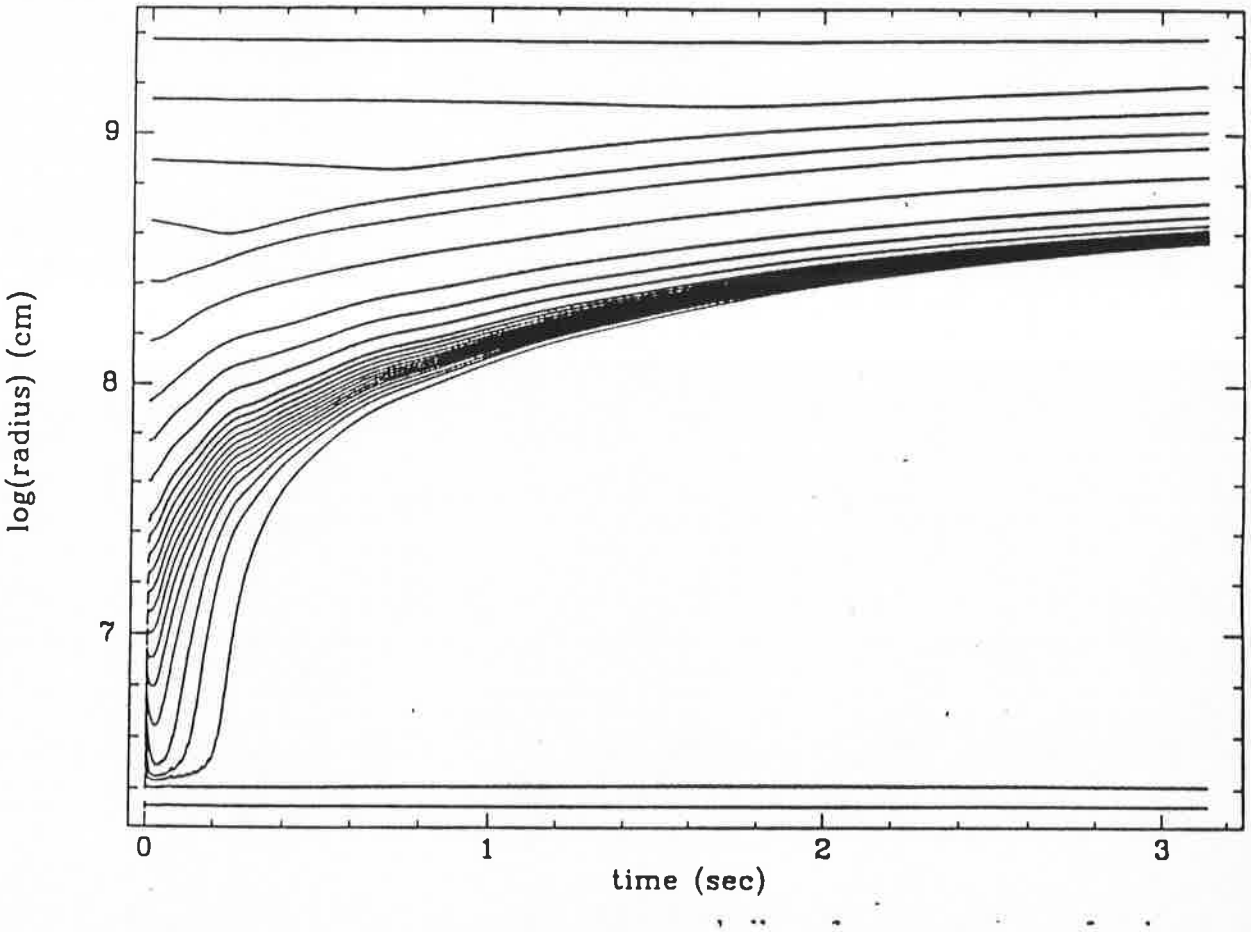

Fig. 29

Fig. 30

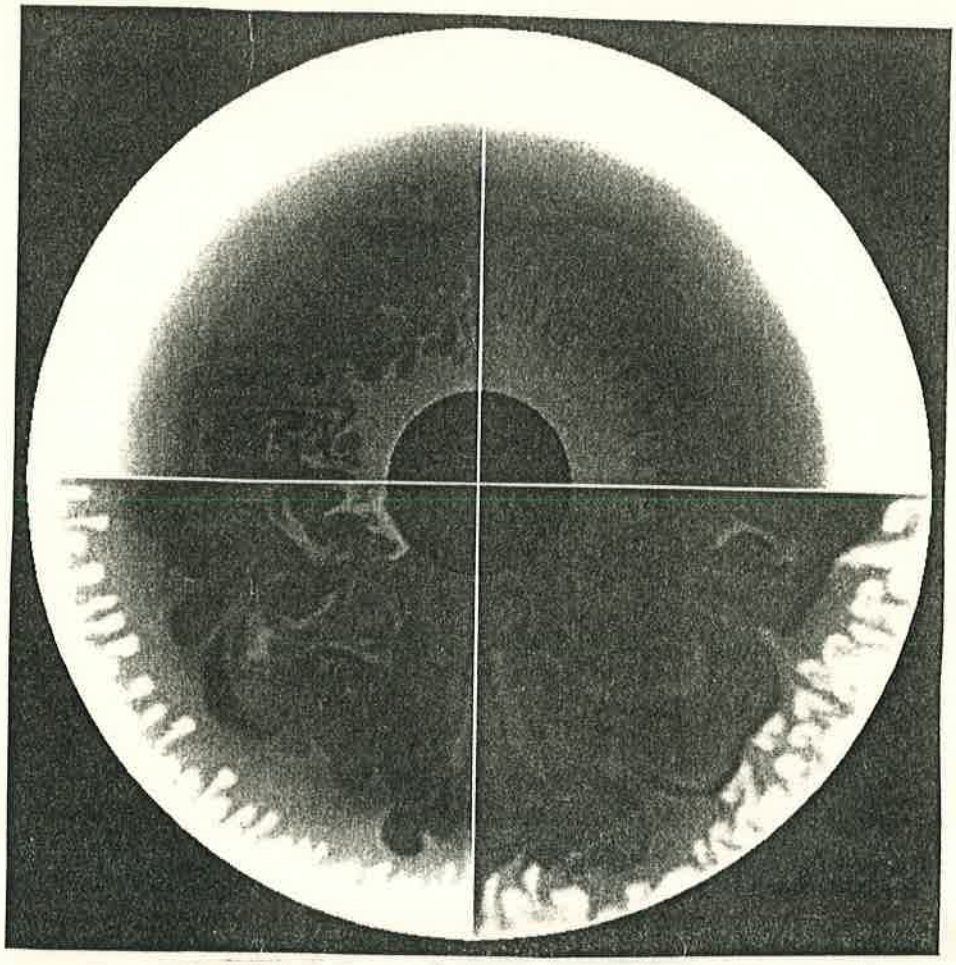

Fig. 31

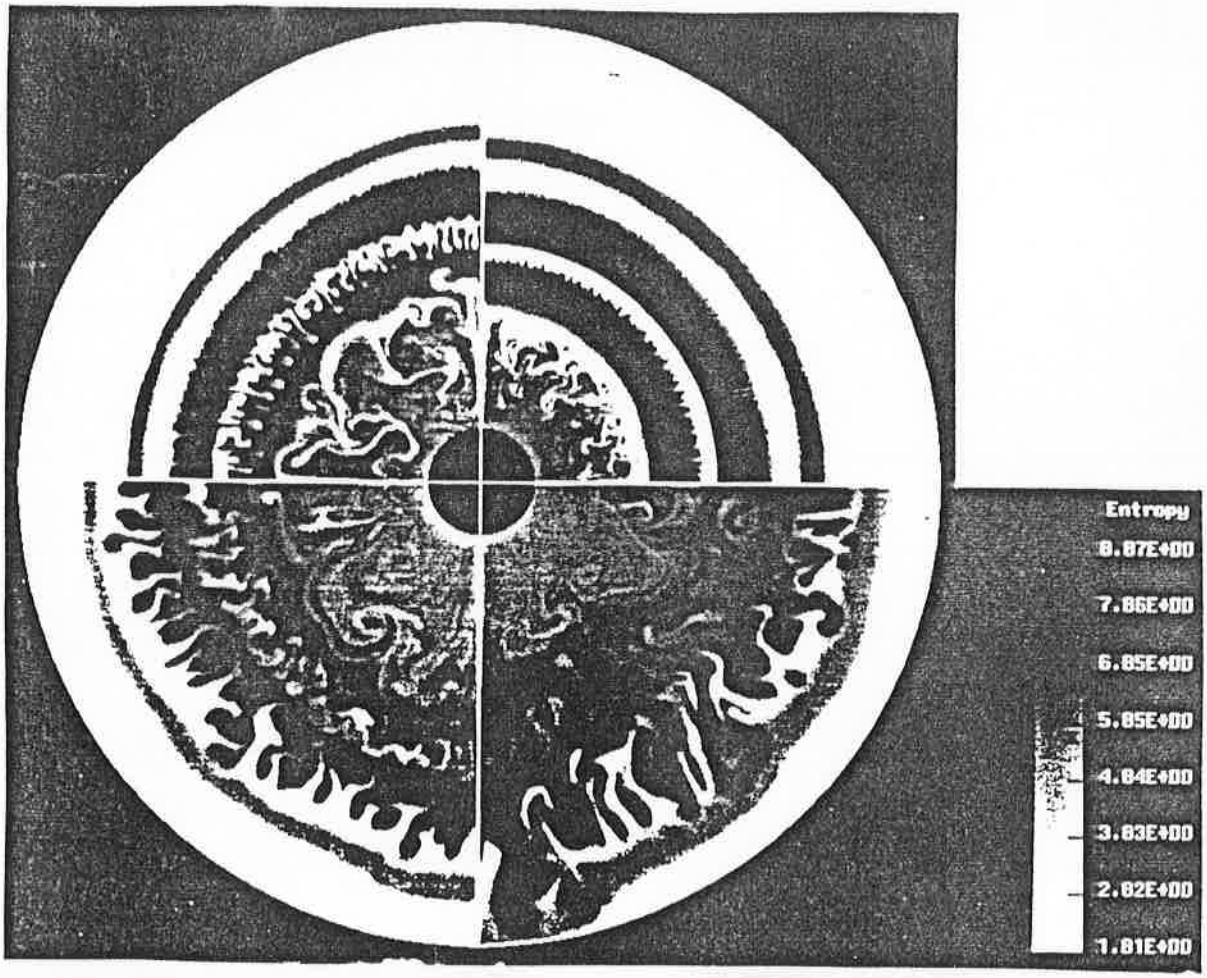
Entropy
8.87E+00
7.86E+00
6.85E+00
5.85E+00
4.84E+00
3.83E+00
2.82E+00
1.81E+00

Fig - 32

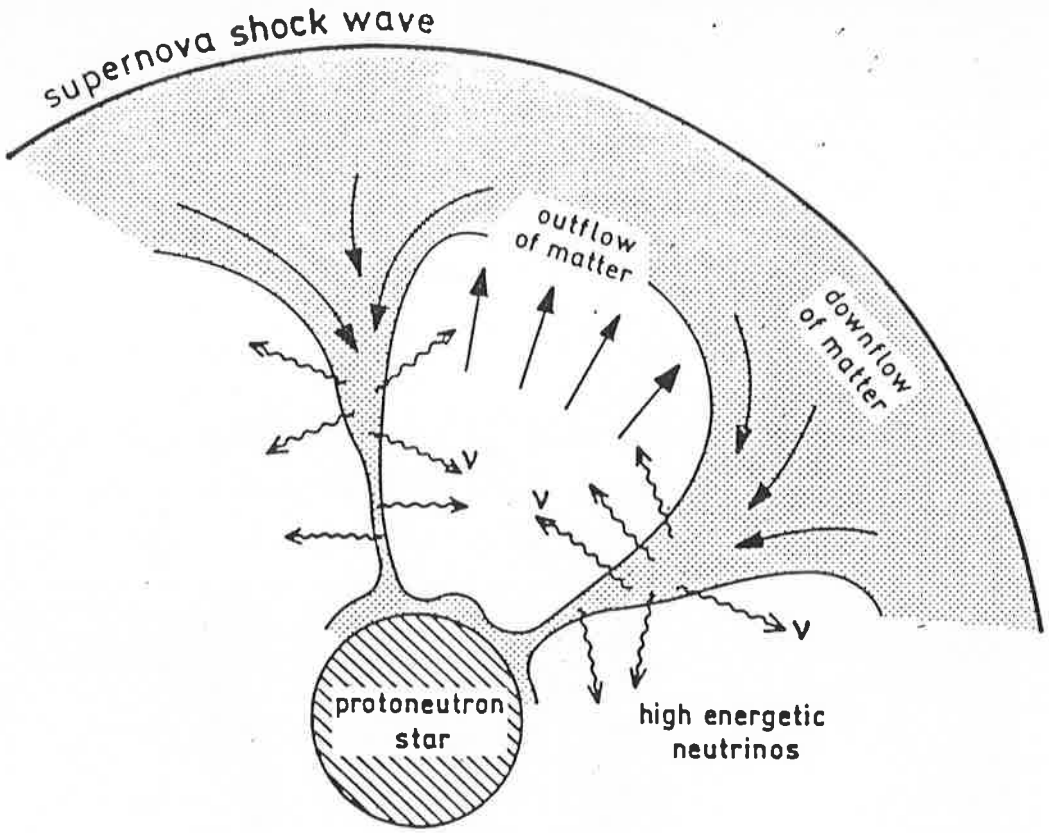
supernova shock wave
outflow of matter
downflow of matter
ν
ν
ν
protoneutron star
high energetic neutrinos

Fig. 33

TABLE 1 Fe Core Masses

Model	Fe Core	2500 km	3500 km	Model	Fe Core	2500 km	3500 km
12S2	1.37	1.47	1.56	15S1	1.41	1.43	1.50
13S2	1.54	1.55	1.66	25S1	1.45	1.63	1.73
15S2	1.30	1.50	1.58	35S1	1.40	1.61	1.71
20S2	1.66	1.85	2.06	15S3	1.30	1.53	1.60
25S2	1.95	1.90	2.24	25S3	1.52	1.52	1.58
30S2	2.04	1.88	2.23	35S3	1.91	1.90	2.12
35S2	2.03	1.85	2.18	15ST	1.63[a]	1.55	1.68
15N2	1.20[a]	1.34	1.38	25ST	1.61	1.72	1.83
20N2	1.69	1.53	1.69	35ST	1.63	1.84	2.06
25N2	1.49	1.71	1.80	25N1	1.37	1.51	1.59
30N2	1.68	1.84	2.04	35N1	1.62	1.56	1.69
35N2	1.63	1.85	2.06	15N3	1.25[a]	1.44	1.50
				25N3	1.53	1.76	1.90

[a] Implosive burning in progress. Iron core poorly resolved.